(12)

AD

AMMRC TR 78-14
VOLUME 2

ENERGY

BRITTLE MATERIALS DESIGN, HIGH TEMPERATURE GAS TURBINE

VOLUME 2
CERAMIC TURBINE ROTOR TECHNOLOGY

12TH INTERIM REPORT FOR THE
PERIOD JANUARY — SEPTEMBER 1977

Arthur F. McLean, Robert R. Baker

Date Published — March, 1978

Prepared for
ARMY MATERIALS AND MECHANICS RESEARCH CENTER
Watertown, Massachusetts 02172

Contract Number DAAG-46-71-C-0162
Agency Accession Number DA-OD 4733

FORD MOTOR COMPANY
ENGINEERING AND RESEARCH STAFF
DEARBORN, MICHIGAN 48121

U. S. DEPARTMENT OF ENERGY

Division of Transportation Energy Conservation

The findings in this report are not to be construed as an official Advanced Research Projects Agency, Department of the Army, or U.S. Government position, either expressed or implied, unless so designated by other authorized documents.

Mention of any trade names or manufacturers in this report shall not be construed as advertising nor as an official indorsement or approval of such products or companies by the United States Government.

DISPOSITION INSTRUCTIONS

Destroy this report when it is no longer needed.
Do not return it to the originator.

Printed in the United States of America

Available from

National Technical Information Service
U.S. Department of Commerce
5285 Port Royal Road
Springfield, Virginia 22161

Price: Printed Copy $6.50
Microfiche $3.00

(18) (19)
AMMRC TR-78-14 -VOL-2
VOLUME 2
Distribution Category UC-96

(6)
BRITTLE MATERIALS DESIGN, HIGH TEMPERATURE GAS TURBINE.

VOLUME 2. CERAMIC TURBINE ROTOR TECHNOLOGY.

(9)
12TH INTERIM REPORT FOR THE no. 12,
PERIOD JAN[redacted] — SEP[redacted]77,

(10) Arthur F. McLean Robert R. Baker

FORD MOTOR COMPANY
ENGINEERING AND RESEARCH STAFF
DEARBORN, MICHIGAN 48121

(11)
Date Published — Mar[redacted]78

(12) 93 p.

Prepared for
ARMY MATERIALS AND MECHANICS RESEARCH CENTER
Watertown, Massachusetts 02172

(15)
Contract Number DAAG-46-71-C-0162, ARPA Order-1849
Agency Accession Number DA-OD 4733

U.S. DEPARTMENT OF ENERGY

Office of the Assistant Secretary for Conservation and Solar Applications
Division of Transportation Energy Conservation

ABSTRACT

The progress in the last nine months on ERDA supported programs within the joint DARPA/ERDA supported "Brittle Materials Design, High Temperature Gas Turbine" Program is reported on in this volume. Volume 1 covers the progress on the DARPA supported Ceramic Turbine Testing Program.

Investigations of the materials used to fabricate duo-density ceramic turbine rotors were conducted on injection molded reaction bonded and hot pressed silicon nitride. The starting silicon powder, used to injection mold rotor blade rings, was found to contain contaminates in the form of iron and chromium. Microstructural examination of both silicon nitride test bars and rotor blades indicated a definite correlation between strength and the size of microscopic flaws due to contamination. Magnetic separator equipment was ordered and received so that all starting silicon powder can be cleaned in-house. Approximately 30 hot pressings were made with various purity level starting powders and a variety of hot pressing aids. The high temperature strength will be determined to identify the best candidates for further study.

The injection molding process, utilized to fabricate rotor blade rings, was improved by optimizing the molding parameters with the automated control system and improving the molding mixture. The installation of nozzles, to apply mold release, and air blast jets, to clean the die and evenly distribute the mold release, resulted in a noticeable improvement in the surface finish of the blade rings. Significant improvements were made in the hot press bonding process used to fabricate duo-density turbine rotors. Control of the hot pressing load was refined and temperature measurement improved. The graphite tooling was redesigned and blade filling process was modified. These two changes resulted in the most significant improvement in the yield of hot pressings to date; 70% of the rotors fabricated were free of flaws induced by hot pressing. Alternate approaches were investigated to produce duo-density turbine rotors.

Duo-density turbine rotors were tested in the cold spin pit to evaluate the hot press to reaction sintered bond joints and the effect of I.D. voids, in the blade ring rim, on blade failure speeds. Degradation of the room temperature strength of the reaction bonded silicon nitride rotor blades was identified as resulting from the press-bonding operation. Blade strength decreases of 14 to 38% were measured by the blade bend test. Analysis of the blades indicated they change from a shiny black to a gray color after hot pressing with a corresponding increase in non-uniform porosity; phase analysis indicated that the reaction bonded silicon nitride had changed from an average of 70% α, 29% β before press bonding to an average of 22% α, 75% β and 3% silicon oxynitride after press-bonding.

A procedure for determining whether statistically significant differences exist between two sets of data, known as the 'Hypothesis Testing' was outlined. The test was applied to data from duo-density turbine rotors and showed that blade strength did deteriorate after the press-bonding operation. Use of proof-testing as a means of enhancing the accuracy of life predictions was discussed. Analytical relations were derived for predicting the survival probability of a proof-tested component, and a procedure was outlined for maximizing the effectiveness of a proof-test. Life prediction relations derived in the previous report were applied to the first-stage turbine rotor. Several disk contour modifications were studied as means of improving the life of the rotor under the DARPA duty cycle. The study showed that for given design constraints (space, inertia, etc.) and using material utilization as the criterion, the optimum disk configuration derived on the basis of fast fracture (time independent) mode of failure differed from the configuration derived from life considerations when the material is subject to static fatigue.

FOREWORD

This report is the twelfth technical report of the "Brittle Materials Design, High Temperature Gas Turbine" program initiated by the Defense Advanced Research Projects Agency, DARPA Order Number 1849, and Contract Number DAAG-46-71-C-0162. This is an incrementally-funded seven year program.

Since this is an iterative design and materials development program, design concepts and materials selection and/or properties presented in this report will probably not be those finally utilized. Thus all design and property data contained in the semi-annual reports must be considered tentative, and the reports should be considered to be illustrative of the design, materials, processing, and NDE techniques being developed for brittle materials.

In fiscal year 1977, the Energy Research and Development Administration (ERDA), now Department of Energy (DOE), joined forces with DARPA to support this project.

The ERDA Division of Transportation (TEC), started to support process development to improve the quality of duo-density silicon nitride turbine rotors, and ERDA's Division of Conservation Research and Technology (CONRT), supported some of the work on non-destructive evaluation of ceramics and ceramic materials characterization. DOE has delegated project management responsibility to the NASA Lewis Research Center for the TEC Heat Engine Highway Vehicle Systems Program. This includes work under the TEC/AMMRC Heat Engine Systems Materials and Components Technology Program. The Army Materials and Mechanics Research Center continued to function as the technical monitor of the overall program.

The progress made on the DARPA Ceramic Turbine Testing Program is presented in Volume 1 while the progress on the ERDA Ceramic Turbine Technology and Ceramic Turbine Materials and NDE Technology Programs is presented in this Volume. This work was supported under ERDA/DOD (now DOE/DOD) Interagency Agreement EC-77-A-1017 between TEC and AMMRC.

The principal investigator of this program is Mr. A. F. McLean, Ford Motor Company, and the technical monitor is Dr. E. S. Wright, AMMRC. The authors would like to acknowledge the valuable contributions in the performance of this work by the following people.

Ford Motor Company

N. Aron, R. J. Baer, J. H. Buechel, D. J. Cassidy, J. C. Caverly, G. C. DeBell, A. Ezis, E. A. Fisher, D. L. Hartsock, P. H. Havstad, J. A. Herman, R. A. Jeryan, C. F. Johnson, J. A. Mangels, W. E. Meyer, A. Paluszny, G. Peitsch, J. R. Secord, L. R. Swank, W. Trela, T. J. Whalen, R. M. Williams, W. Wu

Army Material and Mechanics Research Center

G. E. Gazza, E. M. Lenoe, R. N. Katz, D. R. Messier, H. Priest

ERDA-TEC Project Officer — R. B. Schulz

ERDA-CONRT Project Officer — F. C. Moore

ERDA-NASA Lewis Project Officer — C. P. Blankenship

TABLE OF CONTENTS

LIST OF ILLUSTRATIONS

LIST OF ILLUSTRATIONS

LIST OF TABLES

1.0 INTRODUCTION

In July, 1971, the Defense Advanced Research Projects Agency of the Department of Defense jointly sponsored a program with Ford Motor Company to develop and encourage the use of brittle materials for engineering applications. The major program goal of the "Brittle Materials Design — High Temperature Gas Turbine" program was to prove by a practical demonstration that efforts in ceramic design, materials, fabrication, testing and evaluation could be drawn together and developed to establish the usefulness of brittle materials in demanding high temperature structural applications.

The replacement of high cost nickel-chrome superalloys in gas turbines with low cost, higher temperature capability ceramics offers significant advances in efficiency, materials utilization and power per unit weight. The vehicular turbine project was organized to design and develop an entire ceramic hot flow path for a high temperature (2500°F) vehicular gas turbine engine (Figure 1.1).

The progress of the gas turbine engine has been and continues to be closely related to the development of materials capable of withstanding the engine's environment at high operating temperature. Since the early days of the jet engine, new metals have been developed which allowed a gradual increased in operating temperatures. Today's nickel-chrome superalloys are in use, without cooling, at turbine inlet gas temperatures of 1800°F. However, there is considerable incentive to further increase turbine inlet temperature in order to improve specific air and fuel consumptions. The use of ceramics in the gas turbine engine promises to make a major step in increasing turbine inlet temperature to 2500°F. Such an engine offers significant advances in efficiency, power per unit weight, cost, exhaust emissions, materials utilization and fuel utilization. Successful application of ceramics to the gas turbine would therefore not only have military significance, but would also greatly influence our national concerns of air pollution, utilization of material resources, and the energy crisis.

In fiscal year 1977, ERDA joined forces with DARPA to support the program. The ERDA Division of Transportation, working closely with NASA-Lewis, started to support process development to improve the quality of duo-density silicon nitride turbine rotors, and ERDA's Division of Conservation Research and Technology supported some of the work on non-destructive evaluation of ceramics and

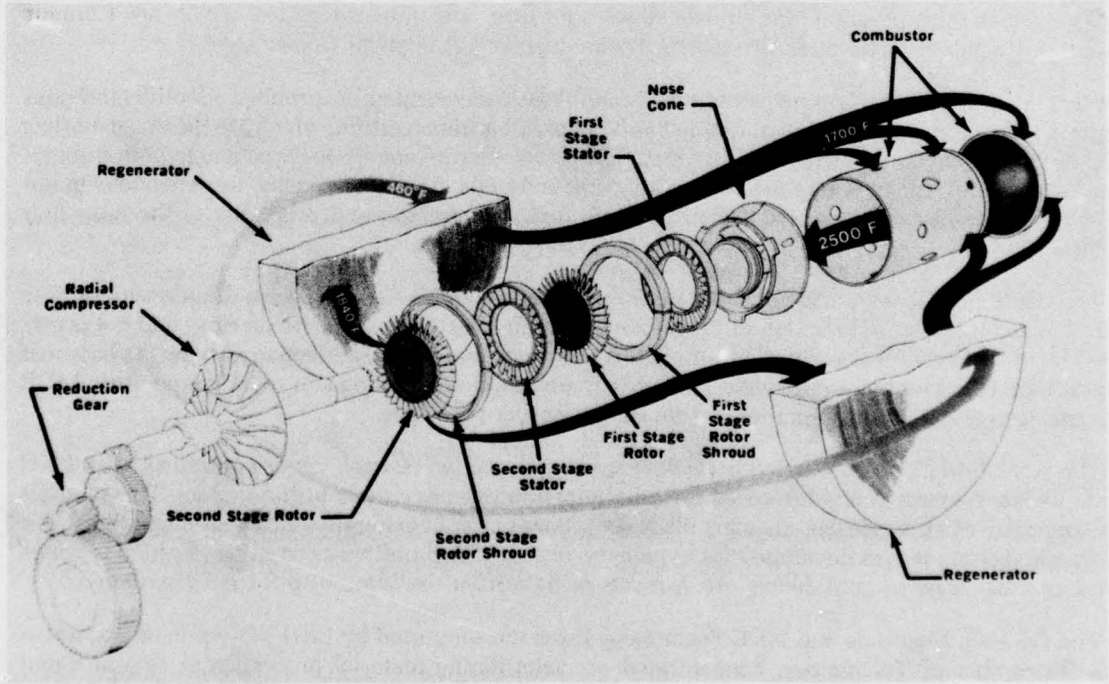

Figure 1.1 — Schematic View of the Vehicular Gas Turbine Engine Flowpath

ceramic materials characterization (Figure 1.2). The Army Materials and Mechanics Research Center continued to function as the technical monitor of the overall program.

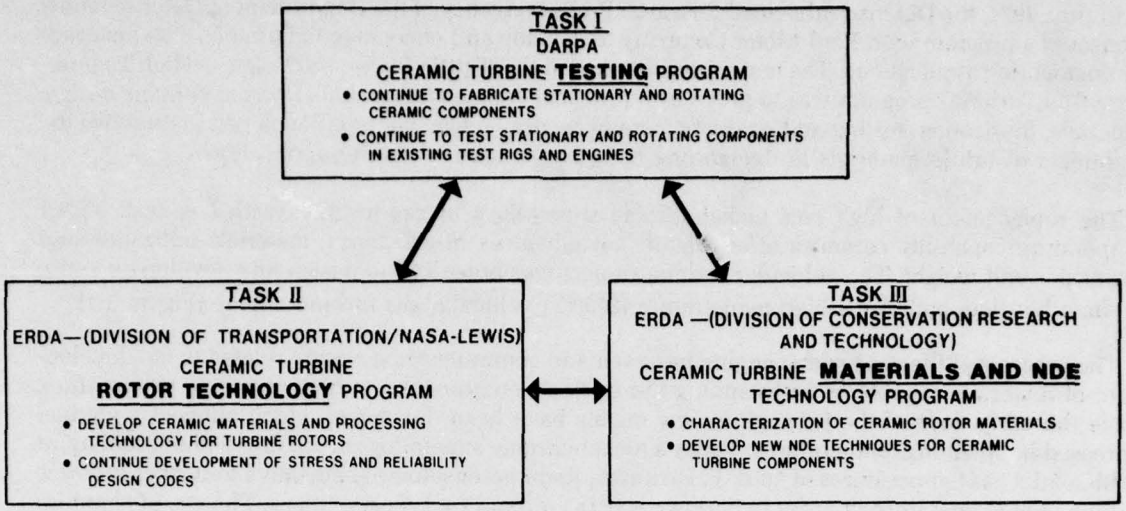

Figure 1.2 — DARPA/ERDA Supported Tasks in the "Brittle Materials Design, High Temperature Gas Turbine" Program

During the past nine months, the DARPA portion of the program was specifically oriented toward the evaluation of the reliability of state-of-the-art ceramic components which were developed over the previous five and one half years. Volume 1 of this report covers the DARPA Ceramic Turbine Testing Program and represents the 12th report of progress. This volume covers the progress on ERDA supported work on Ceramic Turbine Rotor Technology and Ceramic Turbine Materials and NDE Technology Programs.

The Turbine Rotor Technology Program, supported by ERDA Division of Transportation, focused on continued development of ceramic materials and process technology used to fabricate ceramic turbine rotors. The program was broken down into three separate categories, which are Ceramic Materials Technology, Ceramic Processing Technology and Analytical Codes.

Work in the area of Ceramic Materials Technology concentrated on problem identification and continued development of reaction bonded and hot pressed silicon nitride which are the two materials used in fabricating duo-density turbine rotors (Figure 1.3). Improvements were sought in both strength and "m" value of injection molded rotor blade ring materials of 2.7g/cc density. Investigations in hot pressing technology were carried out to improve both the strength and reliability of the rotor hub material.

The continued development of Ceramic Processing Technology as applied to duo-density turbine rotors concentrated on fabrication improvements on both injection molded blade rings and hot press/press bonding of rotor hubs. Considerable effort was needed and was spent on modifying the hot press bonding process to increase the yield of usable rotors. Cold spin testing and room temperature MOR strength tests were used to monitor improvements in the processes.

The Analytical Codes continued to be developed and applied through the use of statistical and 3-D finite elements stress computer codes for reliability analysis of ceramic turbine rotors. This analysis was required to effect design changes made as a result of data generated on material strengths. An analytical technique was developed for hypothesis testing which utilizes a computer program to determine, at what level of confidence, are two sets of data from the same or different populations.

The Ceramic Materials and NDE Technology Program, supported by ERDA Division of Conservation Research and Technology, concentrated on determining material properties of ceramics and evaluating new NDE techniques.

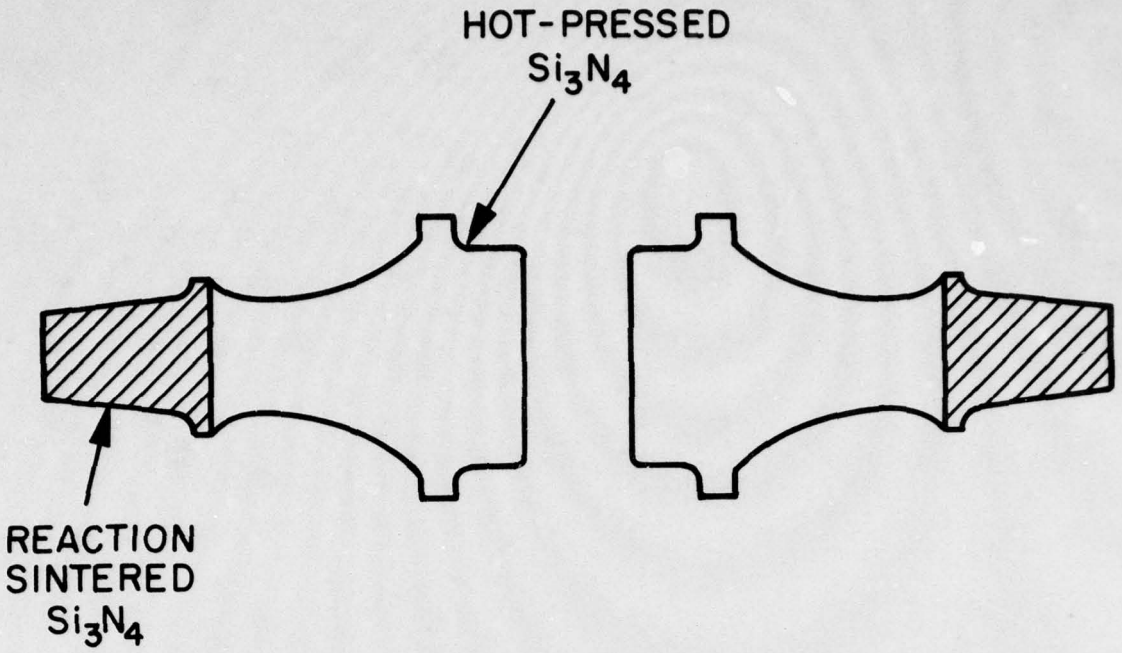

Figure 1.3 — Duo-Density Ceramic Turbine Rotor

The characterization of hot pressed and reaction sintered silicon nitride included determining strength, creep, stress rupture and elastic properties of these materials for design purposes. A study was also initiated on the relationship of material composition and processing variables on the fracture mechanisms, microstructure and strength of these two forms of silicon nitride.

New ceramic NDE techniques were evaluated and applied to duo-density turbine rotors. The primary emphasis was on the reaction sintered silicon nitride rotor blade ring utilizing micro focus x-ray radiography.

2.0 FUTURE PLANS

Work during this reporting period under the DOE (ERDA)-sponsored portion of the program and reported herein focused on development of ceramic materials and process technology used to fabricate duo-density silicon nitride turbine rotors. While significant improvements were made which resulted in an increased yield of duo-density rotors made for testing under the ARPA-sponsored portion of the program, several areas were identified which limited the rotor materials from achieving their strength potential. For example, cold spin testing revealed that blades which failed in the lower-speed range had internal flaws not detected by NDE. Also, it was shown that the bend strength of blades after hot press bonding was lower than before; this material degradation was confirmed by microstructure analyses. These problems form the basis for future plans aimed at improving the duo-density silicon nitride rotor.

In the past, efforts to improve rotor quality have been closely coordinated with the need to fabricate rotors for material and spin testing. During the next reporting period, the need to make rotors for testing will be relaxed and emphasis will be placed on quantifying and resolving rotor material degradation. As a result, fabricated rotors will be cut up to help make flaws more accessible to NDE and blades will be fractured to assess material degradation. The primary objective of this next phase will not be to make rotors, but to define the process for making improved rotors.

Under plans to improve the quality of injection molded rotor blade rings, recently acquired microfocus X-ray equipment will be used to examine separate, cut-off parts of blade rings in an effort to detect the type of internal voids previously revealed in cold spin testing. Parallel efforts in the injection molding process will continue with emphasis on utilization of the Hunkar adaptive process control unit (See 3.1) to maintain a programmed flow rate of mold material into the die cavity during injection.

In the area of hot press bonding, experiments will be conducted to quantify blade strength degradation as a function of hot press bonding conditions and to develop the conditions for minimum blade degradation. Special attention will be paid to the sensing of parameters (particularly temperature) and the control of the hot press bonding process. The objective is to work toward fully automatic control with safety features to facilitate consistent operation without manual monitoring.

During this reporting period, a small effort was initiated to investigate molten glass to replace the graphite wedge system as the restraining mechanism in the hot press bonding process. Although this approach has not proved successful as yet, a small effort will continue under future plans including the evaluation of molten metal as the restraining media.

3.0 CERAMIC ROTOR FABRICATION TECHNOLOGY

Introduction

The duo-density silicon nitride rotor concept utilizes reaction bonded silicon nitride for the complex shaped creep resistant blades and hot pressed silicon nitride for the high strength rotor hub. The blades are formed by injection molding a one piece blade ring consisting of all 36 blades and the blade ring rim. The green preform, made of silicon particles and an organic binder, is subsequently burned out, to remove the binder, and then heated in a nitrogen atmosphere to convert the silicon to silicon nitride. The silicon nitride blade ring, after encapsulation in a blade fill, is placed in a hot press. Silicon nitride powder is then hot pressed to form the hub while simultaneously hot press bonding the hub to the blade ring.

Improvements in both the injection molding and hot press bonding processes were sought in order to improve the quality of duo-density turbine rotors. During the last reporting period several improvements were made to the injection molding process utilizing the automated control system[11]. The hot press bonding process was modified with the introduction of the simplified two piece concept which eliminated previously encountered problems[11]. However further improvements were required as all rotors produced exhibited blade and/or rim cracking induced by hot pressing.

Summary

The injection molding process, utilized to fabricate rotor blade rings, was improved by optimizing the molding parameters with the automated control system. The installation of nozzles to apply mold release and air blast jets, to clean the die and evenly distribute the mold release, resulted in a noticeable improvement in the surface finish of the blade rings.

Significant improvements were made in the hot press bonding process used to fabricate duo-density turbine rotors. Control of the hot pressing load was refined by modifying the hydraulic pressure regulating system. Some initial experiments conducted with a radiation pyrometer coupled to an automatic temperature control unit were successful. The graphite tooling was redesigned to provide more consistent action of the blade ring restraining wedges. The blade filling process was modified to more accurately control the thickness of boron nitride used as a barrier material. These last two changes resulted in the most significant improvement in hot pressing to date as 70% of the rotors fabricated were free of flaws induced by hot pressing.

Two alternate approaches were investigated to produce duo-density turbine rotors. A large graphite ring, which replaced the wedge assembly, failed to provide adequate support to the blade filled blade ring and resulted in cracked blades. Investigations of another concept which used glass to replace the blade fill and wedge assembly indicated a major problem in containing the high pressure molten glass.

3.1 INJECTION MOLDING OF ROTOR BLADE RINGS

As reported in the last report[11], increased yields of improved quality blade rings were obtained after installation of the automatic process control unit. During this reporting period, attempts were made to refine and improve the automatic control to gain further yield and quality improvements.

Further optimization of parameters was made with respect to times and temperatures used in the process. The temperature comparator unit which opens the die inserts at a given component temperature[11] was redesigned for more accuracy. The previous unit was found to be susceptible to false signals due to a high ambient RF noise.

Further automation of the process of blade ring molding was also made. A process of automatically applying a measured amount of mold release in a very uniform manner was developed. A system of four mold release sprayers, four air blast jets, and two electronic timers was installed in the molding system. First, jets of high pressure air cleaned the die cavity. Mold release was then introduced into the cavity area as a cloud of fine mist. Precise timing regulated the amount of mold release used. A second timed blast of high pressure air distributed the mold release in the die cavity. It was found that this system applied a much more uniform application of mold release than previous manual spraying of the die cavity. The improved part yield as reflected in cracks detected in the as molded components is shown in Figure 3.1. The bottom curve represents blade rings having no visible defects, in the as molded state, under 70x microscopic inspection. The top curve represents usuable test blade rings and includes those molded with no cracks or other functional defects and less than two minor surface imperfections. The number of parts refers to the total number of blade rings molded during a particular stage of control development. It should be noted that flaws were detected in some of these components after subsequent processing steps. Improved NDE techniques aimed at detecting these flaws in as molded parts are being investigated.

The overall part quality was also improved as evidenced by increased yields after the burnout inspection and nitrided part inspection. The surface finish of the blade rings was noticealy improved at all stages of processing, following introduction of the automatic mold release system. An added benefit of better surface finish was improved ease of flaw detection during visual inspection.

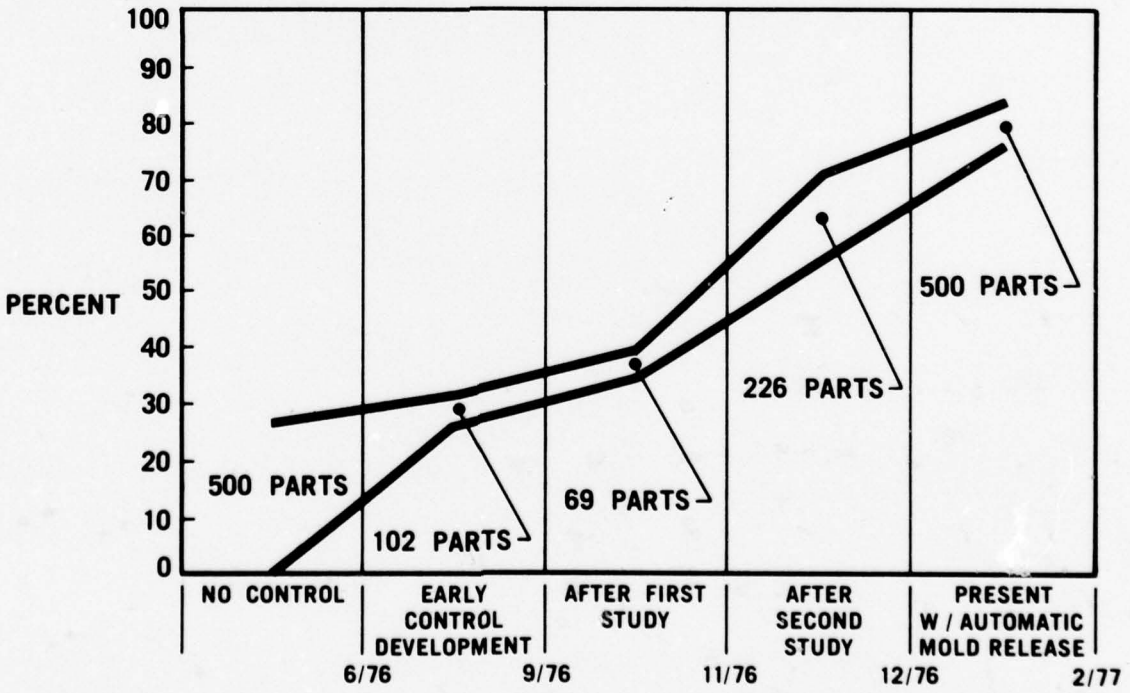

Figure 3.1 — Yield of Good As-molded Blade Rings Versus Process Development

In an effort to further improve quality of molded blade rings, an adaptive process control unit manufactured by Hunkar Laboratories Inc. was installed on the Reed Prentice injection molder. This system interfaces with the Ford automatic control system and controls machine operation from the time the inject command is given until the plunger retract command is received. A solid state logic module controls a hydraulic solenoid valve and through modulation of the valve maintains a programmed flow rate of material into the die cavity during injection. A second module allows holding pressure to be profiled once the material has filled the die. The amount of material prepacked in the barrel for each shot, the remaining cushion after a shot, and the transition point for the transfer from injection profile to hold profile are controlled by a third module. A monitor module gives an output of ram position and velocity as well as cavity and hydraulic pressure. The values of these outputs can be displayed on an osciliscope. This system is now undergoing checkout and debugging.

3.2 HOT PRESS BONDING OF DUO-DENSITY ROTORS

Introduction

The duo-density rotor concept utilizes the high strength of hot-pressed silicon nitride in the hub region where stresses are highest but temperatures are moderate and, therefore, creep resulting from the use of a magnesium densification additive is minimized. The process consists of hot pressing the hub, from silicon nitride powder, while simultaneously hot press bonding the hub to the reaction sintered silicon nitride blade ring. The primary fabrication approach, the simplified two piece design, was introduced in the first quarter of FY 77 and described in some detail in reference 11. Figure 3.2 shows the blade ring encapsulated in slip cast reaction sintered silicon nitride blade fill material which protects the blades from the high temperature/carbonatious atmosphere and supports the blade ring rim during hot pressing. A graphite wedge system was used to apply the radial restraining load to the outer diameter of the encapsulated blade ring. A 1000 pound wedge load was used to counter balance the 1000 psi central pressure which was held for three hours at temperatures of 1700 to 1775°C. The hub was hot pressed from silicon nitride powder with 3½ w/o magnesium oxide added before wet milling with tungsten carbide balls.

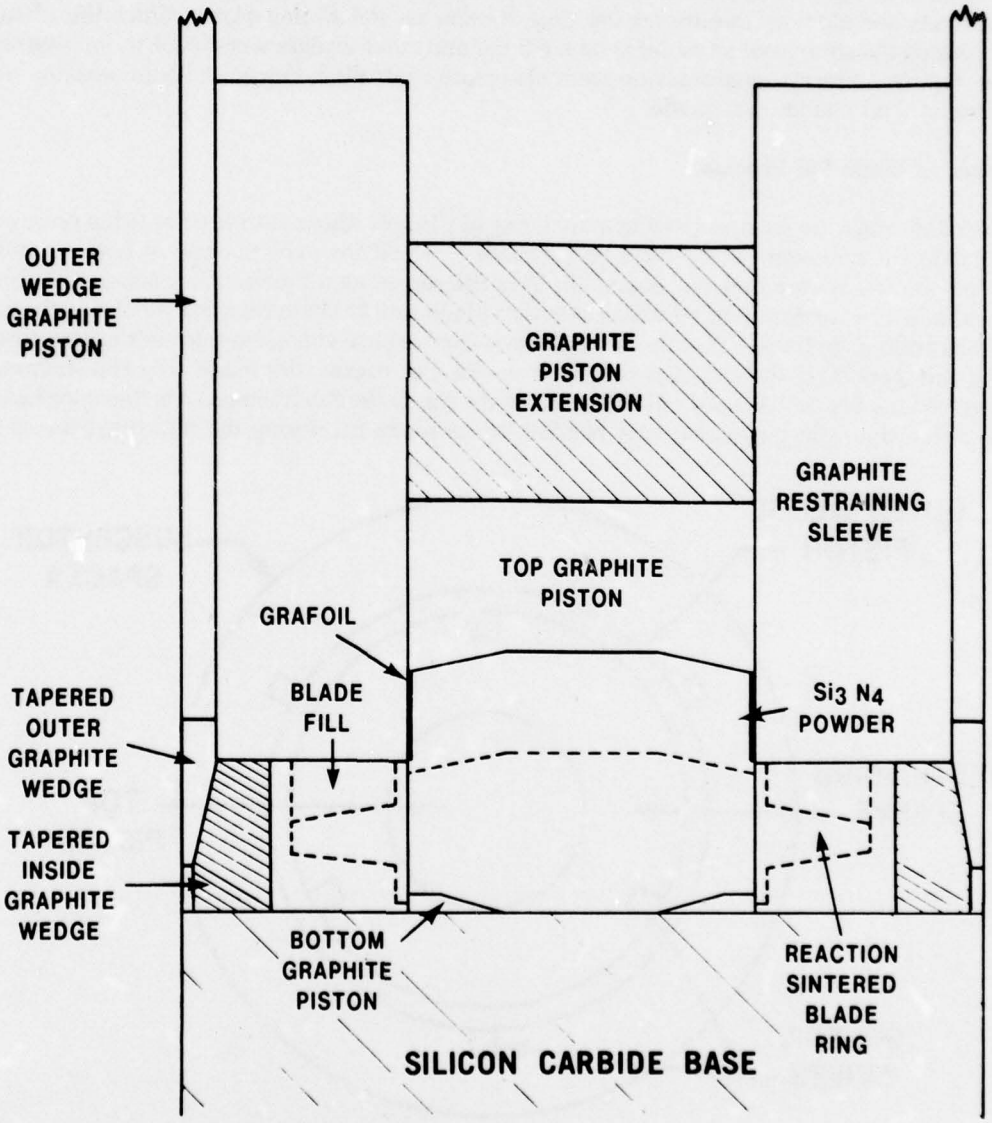

Figure 3.2 — Simplified Two-piece Configuration

The major problem areas with this and earlier concepts were blade cracking and blade ring rim distortion/cracks on an inconsistent basis. Two changes to the process were made which resulted in a major improvement in quality and much more consistent results.

Outer Wedge Load Tooling Modifications

A set of new graphite tooling was carefully cleaned and hand polished and a normal hot pressing made. Inspection of the outer wedge graphite piston and mating graphite restraining sleeve and susceptor spacer, showed evidence of heavy rubbing which occured during the run. This rubbing action must have been due to differential thermal expansion of the concentric graphite cylinders as a clearance existed when the parts were assembled in the cold condition. Such an interference condition reduced the wedge restraining load actually obtained at the wedges due to inconsistent friction drag on the sliding component. The radial clearances between the outer wedge piston and the inner sleeve and outer spacer were increased from 0.0015" to 0.022". In order to center the tooling over the blade filled blade ring six strips of 0.015" thick Grafoil were placed between the outer wedge loading cylinder and the mating cylinders as shown in Figure 3.3. The Grafoil strips were staggered in a circumferential direction to take advantage of the increased radial flexibility of the thin outer wedge loading cylinder when loaded at 3 points. The differential thermal expansion of the tooling then produced much lower radial loads and thereby minimized the drag friction on the sliding piston. Since this change was incorporated the shiny contact patterns on the inner and outer wedges were much more consistent and blade ring rim deformations/cracking were also more controlled. However blade cracking persisted until the second change was made.

Changes in Blade Fill Process

The blade rings are encapsulated in a thick ring of slip cast silicon nitride prior to hot press bonding. This blade fill operation is a multi-step process[10] which involves the use of boron nitride (BN) between the blade ring and the blade fill. The BN serves as a lubricant for subsequent blade fill removal and as a barrier material which prevents blade ring to blade fill bonding during the nitriding step. Controlling the thickness of the BN was the second critical change in rotor fabrication carried out during this period. If the BN was too thick in the rim region, the blade ring rim deformed and compressed the BN until the BN either supported the rim or the rim fractured. On the other hand, if the BN was too thin, the blade ring was bonded to the blade fill during the nitriding process making

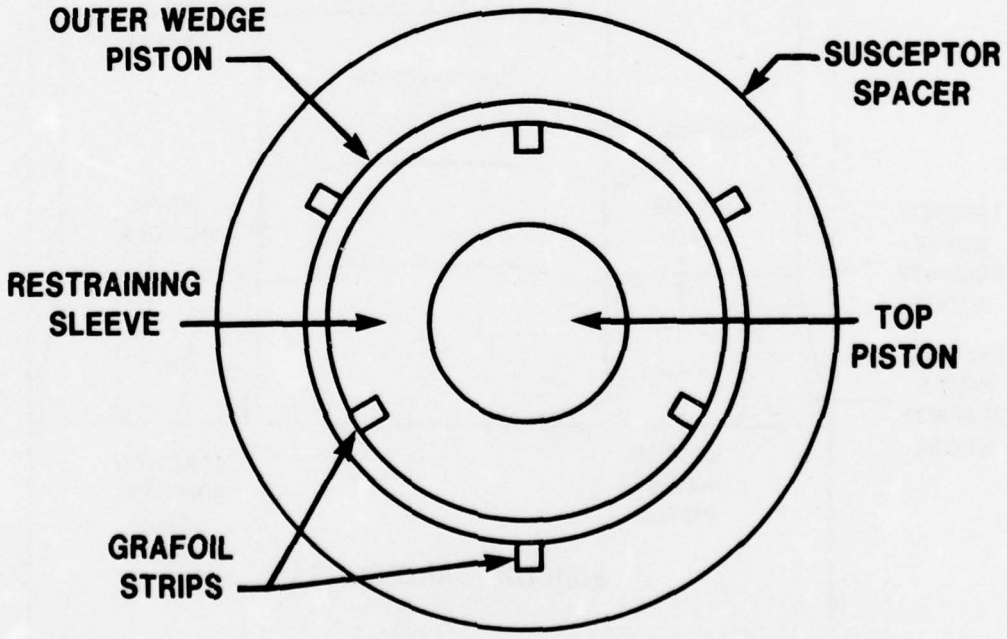

Figure 3.3 — Top View of Graphite Tooling

removal of the blade fill impossible. A thicker coating of BN was desirable on the airfoils so that small motions of the blades were accommodated without resulting in cracking of the blades (Figure 3.4).

Forty-six simplified two piece duo-density turbine rotors were hot pressed with controlled BN thickness and the modified outer wedge loading cylinder design at standard conditions of 1000 psi, 1715°C for 3 hours with 3½ w/o magnesium oxide additive in the silicon nitride powder. As shown in Figure 3.5, 70% (32 out of 46) were free of flaws induced by hot pressing. This represented the most significant improvement in the yield of hot pressings to date.

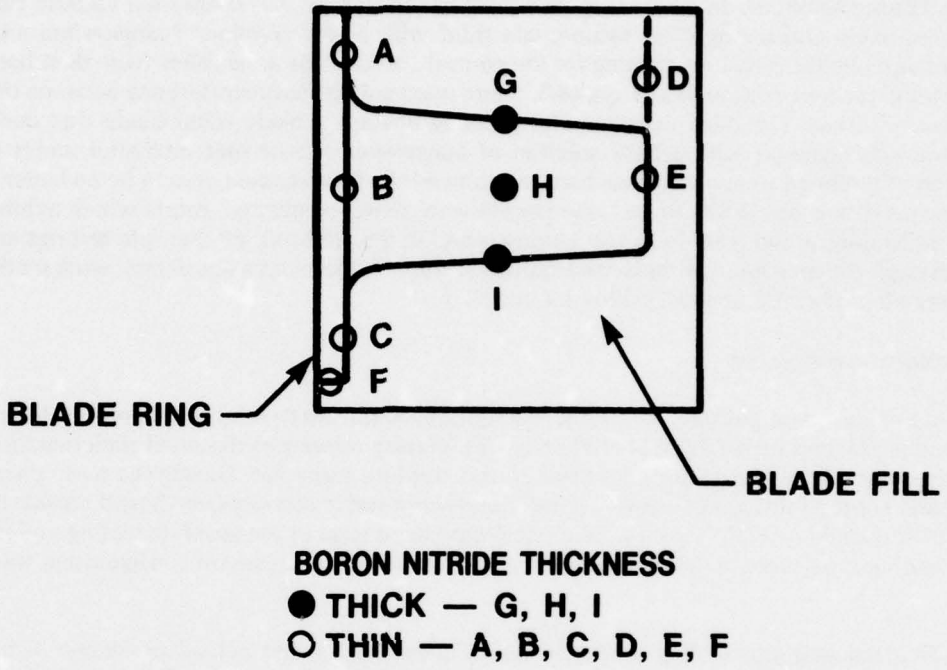

Figure 3.4 — Blade Filled Blade Ring Showing Boron Nitride Layers

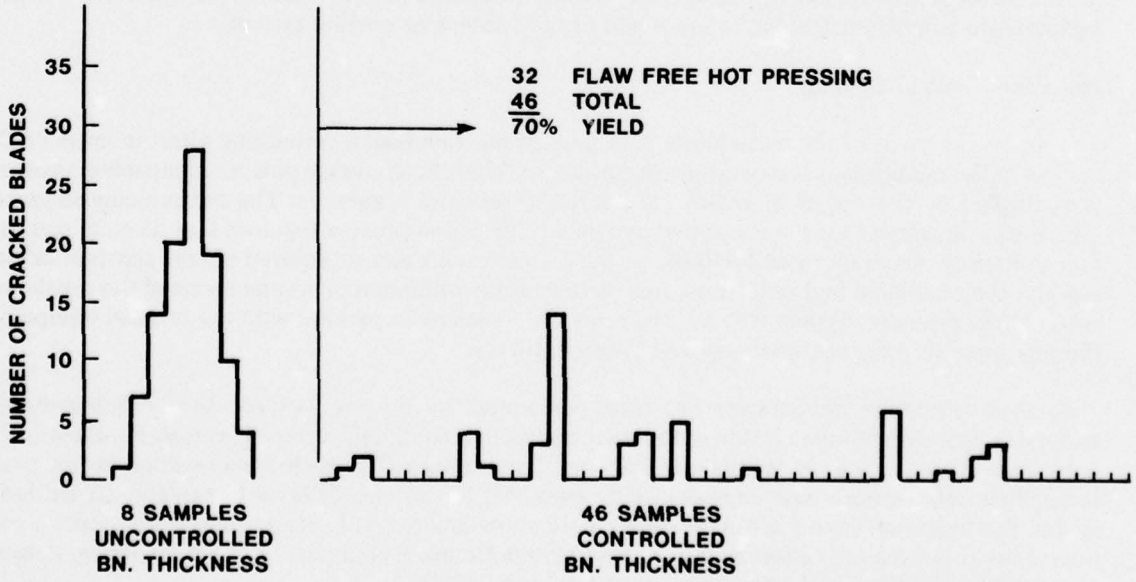

Figure 3.5 — Hot Press Induced Blade Cracks versus Boron Nitride Thickness

Bond Joint

The bond joint between the reaction bonded silicon nitride blade ring and the hot pressed silicon nitride hub is formed during the hot pressing operation. Zyglo inspection of the joint of a rotor fabricated during the development of the process gave a definite indication, initially thought to be a crack. Upon closer examination it was proven to be a low density region in the hot pressed material at the hub/blade ring interface. Three experiments were conducted to eliminate the low density region.

The first two trials involved painting the inner diameter of the blade filled blade ring with magnesium containing solutions. In both cases, one third of the surface was coated with a 50% solution of magnesium oxide and methylethyl ketone, one third with a 50% solution of magnesium nitrate and methanol and one third with no coating for the control section. The assemblies were then hot pressed in the normal process, sectioned and zygloed. There was no discernable difference between the coated and uncoated areas. The third experimental pressing utilized a blade filled blade ring one half on which was impregnated with a 50% solution of magnesium nitrate and methanol under vacuum. Inspection of the bond joint after press bonding showed the impregnated area to be no better than the unimpregnated portion. While these experiments were being conducted, rotors which exhibited low density indications at the bond joint were being tested in the cold spin pit, hot spin test rigs and in the modified engine. Since none of these tests indicated the bond joint was a problem, work on this effort was terminated. (See Volume 1, Tables 3.3 and 3.5)

Temperature Investigation

One of the important parameters for hot pressing silicon nitride powder is the pressing temperature. The induction heated furnace used to hot press duo-density rotors was designed such that the controlling temperature is measured on the outside of the graphite susceptor. During the early phase of the development of the fabrication process experiments were run to correlate inside and outside temperature (1700°C outside — 1775°C inside). Since that time the design of the graphite tooling and the water cooled loading rams were modified, therefore a recalibration of the present configuration was carried out.

The standard graphite tooling was modified *(Figure 3.6)* so that optical pyrometer temperature measurements could be made at both the inside and outside of the furnace. The outside temperature was measured at the normal location while the inside temperature was measured 0.20 inches away from the hot pressed hub. Utilizing this system several hot press runs were made and the inside temperature was observed to be 1715°C while the outside temperature was maintained at the normal level of 1700°C. This system will be used to recheck the correlation of controlling temperature to inside temperature when future changes are made to the furnace or cooling system.

Hot Press Control Systems

The development of the rotor fabrication process has involved a continuing effort to improve the control of the hot pressing temperature and pressure. The silicon nitride powder compaction pressure is controlled by the use of manually set hydraulic pressure regulators. The hot pressing sequence which was developed for the simplified two piece fabrication process required four discrete compaction pressures. Accurate reproducibility of the lower two pressures required almost constant adjustment as the associated hydraulic pressures were near the minimum operating levels of the regulators. New, lower pressure regulators were procured and installed in parallel with the original equipment thereby providing the required sensitivity and accuracy.

Control of furnace temperature has been performed, in the past, by periodically measuring the surface temperature on the outside of the susceptor with a hand held optical pyrometer and manually adjusting furnace power to maintain the desired temperature. This technique resulted in two problems. First, temperature-time reproducibility from run to run was difficult to achieve, particularly during the transition from start-up to steady state operation. Second, steady state temperature variations existed because of differences in optical pyrometer use techniques between operators. A three phase effort to automate the temperature control was initiated.

Phase one of the effort involved the use of available instrumentation and control components to define the automatic control requirements and demonstrate steady state control following a manual start. Phase two will extend the control capability to include the start transient and steady state control with automatic compensation for furnace power variations to provide a constant temperature. Phase three will provide fully automatic control with safety features to allow operation without manual monitoring.

To date, phase one of the effort has been completed. A fixed position radiation pyrometer was installed and a series of tests conducted to correlate with the hand-held optical pyrometer. Additional tests were conducted to calibrate the control elements and identify the control hardware needed to proceed with phase two.

Two successful steady state automatic control attempts were made; the longest for 2:30 hours of the normal 4:00 hours hot press run.

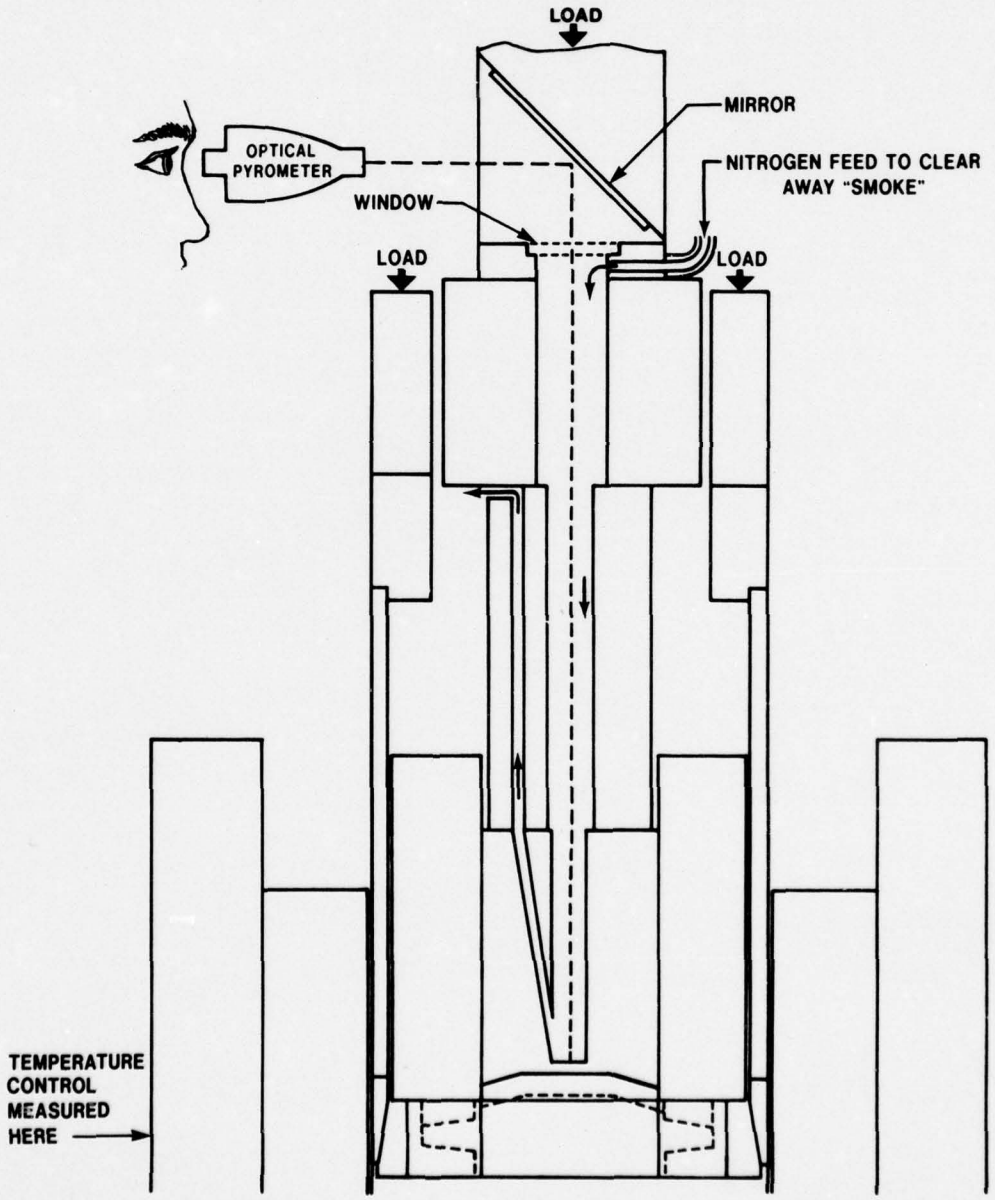

Figure 3.6 — Modification of Graphite Tooling for Inside Temperature Measurement

3.3 ALTERNATE ROTOR FABRICATION CONCEPTS

An alternate approach investigated to produce duo-density turbine rotors eliminated the graphite wedge system and attempted to supply the radial restraining load to the blade fill via a large graphite ring (Figure 3.7). Two fabrication trials were made using this concept. Both rotors exhibited large radial deformations of the blade ring rim indicating plastic flow of the reaction bonded silicon nitride in excess of 4%. Severe blade cracking in the leading edge fillet region was also observed on both rotors. Both of these problems were related to the larger coefficient of expansion of the graphite ring which expanded thermally more than the silicon nitride assembly.

A small effort on another alternate approach to fabricate duo-density rotors was investigated which utilized glass as the restraining mechanism replacing both the graphite wedge system and the silicon nitride blade fill. Graphite tooling, shown in Figure 3.8, was designed and procured. A boron nitride coated blade ring was placed in the bottom of a graphite bucket and soda lime glass powder and plates installed as shown. The furnace temperature was raised, melting the glass, and then pressure was applied to the piston. However, the soda lime glass was so fluid at 1715°C that it permeated the silicon nitride powder and escaped through the clearance between the piston and the bucket. The combination of glass bonding the piston in place and silicon carbide formation between the hot pressed silicon nitride and the bucket sides prevented retraction of the piston.

The bucket was redesigned to incorporate a sleeve of graphite which would slide out with the piston at the end of the run when the piston was retracted and the soda lime glass was replaced by Vycor. However, the Vycor glass still permeated the silicon nitride powder and resulted in severe damage to the blade ring (Figure 3.9).

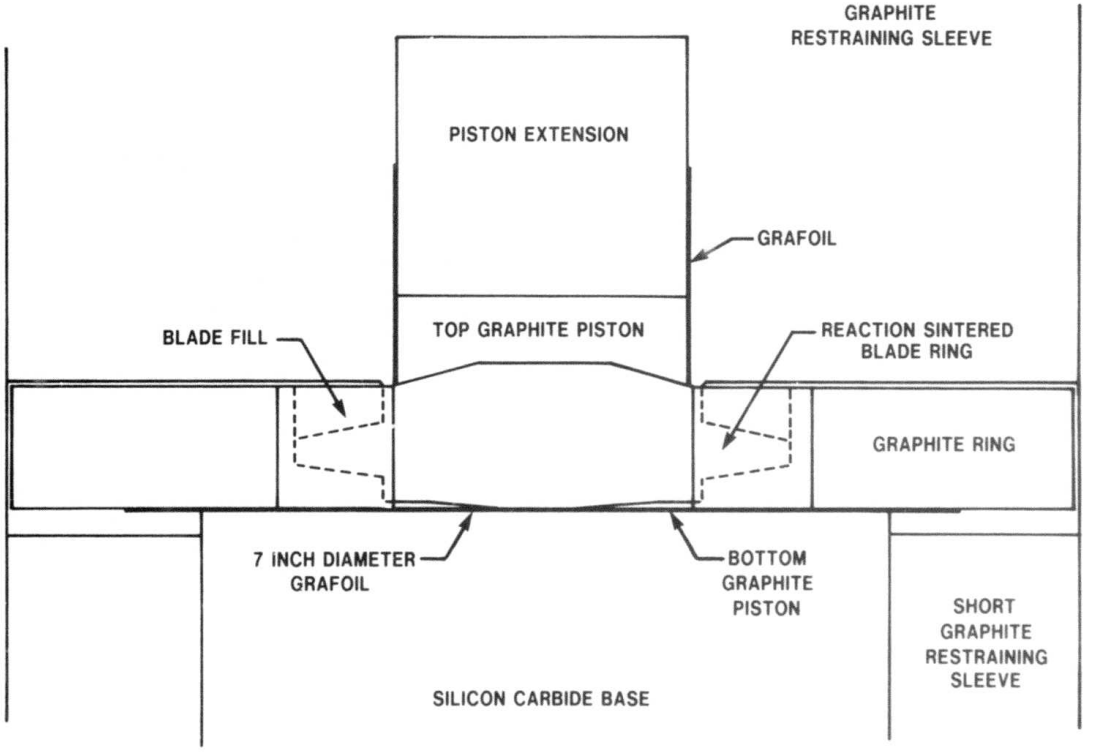

Figure 3.7 — Graphite Wedges Replaced by Ring

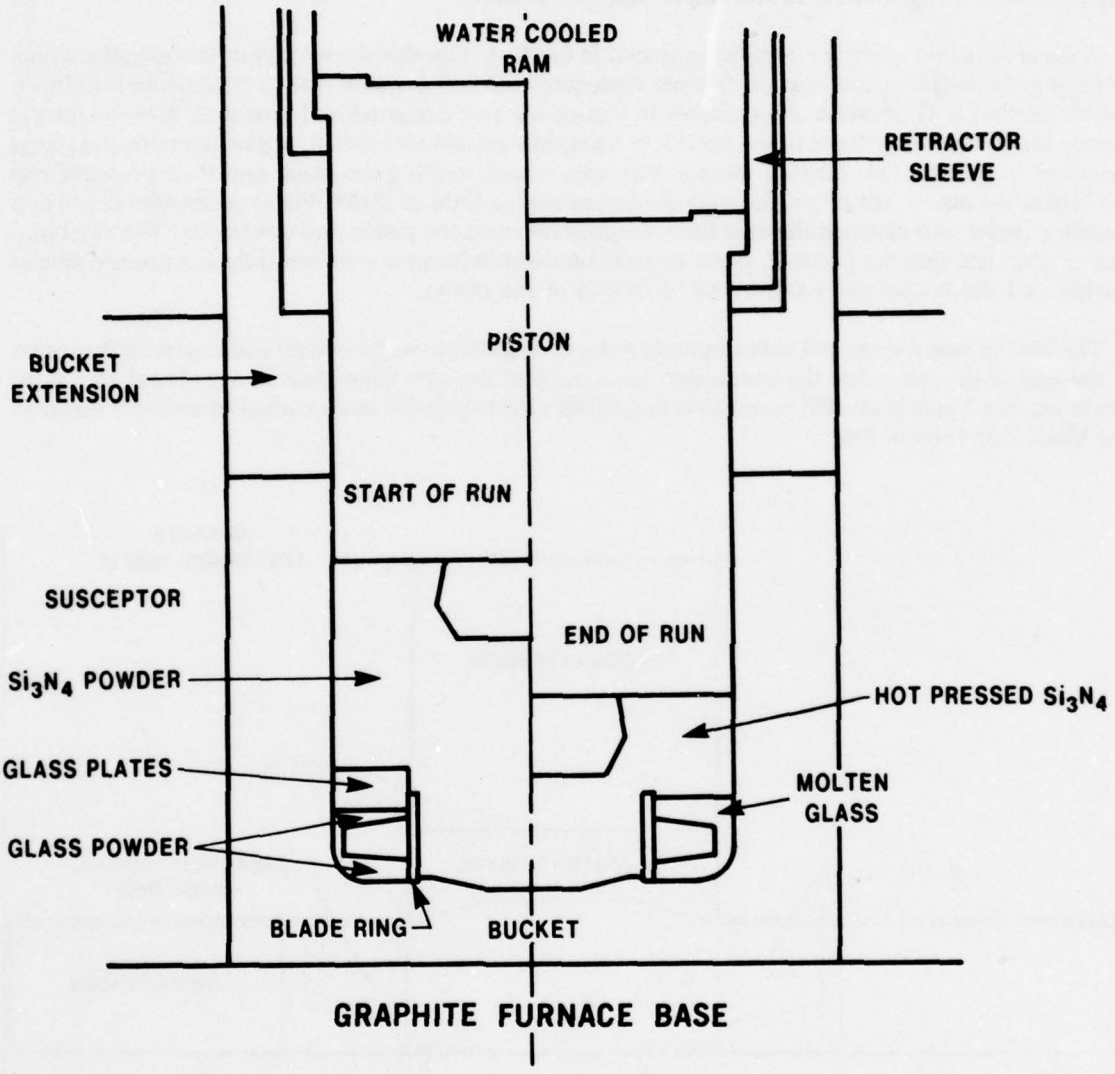

Figure 3.8 — Glass Restraining Concept

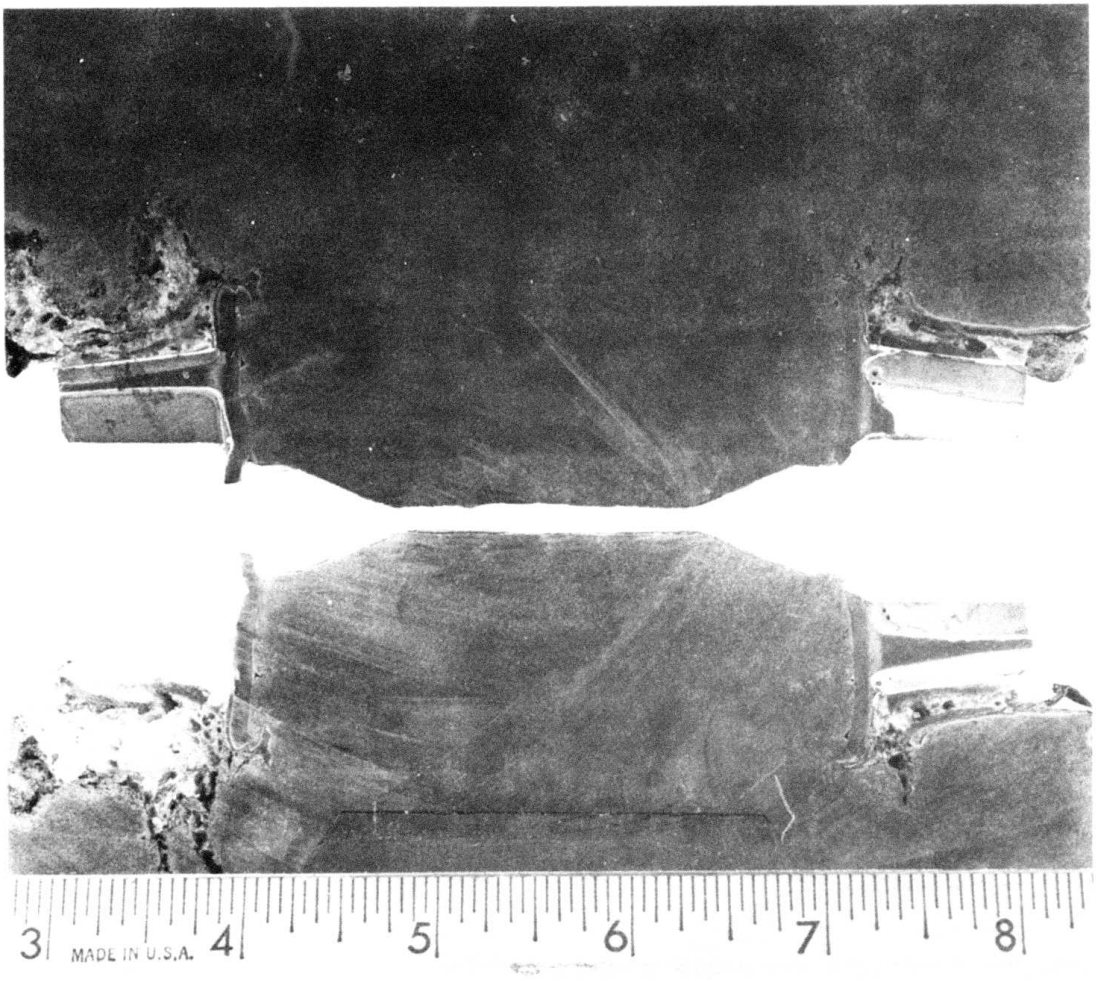

Figure 3.9 — Results of Second Glass Experimental Run

4.0 CERAMIC MATERIALS INVESTIGATIONS

Introduction

The development of ceramic material technology for reaction bonded and hot pressed silicon nitride has been an ongoing activity since the beginning of the Ford/DARPA program, and continued under the ERDA sponsored portion of the FORD/DARPA/ERDA Program. This technology is a very important portion of the systems approach employed in this project for the development of high temperature gas turbine engines. Improvements in materials have been made and characterized so that components could be designed, fabricated and evaluated.

The strength of injection molded reaction bonded silicon nitride was improved by combining the 96% nitrogen/4% hydrogen atmosphere with the nitriding demand temperature control system previously developed [10, 11]. However more work was needed to reduce the scatter in material strength due to both macroscopic and microscopic flaws.

The results of a parametric study on hot pressing parameters consistent with the hub forming process used to make duo-density rotors was presented in the last report [11]. The best material, from this study, was used during this reporting period, to investigate the effects of hot pressing temperature, time and pressure on material quality. In addition some preliminary work was initiated to improve the high temperature strength of hot pressed silicon nitride.

Summary

The starting silicon powder, used to injection mold rotor blade rings, was found to contain contaminates in the form of iron and chromium. Microstructural examination of both test bars and rotor blades indicated a definite linear correlation between strength and the size of microscopic flaws due to contamination. Magnetic separator equipment was ordered and received so that all starting silicon powder can be cleaned in-house.

The mixing of silicon powder and organics, prior to injection molding, was improved with the addition of vacuum capability to the equipment. This, combined with better temperature control during mixing, produced a more homogeneous mix which should result in fewer macroscopic flaws in molded components.

Twenty-two hot pressed samples were fabricated with systematically varied hot pressing temperature, time and pressure. The optimum hot pressing conditions will be determined when the strength data has been generated. Approximately 30 hot pressings were made with various purity level starting powders and a variety of hot pressing aids. The high temperature strength will be determined to identify the best candidates for further study.

4.1 IMPROVEMENTS IN INJECTION MOLDED REACTION BONDED SILICON NITRIDE

During this reporting period a major effort was made to reduce process variability by instituting improved process controls and further development of the automatic molding control system.

Powder Preparation

As reported in Section 4.2 of this report contamination in the form of iron and chromium was detected in the starting silicon powder. This contamination was high enough to produce local strength degradation in the nitrided components. Following evaluation of a magnetic separator to remove iron-chromium contaminates from the starting silicon powder, equipment was ordered so that all starting silicon powder can be screened in-house.

Mixing

Once the starting powder has been cleaned and ball milled to the desired particle size distribution[9], it must be homogeneously mixed with an organic binder so that the resulting mixture can be injection molded to form the green rotor blade ring. In addition to formalizing the mixing procedure, for batches of ceramic molding material, vacuum mixing capability was incorporated into the equipment. The vacuum capability reduces entrapped gas within the granules of molding mix and subsequently reduces the tendency for voids in the molded components.

It was determined that the temperature during mixing effected the homogeneity of the mixture. The viscosity of the molding mix varied widely with temperature and if it was too high or too low a homogeneous mix would not be produced. A readout system was installed on the mixer to monitor the temperature thus insuring that correct temperature was maintained and was repeated from batch to batch.

Molding

Further automation of the injection molding process was found to be necessary in order to improve the consistency of molded components and to reduce the reject rate of green parts. The improvements incorporated into the injection molding system were discussed in section 3.1 of this report.

Burnout

The green injection molded component must be burned out to remove the organic binders, so that the resulting compact of silicon metal particles can be nitrided to form silicon nitride. The green component is buried in charcoal granules [8] and subjected to a specific time/temperature schedule. Monitoring of the burnout process was improved to allow better correlation of burnout results with the actual temperature profile achieved for each batch of components. A two channel recorder was installed to monitor two thermocouples placed near the components within the burnout furnace.

4.2 MICROSTRUCTURE OF INJECTION MOLDED SILICON NITRIDE

Introduction

The previous report [11] described the nitrogen demand nitriding cycle utilized for nitriding injection molded preforms of silicon particles. This cycle controlled the furnace temperature/time schedule automatically to maintain a reasonably steady consumption of nitrogen. This nitriding technique had produced silicon nitride having a very uniform microstructure (uniform fine porosity and fine grain size) and it was concluded that this structure should yield a high strength material [11].

The strength of silicon nitride produced using the nitrogen demand cycle is shown in Table 4.1 (test bars) and Table 4.2 (rotor blades). The variability in strength and density is partially due to molding flaws present in the center of test bars (Figure 4.1). This section describes the fractographic examinations conducted on Ford injection molded reaction bonded silicon nitride to determine the underlying cause for the observed strength variations.

Procedure

Examination of fracture surfaces of both test bars and rotor blades revealed two distinct types of flaws. Some were large macroscopic flaws, resulting from either molding defects or green cracks, which were highlighted by the presence of white alpha silicon nitride whiskers produced during the nitriding cycle (Figure 4.2). Test samples that contained this type of flaw were not included in this investigation. The other types of flaws observed were microscopic in nature and these were investigated in detail.

TABLE 4.1

Strength of RBSN Test Bars Nitrided Using the Nitrogen Demand Nitriding Cycle

Run Number	Measured Density g/cc	Characteristic Strength* Ksi	Weibull Slope	Number of Samples
B55	2.67	49.6	10.5	7
B64	2.62	40.7	9.6	10
B71	2.55	43.4	9.6	7
B75	2.62	40.4	9.0	9
B76	2.62	41.1	13.5	8
B79**	2.69	37.6	9.2	10
B82**	—	38.6	7.5	8

* Four Point MOR — as nitrided surfaces — Strength at 63.2% failure rate
** Furnace shutdown in middle of run

TABLE 4.2

Strength of RBSN Rotor Blades Nitrided Using the Nitrogen Demand Nitriding Cycle

Run Number	Measured Density g/cc	Characteristic Bending Load pounds
B-54	—	107
B-65	2.63	83
B-67	2.71	86
B-70	2.68	88
B-75	2.74	79

The fracture surfaces of test bars from nitrogen demand nitridings and rotor blades from both nitrogen demand and temperature controlled [11] nitridings were examined using Scanning Electron Microscopy. The fracture origins were identified and characterized. If the origin proved to be crystalline in nature, its chemistry was determined using non-dispersive x-ray analysis.

The fracture origins on most samples were easily identified by the presence of fracture mirrors. These mirrors were large on low strength samples and small on higher strength specimens. In the center of these fracture mirrors, the fracture origin was usually identified, under low magnification, as either a dimple or a depression. The fracture origin on very low strength samples, having no readily discernible fracture mirrors, was identified by the dimple or depression.

Results

The identified critical flaws were classified as either a pore or an inclusion. The pores were mostly of the type shown in Figure 4.3, exhibiting a different chemistry than the adjoining matrix indicating they were formed by the pullout of an inclusion. Two distinct types of inclusions were identified. One was very crystalline in nature (Figure 4.4) while the other type contained a structure only slightly different than the adjacent matrix (Figure 4.5).

The flaws in the test bars (Table 4.3) ranged from 39 to 177 microns in diameter and were located, in most cases, below the surface (10 to 125 microns). The pores were of the type previously shown in Figure 4.3 while the inclusions were equally divided between the two types previously shown. The chemistry of the measured inclusions was high in chromium, iron and silicon. Figure 4.6, constructed from the data in Table 4.3, indicated a reasonable correlation existed between flaw size and test bar MOR. Also shown in this figure is the relationship developed by Kinsman using pre-cracked HS130 [6] which is in the same region as the data recently generated.

The flaws in rotor blades (Table 4.4) ranged from 35 to 138 microns in diameter and were located, in most cases, below the surface (25 to 250 microns). Chemistry and types of flaws were generally the same as for test bars. Figure 4.7, constructed from the data in Table 4.4, again showed a correlation between flaw size and blade bending load.

An investigation into the source of the chromium and iron contamination revealed that the starting silicon powder contained 0.04 w/o chromium and 0.87 w/o iron (Table 4.5). Approximately 0.25 w/o of the iron was metallic (from the initial ball milling operation by the vendor) while the remainder was iron silicide probably formed during the reduction process used in producing the silicon. The chromium impurity was also in the form of a silicide. The increase in iron, from 0.87 to 1.71 w/o after nitriding, was due to the addition of iron oxide which was used as a nitriding aid. The increase in chromim contamination was probably due to in house powder processing performed in stainless steel equipment.

Discussion

The general pore size of Ford reaction bonded silicon nitride is quite uniform and fine (Figure 4.8) with the maximum pores being about 30 microns. The larger pores identified in this study could be the result of nitriding exotherms, molding flaws or pullout from inclusions.

The type of pores resulting from a nitriding exotherm (Figure 4.9) were found to be small, less than 40 microns [11], and were not typical of those considered in this investigation but were addressed previously [10, 11]. Pores resulting from molding flaws (shown in Figure 4.1) were much larger, in the order of 75 to 150 microns, and were discussed in Section 4.1. Inclusions and large pores, due to pullout of inclusions, were shown to reduce the strength of reaction bonded silicon nitride as a function of their size. Reducing the contamination, in both the starting silicon powder and during in house processing, should result in a higher, more consistent strength material.

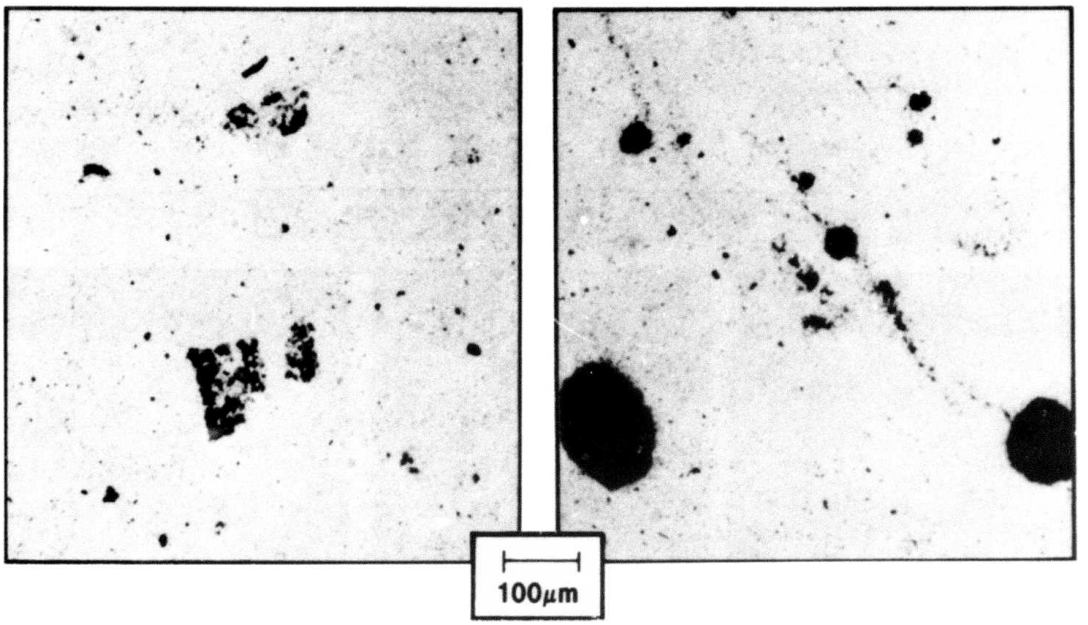

Figure 4.1 — Typical Molding Flaws in Injection Molded Test Bars

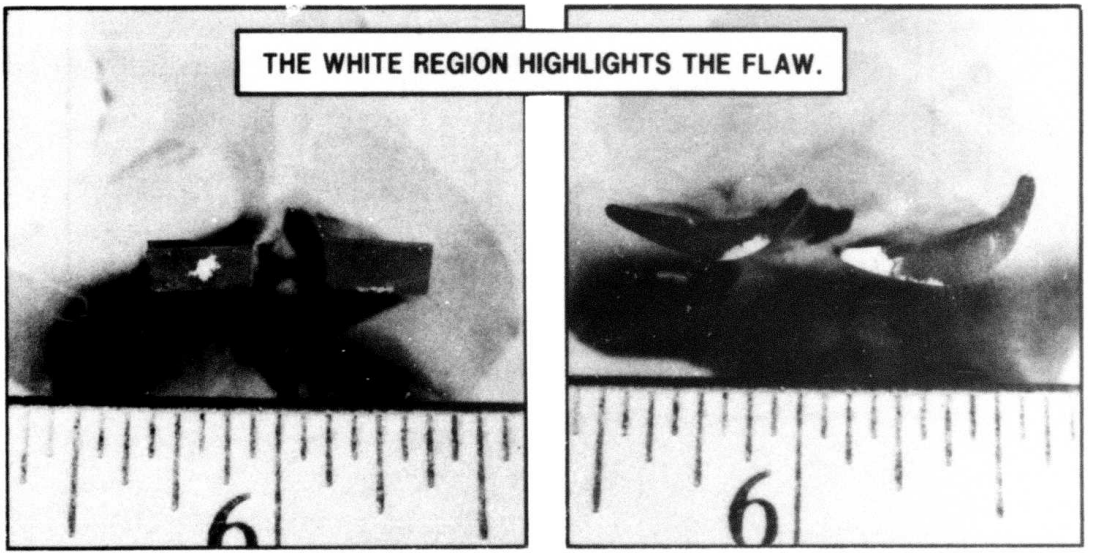

Figure 4.2 — Macroscopic Flaws in Test Bars and Rotor Blades

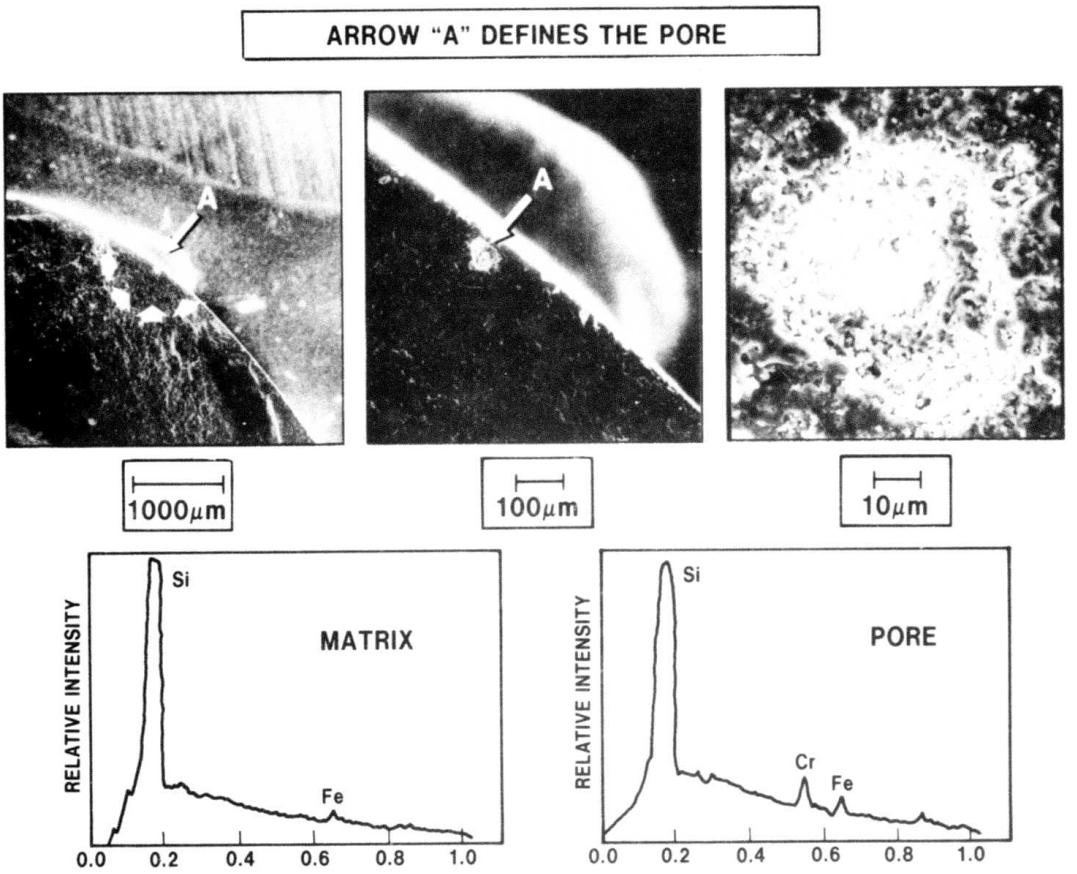

Figure 4.3 — Analysis of Pore from Rotor Blade 1773 #30

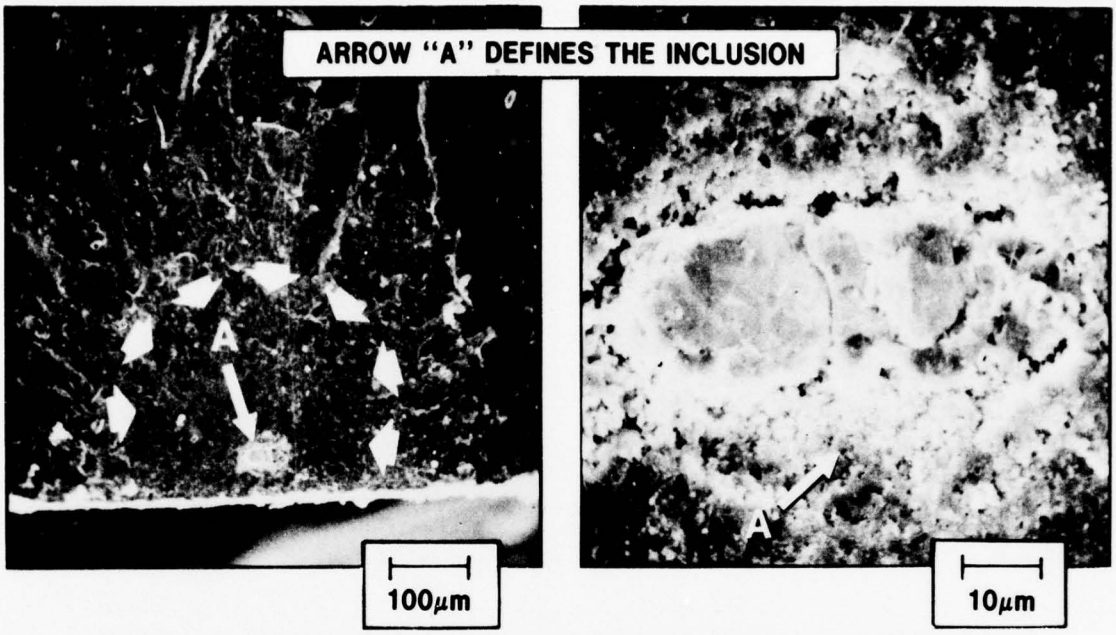

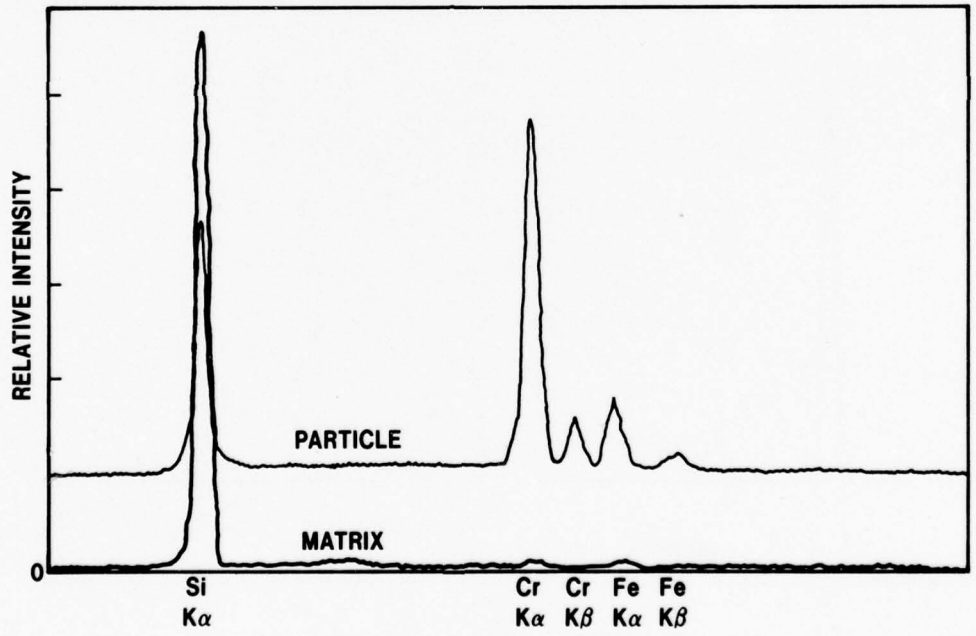

Figure 4.4 — Analysis of Inclusion from Sample B55 #6

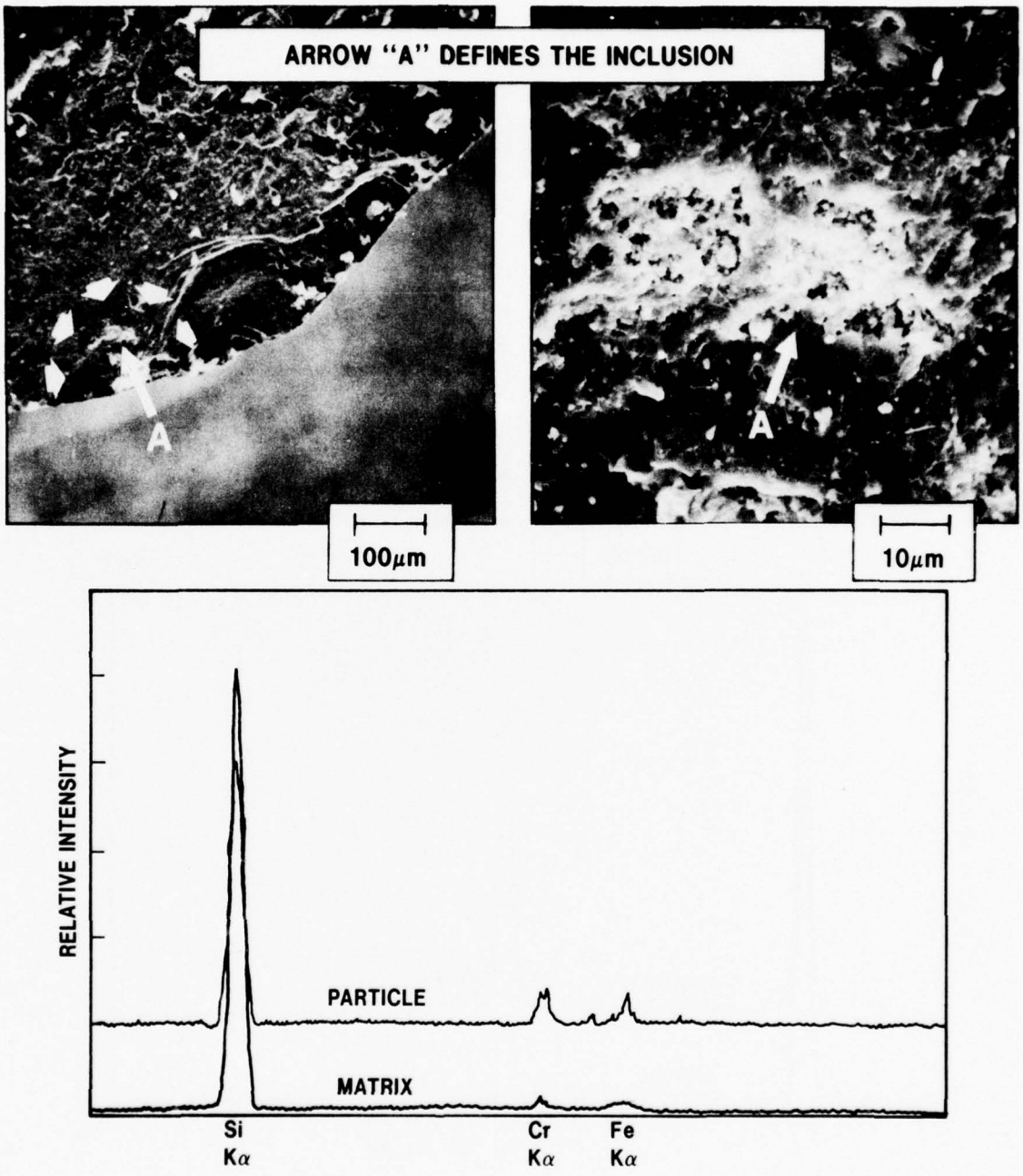

Figure 4.5 — Analysis of Inclusion from Sample B64 #18

TABLE 4.3

Characterization of Flaws from Test Bars

Test Bar Number	Nitriding Number	MOR Ksi	Flaw Size Microns	Flaw Type	Location Microns from Surface	Chemical Composition
1	B55	38.1	76	Inclusion	100	Cr, Si, Fe
2		46.0	76	Pore	50	—
7		52.5	39	Pore	15	—
9	B64	36.7	150	LO Density Area	125	—
18		43.9	47	Inclusion	100	Cr, Si, Fe,
19		41.7	72	Inclusion	100	—
22		37.4	92	Inclusion	100	Cr, Si, Fe
1	B75	35.2	177	Pore	60	—
2		39.6	101	Pore	20	—
3		43.9	101	Pore	20	—
6		33.1	117	Pore	At Surface	—
8		42.8	88	Pore	At Surface	—
9		42.4	53	Pore	10	—

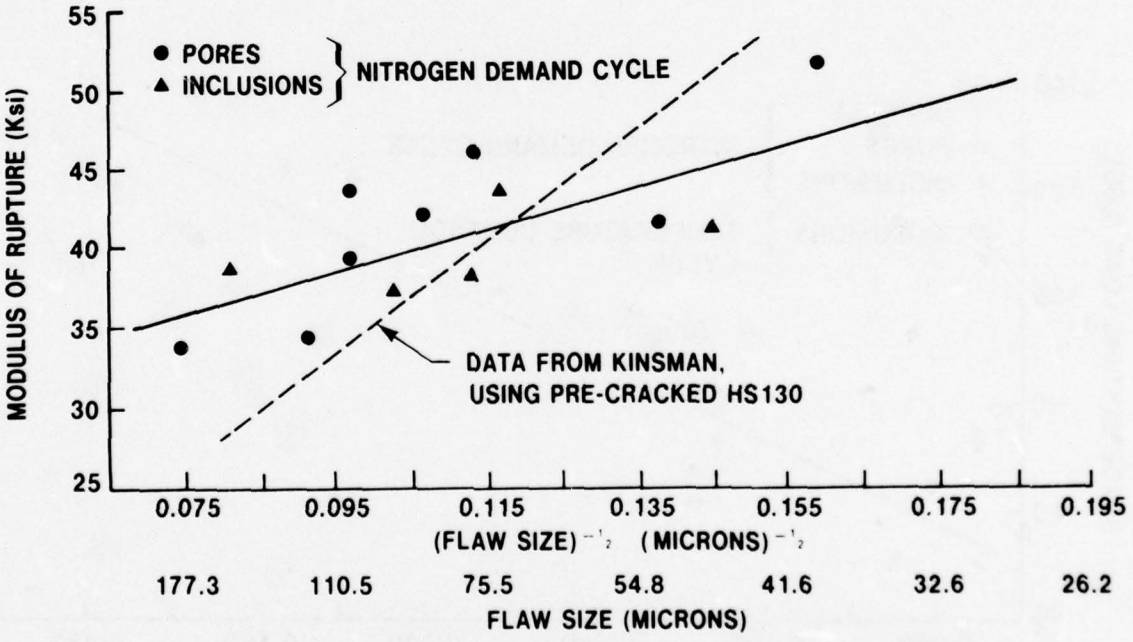

Figure 4.6 — Test Bar MOR versus Flaw Size

TABLE 4.4

Characterization of Flaws from Rotor Blade Rings Tested in Blade Bend Test

Blade Ring & Blade Number	Nitriding Number	Blade Bending Load pounds	Flaws Size Microns	Flaw Type	Location Microns from Surface	Chemical Composition
1737 — 21	B54	110	35	Pore	180	—
11		122	45	Inclusion	65	—
1778 — 19	B56	50.5	138	Inclusion	40	—
23		68.5	88	Surface	At Surface	—
1773 — 17	B56	79.8	88	Inclusion	168	—
30		62	87	Pore	25	Si, Fe, Cr
1386 — 17	B48*	91	76	Inclusion	60	Si, Fe
11		96	75	Inclusion	250	Si, Cr, Fe
9		84	95	Surface	At Surface	—
1410 — 21	B48*	97	67	Inclusion	150	Si, Cr
23		81	89	Inclusion	60	Si, Cr, Fe
19		94	83	Inclusion	170	Cr, Si, Fe
2180 — 4	B75	68	85	Pore	85	Si, TRACE Cr, Fe
9		75	88	Inclusion	63	Si, Cr, Fe
2063 — 12	B70	101	57	Pore	168	Si, Fe, TRACE Cr

* Temperature control cycle

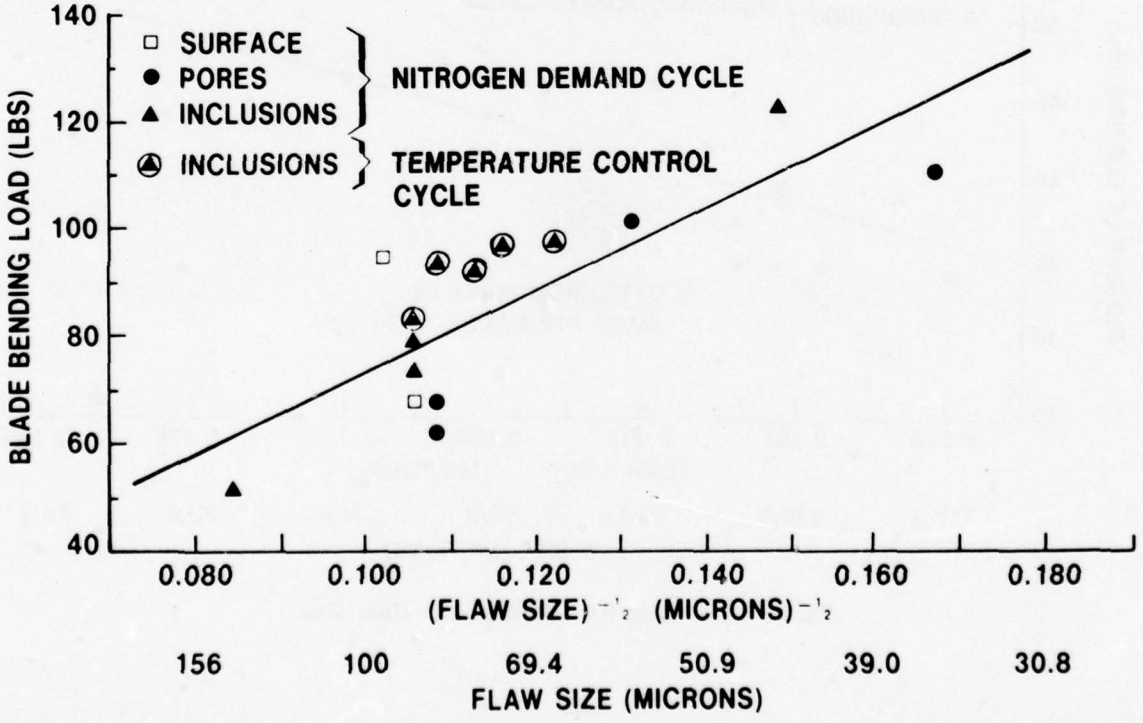

Figure 4.7 — Rotor Blade Bending Load versus Flaw Size

TABLE 4.5

Impurity Analysis of Silicon and Si_3N_4

	Fe*	Cr*
Starting Silicon	0.87	0.04
Final Si_3N_4	1.71	0.06

* Weight percent

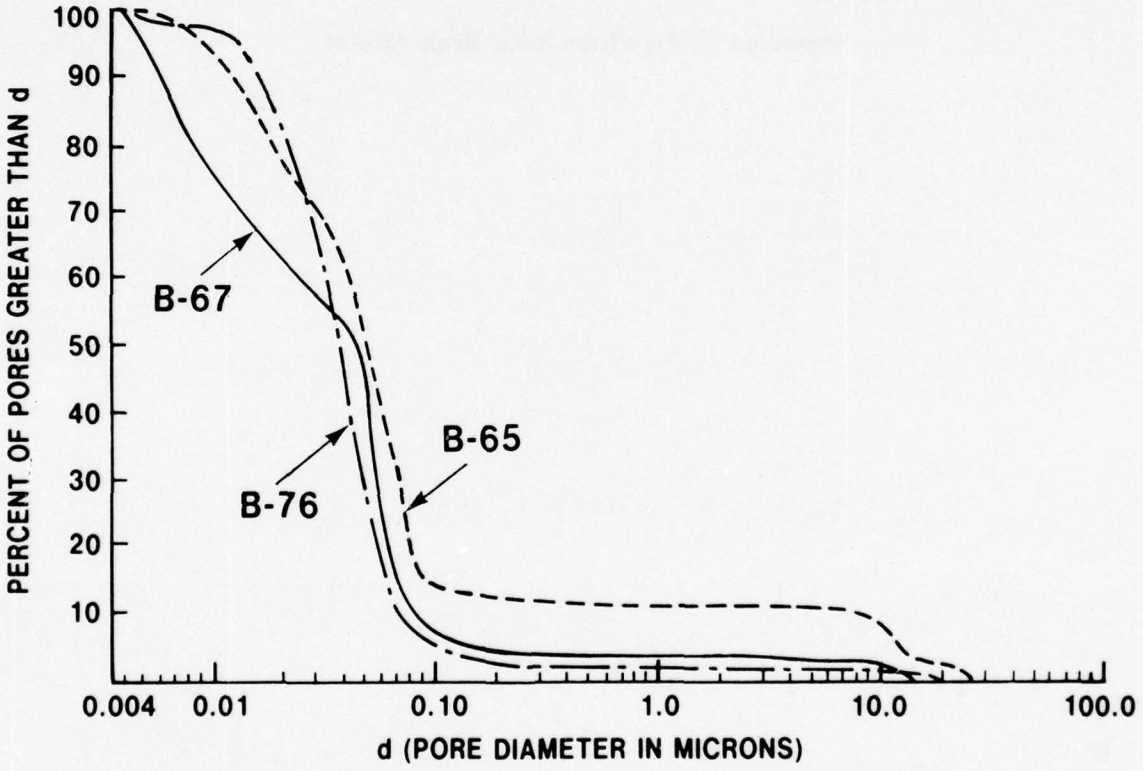

Figure 4.8 — Typical Pore Size Distributions for 2.7g/cc RBSN

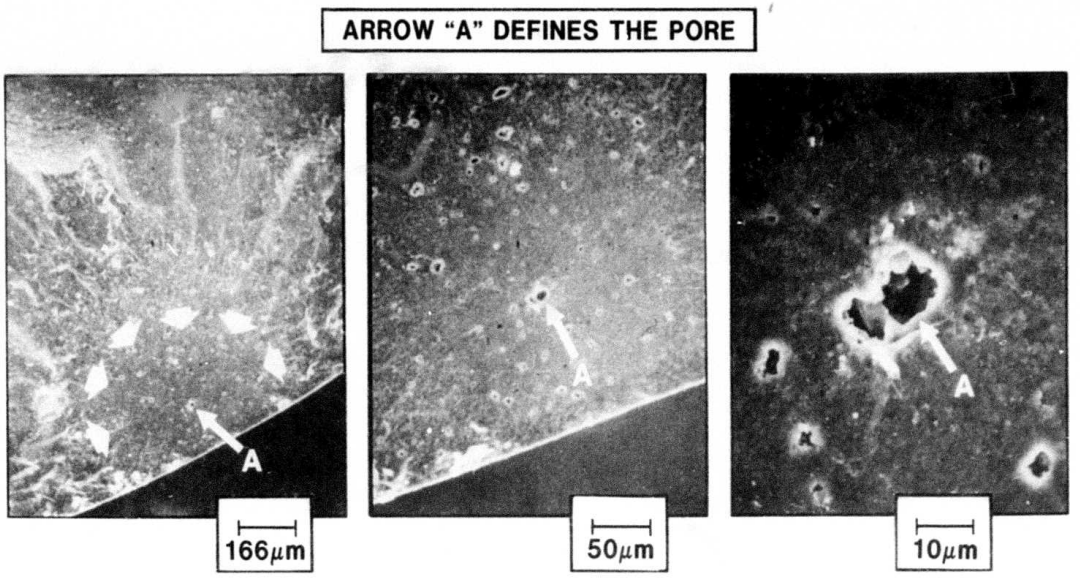

Figure 4.9 — Pore from Rotor Blade 1386 #3

4.3 IMPROVEMENTS IN HOT PRESSED SILICON NITRIDE

Introduction

The last interim report [11] presented the results of a parametric study on hot pressed silicon nitride which included such variables as starting powders (CP-85,KBI), MgO content (2-7w/o), powder milling (wet, dry, WC, $A1_2O_3$,24-72hours) and pressing pressure (500-5000 psi). The best material was produced by WC milling and contained 5w/o MgO densification additive. This study was continued during this reporting period by fixing the powder processing and varying the hot pressing conditions. An additional investigation was initiated to improve the high temperature strength by applying grain boundry engineering strategies.

Hot Pressing Parameter Study

Preliminary investigations were initiated to study the effect of the hot pressing temperature, time and pressure on the material quality. Controlled phase AME silicon nitride powder (CP-85) with 5 w/o magnesium oxide densification additive was processed per the following fixed procedure.

The silicon nitride powder and additive was wet milled with tungsten carbide cylinders in reagent grade absolute methanol. The powders were milled until the average particle size (by weight) was approximately 1.3 microns, dried and then dry ball milled to break up large agglomerates. The powders were then passed through a two tier screening apparatus with the bottom screen being 100 mesh.

Two hundred and twenty-five grams of the screened powder was poured into a cylindrical graphite die where the piston and base had been previously coated with boron nitride. Experimental hot pressings were then made under various fabrication conditions. The ranges of hot pressing parameters investigated were: temperature (1500-1750°C), pressure (1000 to 5000 psi) and time (1 to 7 hours). Twenty-two hot pressed samples were fabricated and are in the process of being diamond ground into appropriate test specimens, for strength evaluation.

Grain Boundary Engineering of Hot Pressed Silicon Nitride[12]

Preliminary investigatory work was initiated to improve the high temperature strength of hot pressed silicon nitride by applying grain boundary engineering strategies. The approach is two fold.

1. Reduce the residual impurity content in the starting silicon nitride powder to make the grain boundary $MgSiO_3$ glass more refractory.

2. Develop a densification aid to yield a more refractory glass than $MgSiO_3$ or $MgSi(O,N)_3$.

The first approach was to investigate a variety of commercial grade silicon nitride powders having varying purity levels. Six powders were obtained, five containing high alpha fractions and one which was almost 100% amorphous. Two and five weight percent magnesium oxide was used as the densification additive.

The second approach was to investigate oxide pressing aids other than magnesium oxide such as: yttria stabilized zirconia (zyttrite), yttria, and cerium oxide. Table 4.6 shows the chemistry of the starting silicon nitride powders and of the oxide hot pressing aids. The powders were ball milled and loaded into the graphite dies per the procedure used in the hot pressing parameter study. The die assembly was placed into the hot press where the powder was cold pre-compacted to 500 psi and then quickly heated (within 50 minutes) to 1500°C (pyrometer reading on the pressing cavity die wall) in a nitrogen atmosphere. The pressure was increased to 2000 psi when the temperature reached 1500°C. At 1600°C the pressure was increased to 4500 psi and then at 1650°C the pressure was raised to a final load of 5000 psi. The temperature was further raised to 1700°C and then maintained for three hours. The ram movement was measured with a dial indicator and compaction curves were constructed for each run. Approximately thirty hot pressed pucks have been made. The pucks were cleaned by sand blasting and the densities measured using Archimedes' principle. All pucks are in the process of being diamond ground into standard "A" size test bars for strength evaluation.

TABLE 4.6
Chemistry of Commercial Grade Silicon Nitride Powder and Hot Pressing Additives

	AME CP-85B	AME Hi-Purity	Starck	Annawerk	Sylvania SN 402	Sylvania SN 502	Zyttrite (Δ)	Cerium Oxide (CeO_2)	Yttria (Y_2O_3)	Magnesium Oxide (MgO)
α-Si_3N_4*	84.7	~70	93.4	~80	0.5-1	~90				
β-Si_3N_4*	14.3	~30	6.6	~20	Amorphous	~10				
Si_2N_2O*	0.7	0.5-1	<0.5	0.5-1	0	0				
Si(free)*	0.3	0.5-1	0	0.5-1	0	<0.5				
O_2*	1.44	1.89	1.10	2.15	2.61	1.64				
SiO_2*	0	0	<0.5	0	0	0				
Fe**	0.88	0.35	0.02	1.40	<0.01	0.04	0.05	0.01	0.01	0.05
Al**	0.63	0.17	0.05	0.15	0.01	0.01	0.02	0.01	<0.01	0.01
Mg**	0.01	0.01	0.02	0.10	<0.01	<0.01	<0.01	<0.01	<0.01	Base
Ca**	0.20	0.01	0.05	0.20	<0.01	<0.01	0.10	<0.01	<0.01	0.10
Ni**	0.03	<0.01	<0.01	0.02	<0.01	<0.01	<0.01	<0.01	<0.01	<0.01
Cr**	0.01	<0.01	0.02	0.01	<0.01	<0.01	0.01	<0.01	<0.01	<0.01
Ti**	0.08	0.05	0.02	0.05	<0.005	<0.005	0.05	<0.005	<0.005	<0.005
B**	0.0005	0.0005	<0.002	0.008	<0.0002	<0.0002	0.0005	0.01	<0.0002	0.05
Si**			Base				0.30	<0.01	0.03	0.10

*By X-ray Analysis — weight percent
**by Emission Spectrographic Analysis — weight percent
Δ — 12% w/o Y_2O_3 stabilized ZrO_2

4.4 THERMAL EXPANSION OF HOT PRESSED SILICON NITRIDE

Thermal expansion was measured from room temperature to 900°C (1652°F) using a differential expansion technique in which the dimensional changes were compared to those of a calibrated fused SiO_2 sample. One-inch specimens were tested, with flat and parallel ends, ground to a length of 1.000 ± 0.0005". They were supported in a fused SiO_2 tube, and the length changes were transmitted through fused SiO_2 push rods. The rod bearing against the reference sample was mounted on the frame, and that bearing on the test specimen was attached to the movable core of a Theta linear variable differential transformer. The core motion relative to the frame is directly proportional to the difference in expansion of the test sample and the reference sample, and the electrical signal produced is amplified and recorded to provide the expansion data.

Comparative thermal expansion measurements were made on twenty-two samples of hot pressed silicon nitride to evaluate the effects of MgO content, powder milling conditions, powder source, and hot pressing pressures.

The ranges of variables investigated are shown below:

Weight % MgO	1, 2, 3½, 5, or 7
Milling Balls:	WC or Al_2O_3
Milling Fluid:	Methanol or none
Milling Time:	48, 72, or 144 hours
Powder Type:	CP85, CP85 after KBI cleaning, or new CP85
Pressing Pressure:	1500 or 5000 psi (1715°C, 3 hours)

The MgO content was found to be the only significant variable affecting thermal expansion (Figure 4.10).

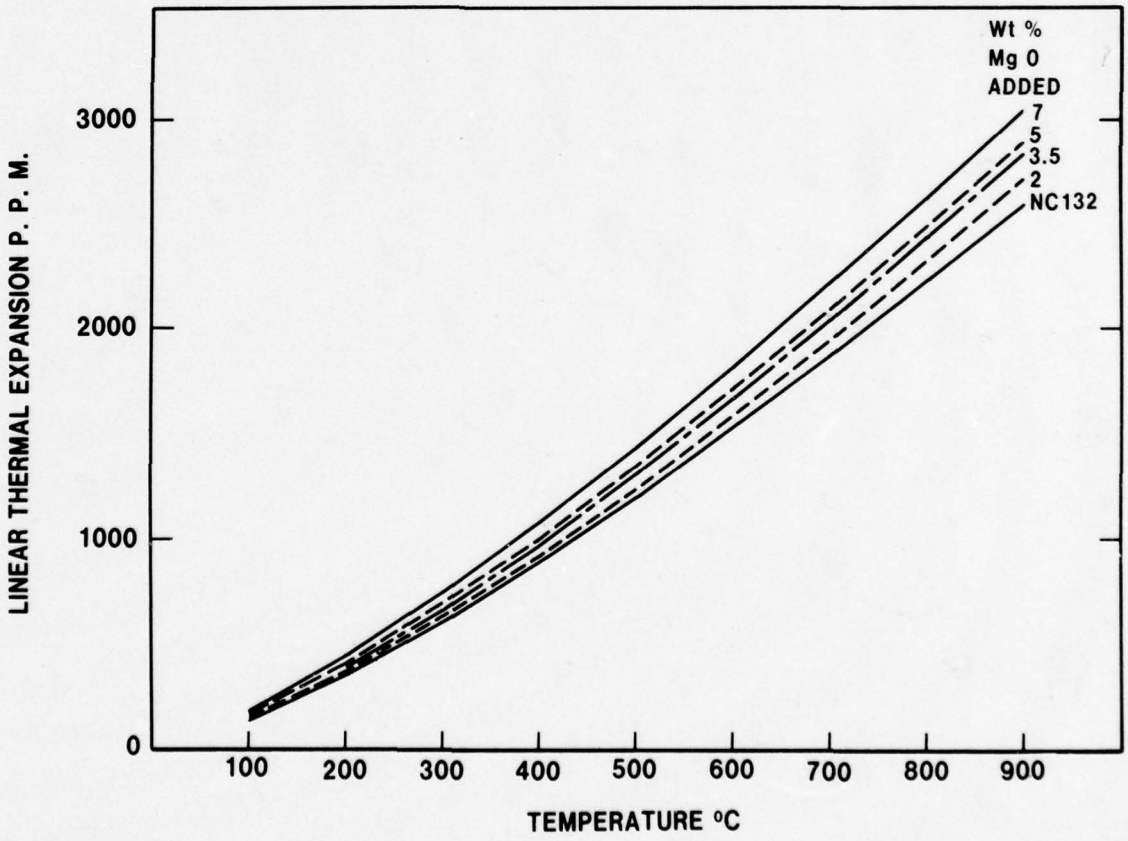

Figure 4.10 — Linear Thermal Expansion of HPSN

5.0 CERAMIC ROTOR BLADE RING INVESTIGATIONS

Introduction

The Ceramic Turbine Rotor Technology Program continued to develop ceramic material and process technology and included both destructive and non-destructive tests to identify problem areas and evaluate process improvements. This Section presents the results of several investigations conducted on injection molded reaction bonded silicon nitride blade rings. Cold spin testing to destruction, room temperature MOR testing of the rim material and blade bend testing before and after hot press bonding all revealed significant problem areas requiring attention.

Summary

Four duo-density turbine rotors were tested in the cold spin pit to evaluate the hot pressed to reaction sintered bond joints and the effect of I.D. voids in the blade ring rim on blade failure speeds. Neither the I.D. voids nor the bond joints failed up to speeds of 96,900 rpm. However, blade failures which occurred from 38,440 rpm to 89,070 rpm were related to surface and internal flaws in the airfoils. Six blades which were free of obvious flaws failed in the 90,060 to 96,900 rpm range.

Room temperature MOR tests on bars cut from the rim area of four reaction bonded silicon nitride blade rings gave characteristic strengths of 25.4 to 33.5 ksi with Weibull slopes ranging from 2.6 to 6.8. Subsurface flaws were responsible for the low Weibull slope which was improved if the flawed test bar data was excluded from the analysis.

Rather severe degradation of the room temperature strength of the reaction bonded silicon nitride rotor blades was identified as resulting from the press-bonding operation. Blade strength decreases of 14 to 38% were measured by the blade bend test. Analysis of the microstructure of the blades indicated they change from a shiny black to a gray color after hot pressing with a corresponding increase in non-uniform porosity. X-ray analysis indicated that the phase composition of the silicon nitride had changed from an average of 70% α, 29% β before press bonding to an average of 22% α, 75% β and 3% silicon oxynitride after press-bonding.

5.1 COLD SPIN TESTING

Introduction

The vacuum spin pit has been used to evaluate ceramic turbine rotor hubs, blade rings and complete duo-density rotors. The facility and test procedures were described in detail in preceding reports[2, 7-11]. During this reporting period, the spin pit was used to qualify twelve duo-density rotors prior to hot testing (Volume 1, Section 3.1.2 of this report). In addition four rotors, fabricated during the development of the simplified two piece hot press bonding process, were spun to destruction to evaluate the hot press to reaction sintered bond joint. This section presents the test results on the four rotors.

Test Results

Rotor 1197, shown in Figure 5.1 mounted in the spin pit ready for testing, had been machined specifically to evaluate the hot press to reaction sintered bond joint. All blades with noted defects and blades with defects in the rim beneath the blades were removed prior to testing. In addition, the blade platform was slotted between each blade through the injection molded blade ring and into the hot pressed hub. The slots interrupted the continuity of the platform and eliminated any tangential load carrying capacity of the rim thereby subjecting the bond joint to nearly pure radial tension. The blades were not machined down to the design diameter but were left at the "as-molded" length to increase the load on the bond joint. The failure speeds for the "as-molded" length blades, Table 5.1, should be increased 18% to be equivalent to design length blades. None of the failures occurred in the bond joint even at 71,000 rpm which for design length blades is equivalent to 83,800 rpm (130% of design speed of 64,240 rpm). Two of the four failures originated from blade surface flaws while the other two failures originated from blade internal flaws.

The remaining three rotors, 1246, 1272 and 1280 were machined to the first stage design tip diameter with a simple tapered disk contour as shown in Figure 5.2. Blades with known defects and blades positioned over defects in the rim were not removed prior to cold spinning. The results are shown in Tables 5.2, 5.3 and 5.4. Since none of the 40 I.D. voids (defects in the rim beneath blades) resulted in failure, even at 95,700 rpm, this type of flaw is not critical to cold spinning. However, gross fabrication flaws in the airfoils, internally and at the surface, were revealed for each test up to 90,000 rpm. Where multiple blade failures occurred in one test, it is believed that the flawed blade(s) was the primary cause of failure with the failure of unflawed blades due to impact from the failed flawed blade(s). Three of the six blades with known gross surface defects failed through the defect while the remaining three did not.

Figure 5.3 shows the largest flaw found during these tests which emphasizes that the nature of the flaw is a gross fabrication defect, it caused a failure at 38,440 rpm on rotor 1246. Figure 5.4 shows the gross fabrication flaw in blade number 11 of rotor 1246 which was noted prior to testing. The inspection report listed it as a 2Bw, i.e. 0.050" long on the convex side of the airfoil. This flaw resulted in failure at 52,270 rpm. Many of the flaws were internal and did not extend to the surface of the blade. Figure 5.5 shows two internal flaws in blade numbers 31 and 32 of rotor 1280 which failed at 80,350 and 81,020 rpm respectively. Figure 5.6 shows the fracture surface of blade 14 of rotor 1280. This 95,700 rpm failure, is typical of the six blades which failed at 90,060 to 96,900 rpm (Table 5.4) and revealed no gross fabrication flaws.

Figure 5.7 is a Weibull distribution of the combined data from rotors 1246, 1272 and 1280. The characteristic failure speed was 97,000 rpm with a Weibull slope of 6.0. Of course it must be emphasized that this distribution includes a preponderance of failures due to gross fabrication defects.

Discussion

This series of tests showed that cold spin blade failures occurring below 90,000 rpm were related to internal and surface gross fabrication flaws in the airfoils. Many of the surface flaws and all of the internal flaws were not detected by the NDE techniques used indicating better techniques are required. More importantly, improvements are required in the fabrication process to eliminate such gross fabrication flaws so that cold spin speeds of 90,000 rpm can be achieved without a large number of failures. Both of these problem areas were addressed in Section 2 of this report, Future Plans.

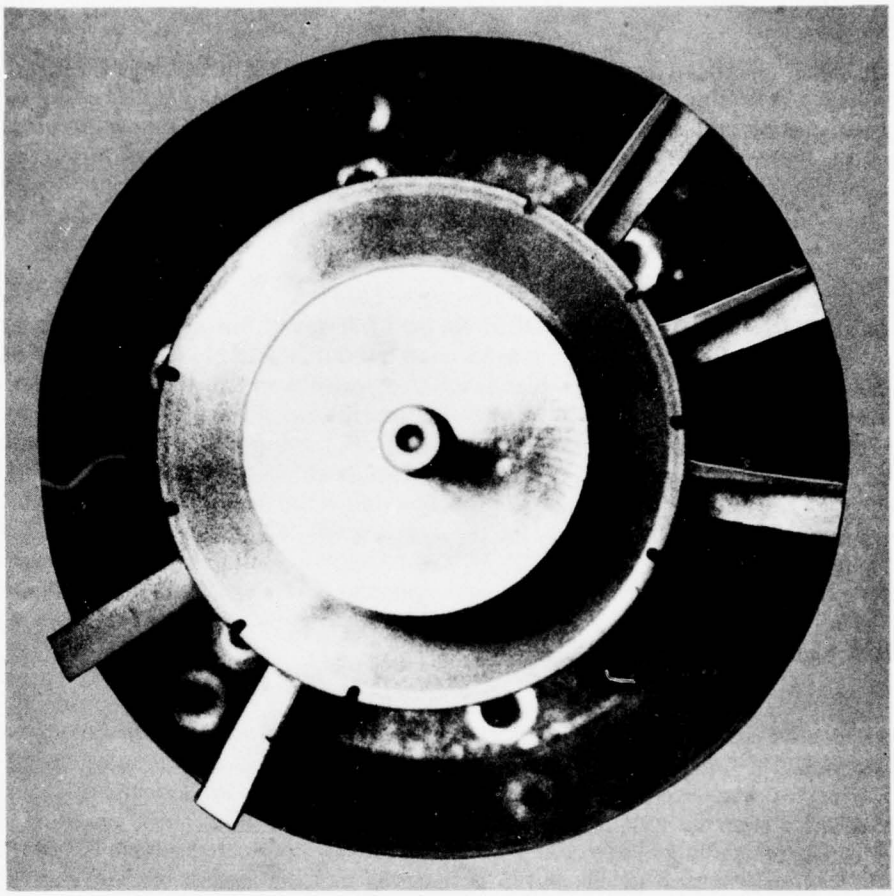

Figure 5.1 — Rotor 1197 Prior to Vacuum Spin Test

TABLE 5.1

Rotor 1197 (Blade Ring 1982) — As Molded Blade Length — 5 Blades

Spin Number	Failure RPM	Failed Blade Number	Before Spin Inspection		Post Failure Examination of Fracture Surface
			I.D. Voids	Blade Crack	
1	43020	25	0	0	Surface Flaw
2	58340	3	0	0	Internal Flaw
3	65690	22	0	0	Surface Flaw
4	71000	28	0	0	Internal Flaw

Blade number 5 intact after 71,000 rpm test.

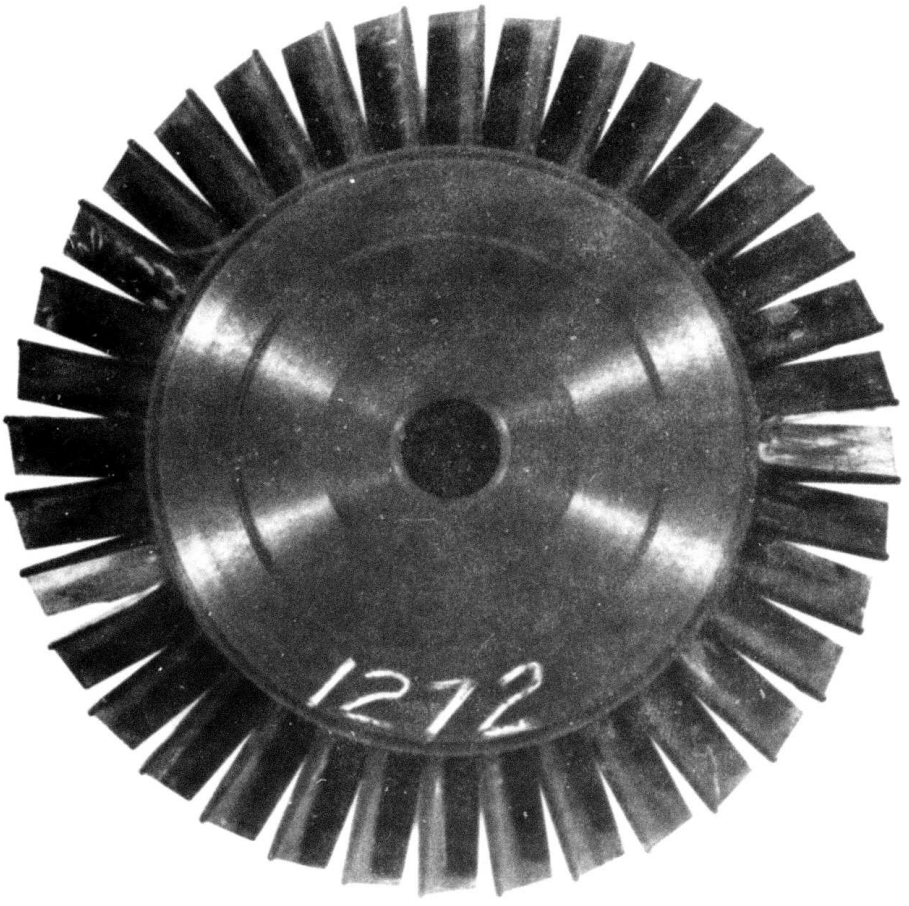

Figure 5.2 — Rotor 1272 Simple Tapered Disk

TABLE 5.2

Rotor 1246 (Blade Ring 2051) — 1st Stage Design Length — 25 Blades

Spin Number	Failure RPM	Failed Blade Number	Before Spin Inspection		Post Failure Examination of Fracture Surface
			I.D. Voids	Blade Crack	
1	38440	13	V*		Surface Flaw
		14	V		No Flaw
2	52270	11	V	2Bw**	Surface Flaw
3	63250	17	V		Surface Flaw
		7			Surface Flaw
4	63220	23			Surface Flaw
5	68400	3			Flaw
		4			Flaw
		5			Blade Chipped
6	70900	36			Flaw
		2			No Flaw
7	71400	8			Flaw
		9	V		No Flaw
		10	V		No Flaw
8	77910	19	V		Flaw
9	78980	20			Flaw
		21			No Flaw
		24			Flaw
10	81450	6			Flaw
		12			No Flaw
		35			No Flaw
11	86950	1	V	1Bw***	No Flaw
		16	V		Flaw
12	85480	5	V		Hub Failure
		22			
		34			

Blades 5, 22 and 34 lost when hub failed.

*Void
**Suction surface indication — 0.050″ long.
***Suction surface indication — 0.025″ long.

TABLE 5.3

Rotor 1272 (Blade Ring 2042) — 1st Stage Design Length — 36 Blades

Spin Number	Failure RPM	Failed Blade Number	Before Spin Inspection		Post Failure Examination of Fracture Surface
			I.D. Voids	Blade Crack	
1	61250	20	V*		No Flaw
		21	V		No Flaw
		22	V	C_3**	Flaw
2	65210	33	V		Internal Flaw
		34			No Flaw
3	71110	18	V	C_3	No Flaw
		19	V		Internal Flaw
		24	V		No Flaw
		25			Surface Flaw
4	72190	12			No Flaw
		13			No Flaw
		14			Internal Flaw
5	74020	4	V		No Flaw
		5	V		Internal Flaw
		6			Surface Flaw
		29			Surface Flaw
6	74310	26			No Flaw
		27			Surface Flaw
7	75190	7			Flaw
		8			No Flaw
		9			No Flaw
8	75190	1			Hub Failure
		2	V		
		3	V		
		10			
		11			
		15	V		
		16	V		
		17	V	C_3	
		23	V		
		28			
		30			
		31			
		32			
		35			
		36	V		

15 blades lost when hub failed.

*Void.
**Leading or trailing edge indication >0.050″ long.

TABLE 5.4

Rotor 1280 (Blade Ring 2040) — 1st Stage Design Length — 36 Blades

Spin Number	Failure RPM	Failed Blade Number	Before Spin Inspection		Post Failure Examination of Fracture Surface
			I.D. Voids	Blade Crack	
1	50050	1			Surface Flaw
		36	V*		No Flaw
2	54570	24			No Flaw
		25			No Flaw
		26			No Flaw
		27	V		Surface Flaw
3	58760	22			No Flaw
		23			Surface Flaw
4	68620	7			No Flaw
		8	V		No Flaw
		9	V		Surface Flaw
		28			Internal Flaw
		29			Internal Flaw
		30			Internal Flaw
5	74560	16	V		No Flaw
		17	V		Surface Flaw
		19			No Flaw
		20	V		No Flaw
		21	V		Internal Flaw
6	80350	31			Internal Flaw
7	81020	32			Internal Flaw
8	87140	2			Internal Flaw
		3	V		No Flaw
		15	V		No Flaw
9	89910	4		1Bw**	Surface Flaw
		10	V		No Flaw
		11			Internal Flaw
10	89070	18			No Flaw
		33			No Flaw
		34			Internal Flaw
11	90060	35	V		No Flaw
12	95700	13	V		No Flaw
		14	V		No Flaw
13	96900	5			No Flaw
		6			No Flaw
		12			No Flaw

*Void.
**Suction surface indication — 0.025″ long.

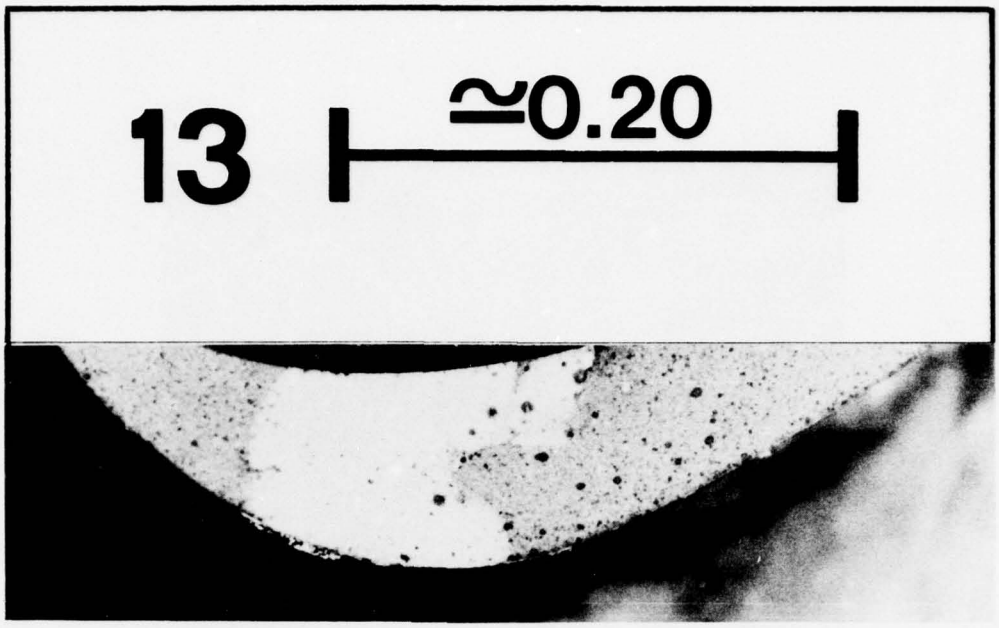

Figure 5.3 — Blade 13 of Rotor 1246 — 38,440 rpm Failure

Figure 5.4 — Blade 11 of Rotor 1246 — 52,270 rpm Failure

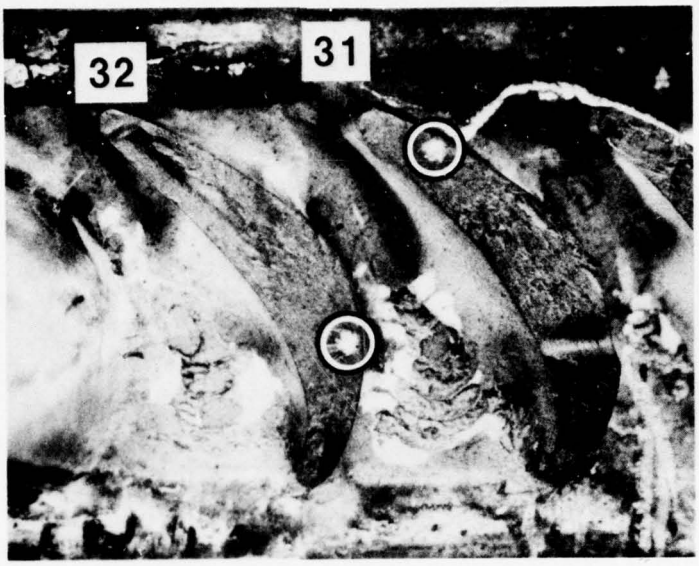

Figure 5.5 — Internal Flaws in Blade 31 (80,350 rpm) and 32 (81,020 rpm) of Rotor 1280

Figure 5.6 — Typical Fracture Surface of Unflawed Blades — Blade 14 of Rotor 1280 (95,700 rpm failure)

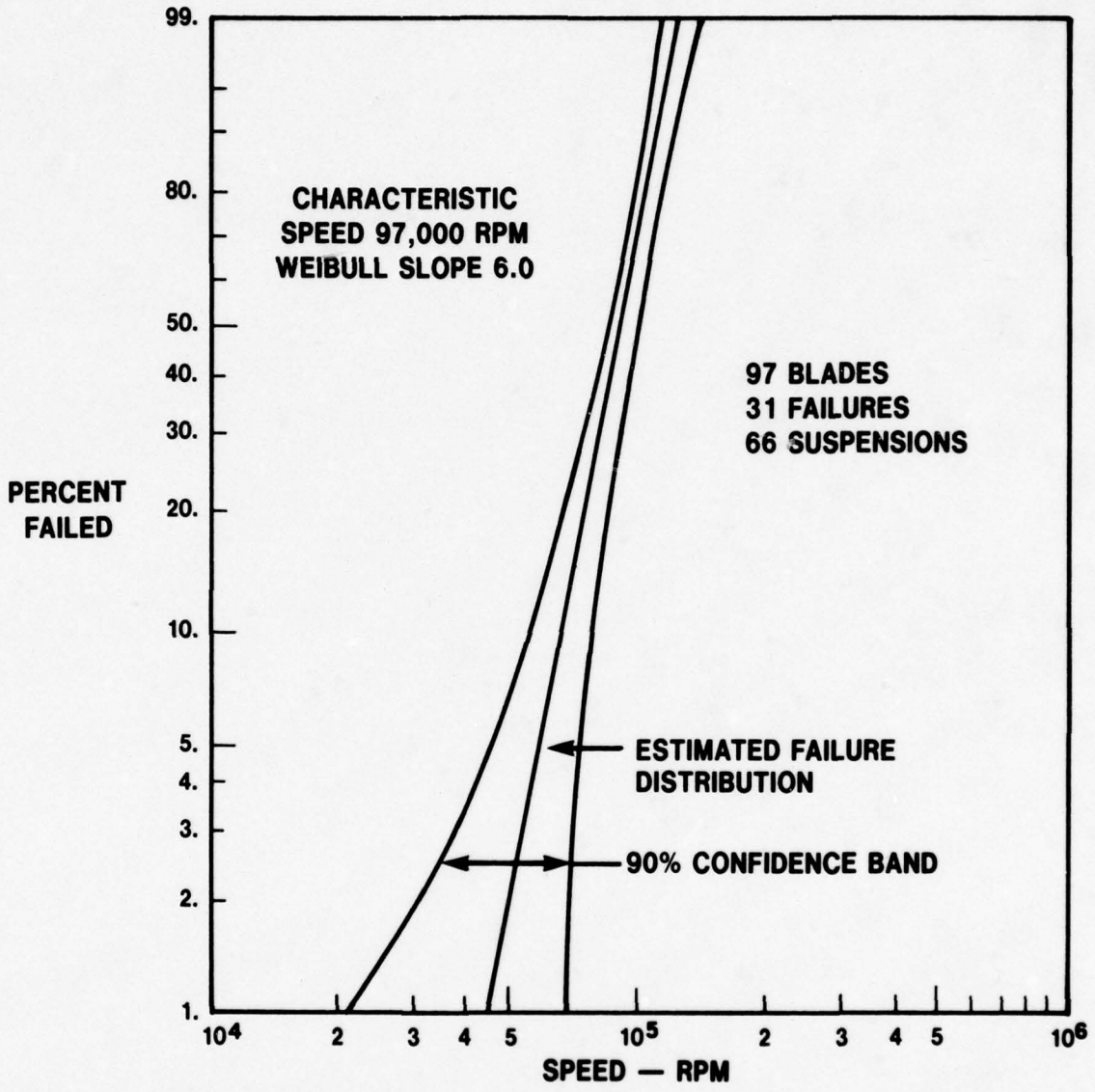

Figure 5.7 — Weibull Distribution of Combined Data from Rotors 1246, 1272, and 1280

5.2 M.O.R. TESTING OF ROTOR BLADE RINGS

Four reaction bonded silicon nitride turbine rotor blade rings, produced by injection molding, were used to determine the room temperature strength of the material. Approximately 15 bars, 1.25" x 0.25" x 0.095", were cut from each rotor blade ring rim. The bars were loaded in a steel fixture with fixed knife edges under four point loading with a constant head speed of 0.5 mm per minute.

Table 5.5 presents all the raw data, including those with clearly visible surface and internal defects. Table 5.6 shows the characteristic strengths to vary from 25.4 to 33.5 ksi and the Weibull modulii ranged from 2.6 to 6.8 for all the raw data. The broken surfaces of the bars were examined and the data for those having white inclusions or pores were rejected. The Weibull parameters for sound bars showed a minor increase in characteristic strength but a significant improvement in Weibull modulus. Eight additional blade rings are under investigation to increase the data base and examine the relationship between type of defect and strength.

TABLE 5.5

Room Temperature M.O.R. Data (KSI)

Blade Ring No.	2047	2155	2251	2256
	21.2	15.6*	12.3*	4.6*
	22.4	21.2	13.7*	12.3*
	23.6	28.0*	15.6*	12.6*
	26.4	28.0	17.0*	12.6*
	26.8	29.2	17.6*	13.4*
	27.4	30.1	25.7	15.1*
	28.0	30.2	25.9	22.4
	29.6	33.2	26.9*	23.2*
	29.6	34.4	28.3*	24.8
	31.4	35.4	30.2*	25.8*
	32.0	35.8*	30.7	27.3*
	33.6	37.0	31.9	28.0*
	35.8	38.0*	32.5*	28.6
		39.2	32.5*	30.3*
				33.6*
				33.9
				36.0

* indicates bar with obvious flaw

TABLE 5.6

Weibull Parameters

Blade Ring No.		All Bars	Flaw-Free Bars
2047	$\sigma\theta$	30.1 (27.8-32.7)	30.1 (27.8-32.7)
	m	6.8 (4.2-8.9)	6.8 (4.2-8.9)
	n	13	13
2155	$\sigma\theta$	33.5 (30.6-36.8)	33.8 (30.7-37.3)
	m	5.7 (3.6-7.5)	6.7 (3.7-9.1)
	n	14	10
2251	$\sigma\theta$	27.0 (23.4-31.1)	—*
	m	3.7 (2.3-5.1)	
	n	14	4
2256	$\sigma\theta$	25.4 (21.2-30.4)	31.1 (24.0-41.8)
	m	2.6 (1.7-3.3)	4.2 (1.5-6.2)
	n	17	5
Combined Values	$\sigma\theta$	29.1 (27.4-30.8)	31.6 (30.1-33.1)
	m	4.0 (3.3-4.6)	6.7 (5.1-8.2)
	n	58	32

$\sigma\theta$ = Characteristic M.O.R. (ksi) — strength at 63.2% failure rate
m = Weibull Modulus
n = Number of bars
Numbers in parentheses represent the 90% confidence band.
* Too few specimens to permit Weibull analysis.

5.3 EVALUATION OF NEW N.D.E. TECHNIQUES

Several N.D.E. techniques were previously considered for the detection of flaws in complex shaped ceramic gas turbine components[11]. These included microfocus X-ray, infra-red thermography, X-ray tomography, electromagnetic excitation, electrostatics, holosonics and mechanical load testing. During this reporting period, feasibility studies were completed on two of these techniques and the equipment was ordered and received for the microfocus X-ray technique.

Infra-Red Thermography

An evaluation of infra-red thermography using silicon nitride rotor blade rings revealed that this technique was not feasible on such complex shaped ceramic parts. This was due to the inability to establish the necessary thermal gradient across the test piece.

Electrostatic Technique

The University of Arizona completed some additional work on the use of an electrostatic technique to detect surface flaws in silicon nitride blade rings. This work involved the use of lighter blade loads than those used in previous tests. Setting a maximum load of 738 grams per blade resulted in a marked reduction of broken blades with detection of root or fillet cracks still possible. The conclusions of the study suggest that an electrostatic technique, using a non-contacting voltmeter as a detector, was a practical N.D.E. tool for locating flaws in rotor blade rings. An automatic system could be set up whereby the blades would be rotated into the test position by a stepped rotary table. Loading would be accomplished by a micropress and the Trek voltmeter detector would move into a preset position at each blade. The disadvantage with this approach is that it only promises to detect flaws in stressed areas and only relatively small portions of the blades can be readily stressed by simple blade loading.

Microfocus X-ray Technique

This technique was described in some detail in the last report[11] with the recommendation that this equipment be obtained and developed as soon as possible. The microfocus X-ray equipment, received late in this reporting period, offers excellent potential for the detection of gross fabrication flaws in rotor blade rings. The panoramic tube, an accessory to this equipment, should permit radial examination of the blade ring rim area to detect sub-surface flaws.

5.4 BLADE STRENGTH DEGRADATION DURING HOT PRESS BONDING

Introduction

Rotors produced during the development of the simplified two-piece hot press bonding concept, described in Section 3.2 of this report, were sectioned to examine the bond joint between the blade ring and the hot pressed hub. During these examinations, it was observed that the reaction bonded blade ring material usually had changed color, from a shiny black to a dull gray. Several rotors were then selected for an investigation into the color changes and possible associated microstructural changes. In addition, a few rotors were subjected to blade bend testing to determine if the strength of the blades was affected by hot press bonding.

BLADE BEND TESTING

The rotor blade bend test[9, 10, 11] was used to determine the affects of hot press bonding on the bend strength of the reaction bonded silicon nitride blades. In order to eliminate any bend strength variability from one nitriding batch to another, blade rings in the "as nitrided" state were compared to hot press bonded blade rings from the same nitriding run.

Seven blade rings from three different nitriding runs were tested and the results compared to five blade rings, which had been further processed into duo-density rotors, from the same three nitridations. Where multiple sets of test data were available for the same nitridation run, in either the as nitrided or press bonded state, the data was combined to obtain a composite Weibull slope, characteristic load and load range. The results are shown in Table 5.7. In all cases, the characteristic loads after

TABLE 5.7

Blade Bend Test Results

Data Set	Condition	Nitriding Number	Blade Ring S.N.	Rotor S.N.	Sample Size	Load Range (Pounds)	Weibull Slope	Characteristic Load* (Pounds)
1	As Nitrided	48	1377	—	18	49-102	6.6	82.4
2	As Nitrided	48	1386	—	15	63-96	13.0	89.5
3	As Nitrided	48	1410	—	19	68-103	14.0	95.3
	Combined Data Sets	1, 2, 3	—	—	52	49-103	9.1	89.9
4	After Hot Pressing	48	1400	1079	15	52-84	11.3	78.0
5	After Hot Pressing	48	1404	1083	29	53-83	8.7	72.8
6	After Hot Pressing	48	1421	1087	16	46-98	5.3	81.3
	Combined Data Sets	4, 5, 6	—	—	60	46-98	6.9	77.0
7	As Nitrided	67	1991	—	31	66-98	11.5	85.4
8	As Nitrided	67	2023	—	26	68-94	10.3	86.1
	Combined Data Sets	7, 8	—	—	57	66-98	11.2	85.7
9	After Hot Pressing	67	2037	1263	16	34-60	6.8	53.0
10	As Nitrided	78	2262	—	12	60-83	8.0	75.2
11	As Nitrided	78	2280	—	20	53-94	9.2	81.2
	Combined Data Sets	10, 11	—	—	32	53-94	9.2	79.1
12	After Hot Pressing	78	2342	1319	13	42-65	15.1	61.6

*Load at 63.2% failure rate

hot press bonding were lower than in the as nitrided state. Table 5.8 summarizes the results and shows the blade strength degradation, due to hot press bonding, to range from 14 to 38%. In order to determine if the 14% strength and 24% Weibull slope degradation observed for nitridation 48 was statistically significant, an analysis of the data was conducted as per the procedure outlined in Section 6.1 of this report. The results show that there is a statistically significant difference in the data before and after hot press bonding. Estimates of the difference and confidence levels are presented in the detailed results of analysis in Section 6.1.

TABLE 5.8

Summary of Blade Bend Test Results

Nitriding Number	As Nitrided		After Hot Pressing		% Change	
	Weibull Slope	Characteristic Load* (Pounds)	Weibull Slope	Characteristic Load* (Pounds)	Weibull Slope	Characteristic Load*
48	9.1	89.9	6.9	77.	−24	−14
67	11.2	85.7	6.8	53.0	−39	−38
78	9.2	79.1	15.1	61.6	+64	−22

*Load at 63.2% failure rate

Color Changes

Color gradients and color changes were observed in the reaction bonded silicon nitride (RBSN) blade rings after the hot press bonding operation. These color gradients or changes occurred in two areas, the blades and the rim. The blade changed color during the hot press bonding operation, going from a shiny black to a light to dark gray color. The light gray was usually present as a case around the perimeter of the blade, while a darker gray color was present in the center of the blade. The color changes present in the rim of the blade rings were more complex. The area of the blade ring next to the bond was usually black. As the distance away from the bond increased, the color changed to a light gray. As the distance was further increased into the blade region, a darker gray region was encountered (Figure 5.8).

Rotor 1182 was studied to evaluate the color gradients present in the bond/rim area. The color gradients in this rotor were typical of all hot pressed rotors examined. The rotor was sectioned, polished and examined using the optical microscope and the electron microprobe.

Figure 5.8 shows the type of color gradients typically found after the hot press bonding operation. Optical micrographs were obtained at various locations within the hub and blade ring (areas marked A through F on Figure 5.8). The micrographs from these areas are shown in Figure 5.9A through F. There was a definite correlation between the color and the porosity of the silicon nitride. The black area of the injection molded blade ring rim (near the bond) appeared to be as dense as the hot pressed hub (Figures 5.9A, B, C). The interface between this black and gray region (Figure 5.9D) showed that the gray region contained much more porosity than the black region. This is, again, shown in Figure 5.9E. The blade region, which has a black color, had less porosity than the gray regions (Figure 5.9F).

That portion of the injection molded rim near the bond region appeared to be densified. The microhardness of the rim was very similar to the hot pressed hub (see Table 5.9) and higher than the values for as nitrided injection molded RBSN.

The bond region was studied in depth using the election microprobe. The magnesium concentration was monitored from the hub to the rim across the bond joint. The result, shown in Figure 5.10, showed that the magnesium had diffused from the hub into the rim area. This diffusion of magnesium into the rim, along with pressure applied to the rim, probably caused densification to occur, yielding the

resulting dense microstructure. It is also interesting to note from Figure 5.10 that the porous regions D and E contain no magnesium only background scatter. This confirms that the magnesium was important to the rim densification observed in the bond region.

A color change, after press bonding, was also noted in the rotor blades as shown in Figure 5.11. After hot pressing, the color had changed from a shiny black to a dark gray-light gray color. This is similar to the gray region that occurred in the rim.

Characterization after Hot Press Bonding

Extensive microstructural analyses were performed on rotor blades after each major processing step in the rotor processing operation; after initial nitriding, after blade fill nitriding, and after hot press bonding. The objective of this work was to identify property changes occurring during the processing steps, to correlate any changes with the observed strength degradation, and to identify possible solutions to the problem.

In this work, 16 as-nitrided, 2 blade-fill nitrided, and 8 hot press-bonded rotor blade rings were studied. The following properties were measured on selected rotor blade rings; bulk density of a rotor blade, color of the blade, general microstructural features, phase composition and oxygen content. The results for each blade ring are given in Table 5.10 with the results summarized for each processing step in Table 5.11. From Table 5.11 the following observations can be noted:

- There was very little change in blade density from the as-nitrided to press-bonding step.
- The color remained the same after blade fill nitriding (shiny black) but changed to gray with a lighter gray case after press bonding (See Figure 5.11).
- The microstructure remained the same after blade fill nitriding (Figure 5.12) but changed after press bonding. After press bonding, a continuous network of fine porosity was formed. Equally distributed within the structure was a network of large grains, which varied in size from blade ring to blade ring as shown in Figure 5.12C and D. These large grains, had a hardness equal to the as nitrided blade rings, while the porous areas had a 40% lower hardness (Table 5.12). A quantitative determination of the increased porosity was made by obtaining the pore size distribution using Mercury Porosimetry. Figure 5.13 shows the pore size distribution of two as nitrided blade rings and two press bonded rotor blades processed in the same nitriding cycle. As shown, the average pore size had increased ranging from 0.03 microns to 0.11 microns.
- The phase composition remained constant through blade fill nitriding but changed to a high β Si_3N_4 composition after press bonding. Also, the amount of Si_2ON_2 was greatly increased after press bonding.
- The oxygen content, as determined using Neutron Activation Analysis (Dr. H. Priest of AMMRC), changed throughout the process; from 1.24% for nitriding to 1.39% after blade fill nitriding to 1.57% after press bonding. The 1.39% after blade fill nitriding may be misleading because of two very diverse readings (See Table 5.10).

In summary, the following can be concluded based on the blade rings studied and the information obtained:

- The data showed that many properties of the blade ring changed after press bonding. All of these property changes (porosity, microstructure, phase composition and oxygen content) could explain the observed strength degradation.
- No such property changes are observed for blade rings subjected to blade fill nitriding. It can be assumed that no strength degradation would be observed after this processing step.

General Discussion

The observed changes that occurred in RBSN during rotor fabrication were all related to temperature or time at temperature. The rotor blade rings were subjected to temperatures of about 1700°C for times of up to three hours. At this temperature, many things can happen to silicon nitride. At 1700°C the α to β silicon nitride phase transformation will occur. At temperatures around 1700°C, Lange and Terwilleger[13] and Greskovich and Rosolowski[14] have observed that it is possible to sinter silicon nitride if the proper additives are present. However, more importantly, at temperatures above 1650°C, Lange and Terwilleger[13] observed that silicon nitride dissociation occurred. They observed that samples heated in a flowing nitrogen atmosphere to about 1650°C for 20 minutes exhibited about a 16% weight loss.

The rotor blade rings were subjected to more severe temperature conditions (1700°C) for longer times (3 hours) than the silicon nitride in Lange's experiments. It is, therefore, reasonable to expect that the silicon nitride rotor blades did undergo some dissociation. The previous results are consistent with this hypothesis. The color changed because density gradients occur. One major observation, in regard to the strength degradation, was the formation of a continuous porous phase. These density gradients and changes in pore distribution could both be the result of silicon nitride dissociation.

The use of a nitrogen over-pressure condition could possibly solve the apparent silicon nitride dissociation. This technique is being used by Greskovich et. al.[14] and Priest et. al.[15] to sinter silicon nitride. Lacking high pressure nitrogen facilities, the silicon nitride blade fill that surrounds each rotor blade ring during press bonding could provide a suitable encapsulating device. However, the blade fill must be impervious to nitrogen and capable of building up from 10 to 100 atmospheres of nitrogen pressure, which the literature suggests is necessary to retard the dissociation at the hot pressing temperature.

The other possible way to retard the dissociation of the silicon nitride is to reduce the hot press bonding temperatures. This step, in conjunction with the current blade fill technology, could reduce the dissociation of the silicon nitride in the blade ring and significantly improve the properties of the blade ring.

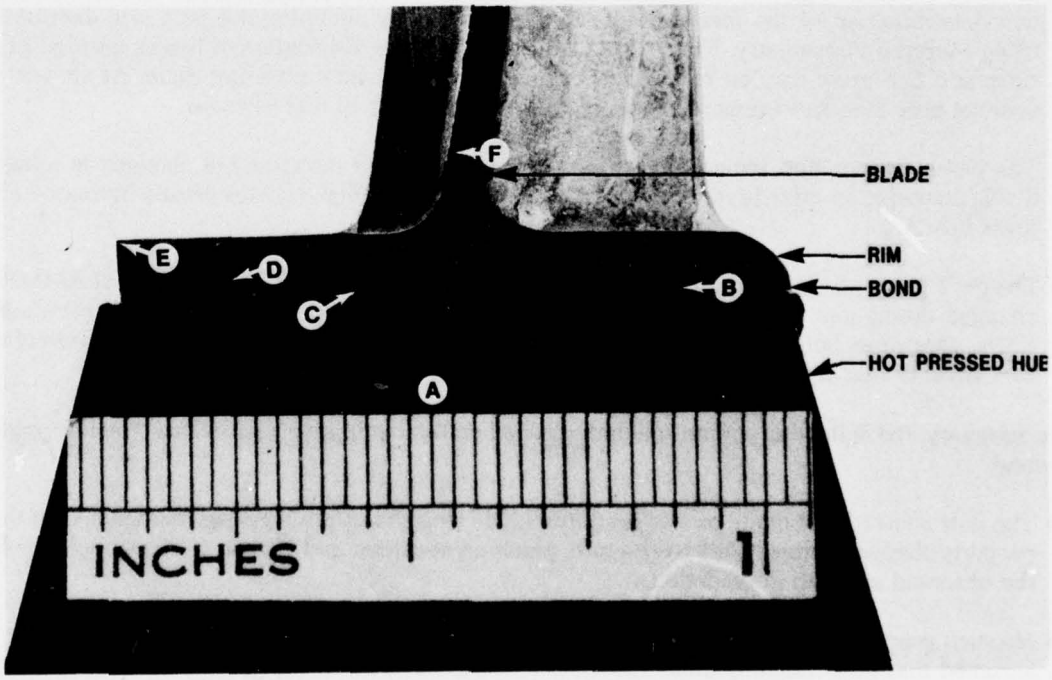

Figure 5.8 — Cross Section of Rotor 1182 Showing Color Gradients

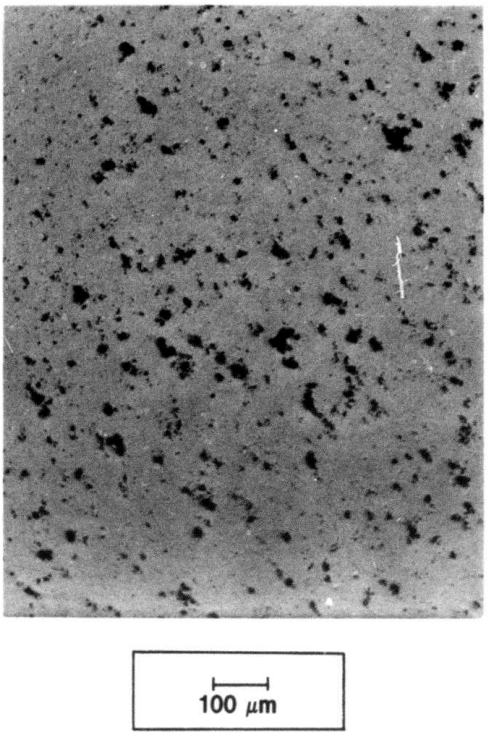

Figure 5.9a — Micrograph of Rotor 1182 Hub Region

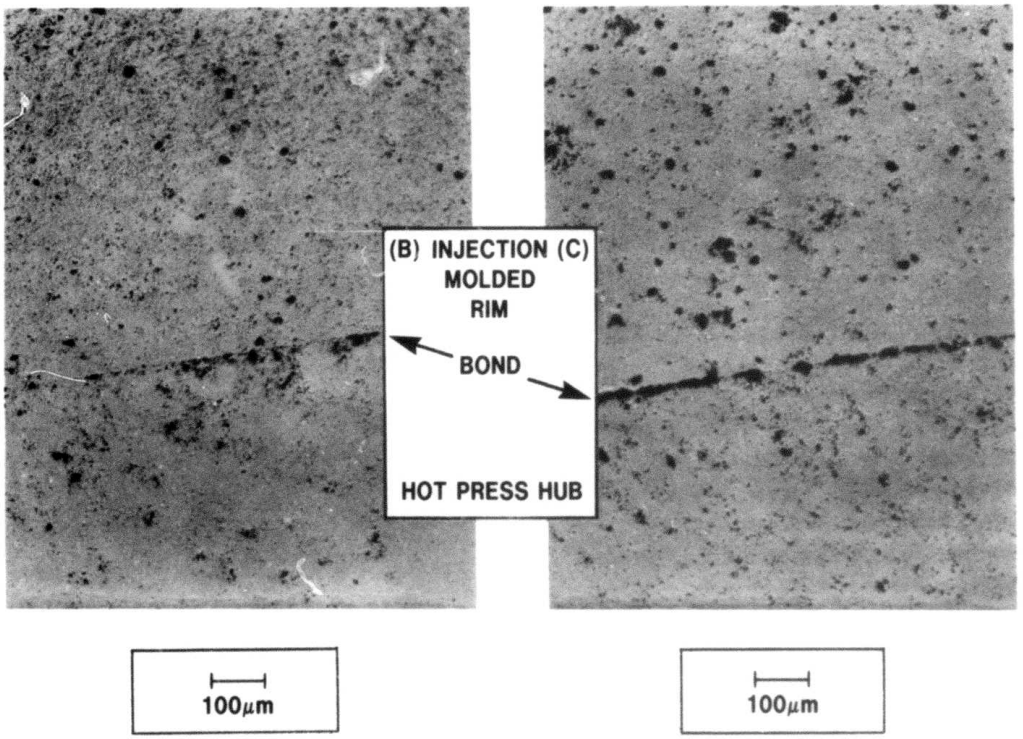

Figure 5.9b,c — Micrograph of Rotor 1182 Bond Region

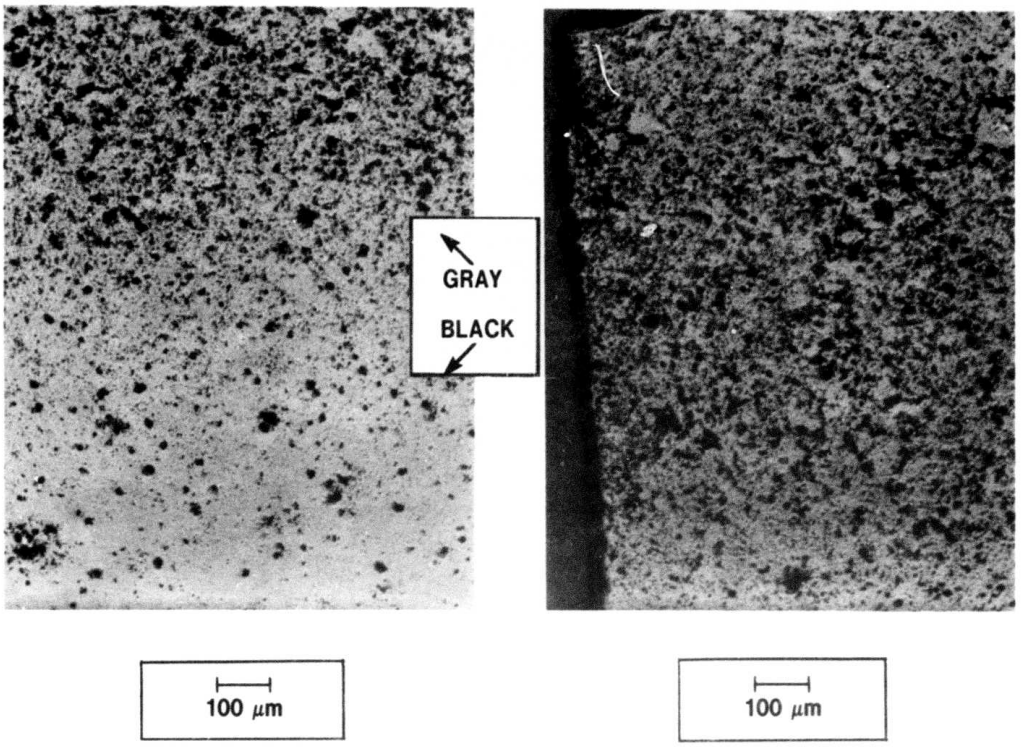

Figure 5.9d,e — Micrograph of Rotor 1182 Rim Region

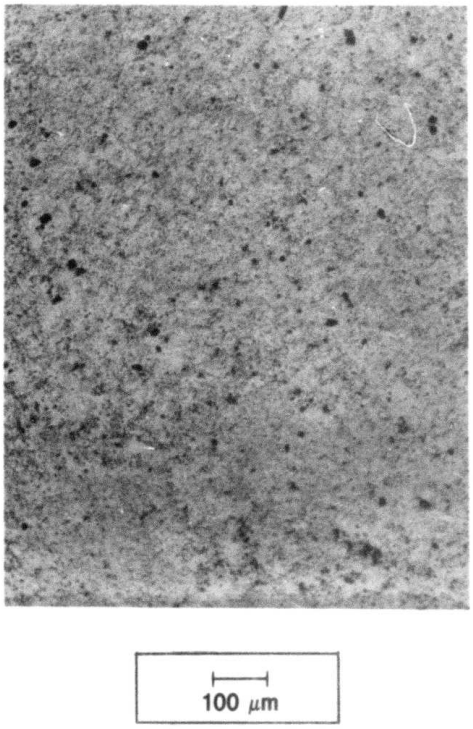

Figure 5.9f — Micrograph of Rotor 1182 Blade Region

TABLE 5.9

Microhardness at Various Locations on Rotor 1182

Location	Color	Vickers Hardness*
Hub	Black	**1670**
Bond Hub Side	Black	**1650**
Rim Side	Black	**1525**
Rim	Gray	**753**
Blade Root	Dark Gray	**976**
Blade	Dark Gray	**1017**
As Nitrided RBSN (BR 2023)	Black	**1178**

* Vickers Diamond Pyramid Indentor 5Kg Load

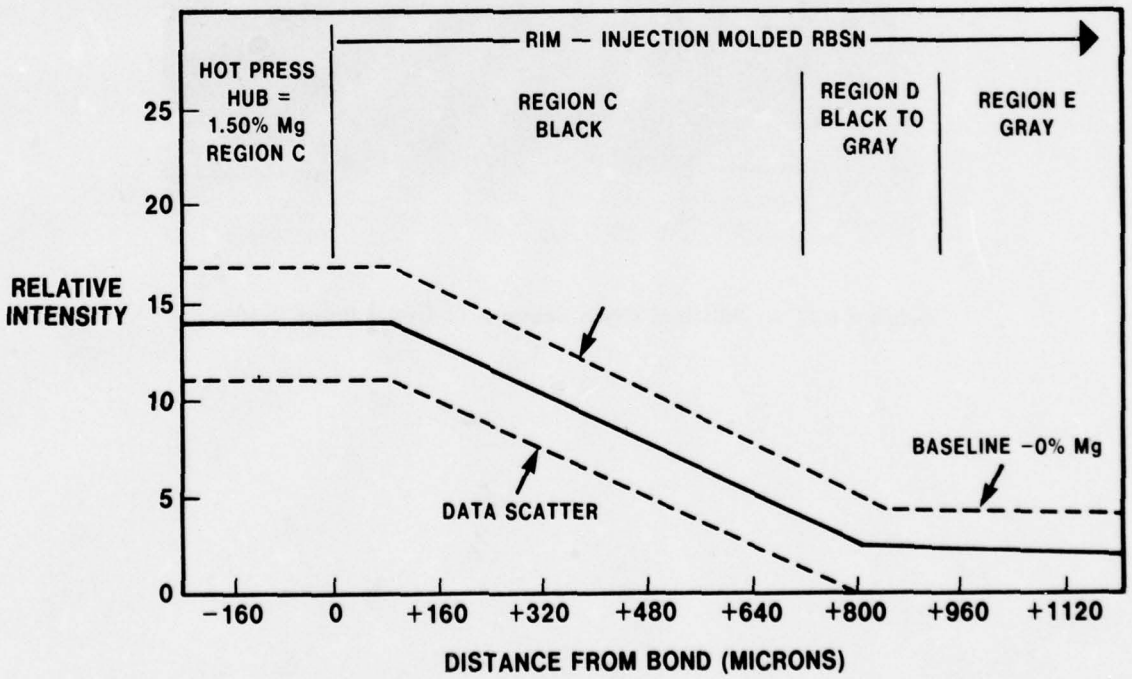

Figure 5.10 — Magnesium Concentration Across the Bond Joint of Rotor 1182

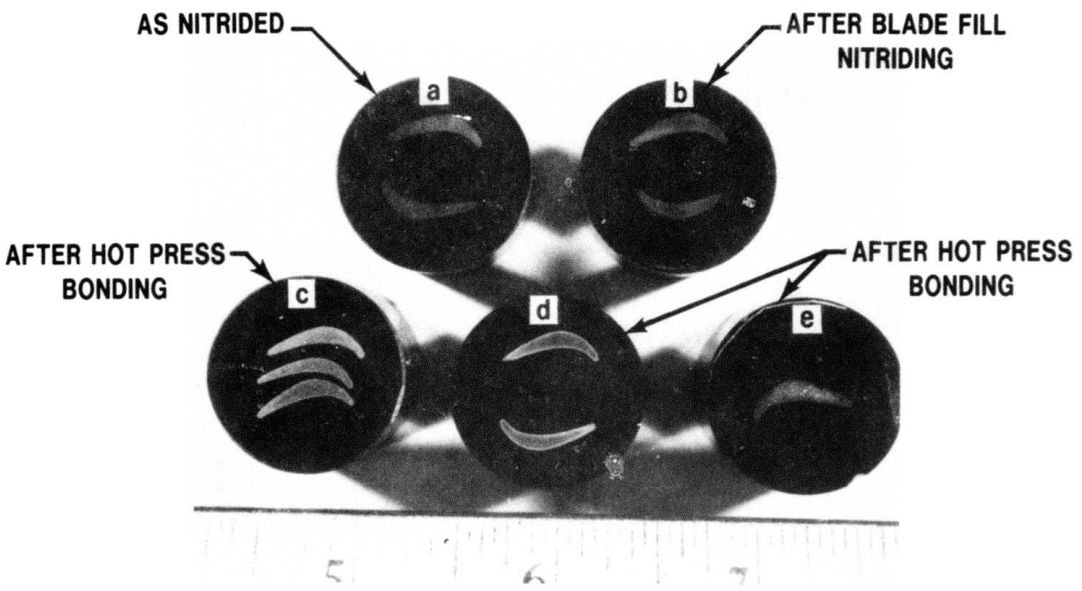

Figure 5.11 — Polished Cross Sections of RBSN Rotor Blades

TABLE 5.10

Characterization of Rotor Blade Rings

Blade Ring S.N.	Rotor S.N.	Nitriding Number	Density g/cc	Color	Micro-Structure	% Phase Composition α	β	Si	Si_2ON_2	SiO_2	Oxygen Content %	Blade Bend Strength (Pounds)
					As Nitrided							
1377	—	48	2.74	SB	UP, SMP	67	31	1.2	0.9	0	1.21	82.4
1386	—	48	2.69	SB	UP, SMP	64	35	0.7	0	0	1.20	89.5
1410	—	48	2.73	SB	UP, SMP	60	40	0	0	0	1.12	95.3
1737	—	54	—	SB	—	73	26	0.7	0	0	—	105.0
1747	—	54	—	SB	—	74	24	0.7	0.7	0	—	109.0
1977	—	65	2.60	SB	UP, MF	76	24	0	0	0	1.32	78.2
1980	—	65	2.66	SB	UP, SMP, MF	80	20	0	0	0	1.39	88.0
1991	—	67	2.74	SB	UP, SMP, MF	80	20	0.5	0	0	1.24	85.4
2023	—	67	2.67	SB	UP, SMP	73	25	0	2.0	0	1.23	86.1
2047	—	70	2.65	SB	—	70	30	0	0	0.4	—	85.5
2063	—	70	2.70	SB	—	62	38	0	0	0.4	—	90.1
2066	—	71	—	SB	—	73	25	0.3	1.2	0	—	—
2155	—	75	2.76	SB	—	62	38	0	0	0	—	79.4
2180	—	75	2.74	SB	—	68	31	0	1.0	0	—	78.1
2198	—	76	2.75	SB	—	69	30	0.4	0	0	—	—
2246	—	76	2.73	SB	—	72	27	0.4	0.6	0	—	—
As Nitrided Averages			2.70	SB	UP, SMP,MF	70	29	0.3	0.4	0.1	1.24	88.6
					After Blade Fill Nitriding							
1815	—	55	2.69	SB	UP, NMP	69	31	0	0	0	1.23	—
2020	—	67	—	SB	UP, SMP, MF	74	26	0	0.3	0	1.55	—
After Blade Fill Nitriding Averages						72	29	0	0.15	0	1.39	—
					After Hot Press Bonding							
1400	1079	48	2.70	G, LGC	NUP	14	84	0	1.5	0	1.69	78.0
1404	1083	48	2.77	G, LGC	NUP, 2P, MF	20	79	0	1.3	0	1.48	72.8
1421	1087	48	2.68	G	SMP	0	99	0	1.4	0	1.92	81.3
1744	1204	57	2.68	DG, LGC	2P	46	51	0	3.1	0	1.26	—
1800	1192	55	2.56	G, LGC	—	27	69	0	4.0	0	1.58	—
1952	1206	65	2.63	SB, GC	NUP, 2P	54	42	0	4.2	0	1.60	—
1982	1197	65	2.70	G, LGC	NUP, 2P	14	84	0	2.2	0	1.49	—
2037	1263	67	2.79	G	UP, 2P, MP	0	96	0.3	3.8	0	—	53.0
Average After Hot Pressing			2.68	G, LGC	NUP, 2P	22	75	0	2.7	0	1.57	71.2

LEGEND:

COLOR
- SB = Shiny Black
- DG = Dark Gray
- G = Gray
- GC = Gray Case
- LGC = Light Gray Case

MICROSTRUCTURE
- UP = Uniform Porosity
- NUP = Non Uniform Porosity
- NMP = No Metallic Phase
- SMP = Some Metallic Phase
- MP = Metallic Phase
- 2P = 2nd Phase
- MF = Molding Flaws

TABLE 5.11

Average Values for Various Rotor Blade Ring Process Steps

	No. of Samples	Blade Density	Color	Microstructure	% Phase Composition α	β	Si	Si_2ON_2	SiO_2	Oxygen Content
After nitriding	16	2.70	Shiny Black	Uniform Porosity, Metallic Phase, Molding Flaws	70	29	0.3	0.4	0.1	1.24
After blade fill nitriding	2	2.69	Shiny Black	Uniform Porosity, Metallic Phase	72	29	0	0.15	0	1.39
After hot press bonding	8	2.68	Gray/ light gray case	Non-uniform fine porosity, 2nd phase	22	75	0	2.7	0	1.57

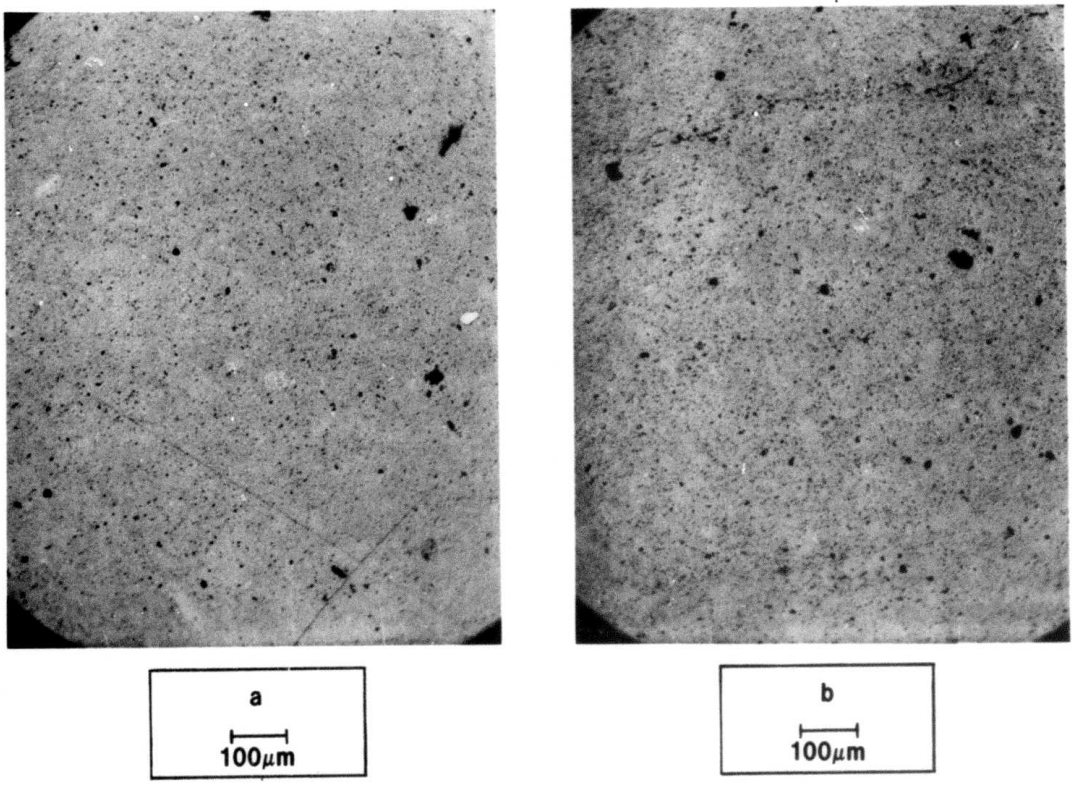

Figure 5.12a,b — Typical Microstructure of RBSN Rotor Blade Rings after: a. Initial Nitriding b. Blade Fill Nitriding

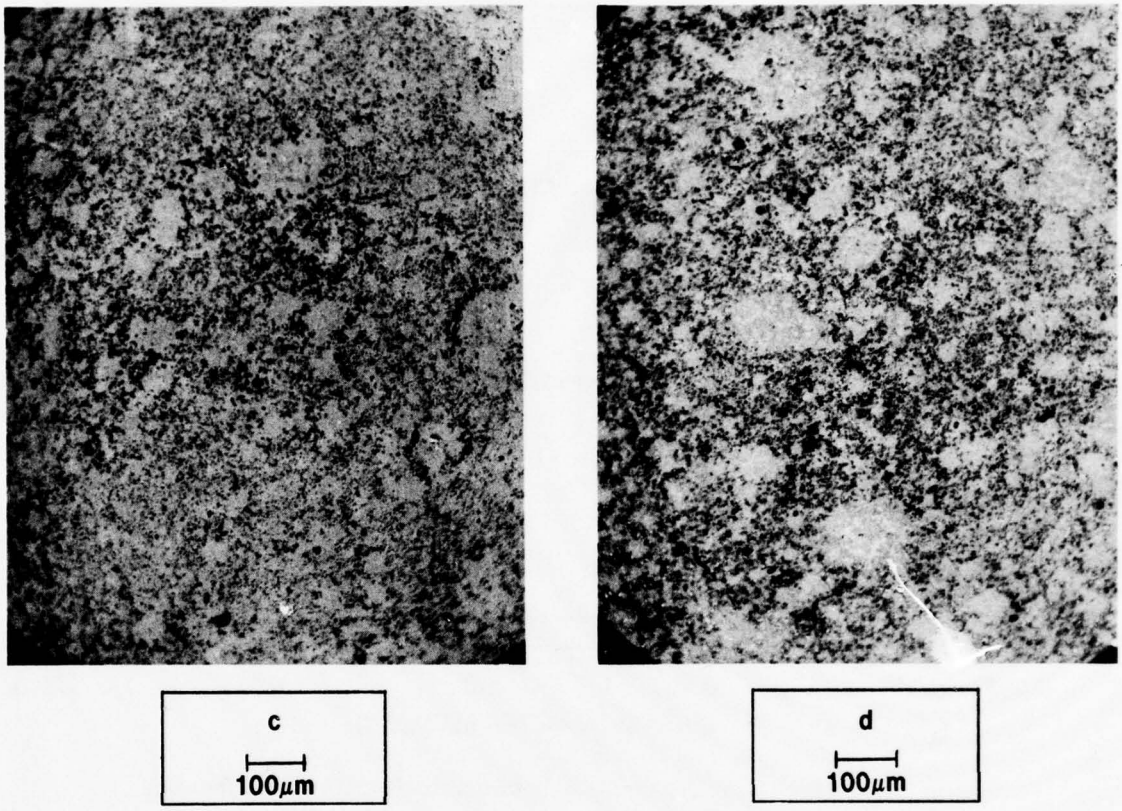

Figure 5.12c,d — Typical Microstructure of RBSN Rotor Blade Rings after: c. Hot Press Bonding (1083) d. Hot Press Bonding (1263)

TABLE 5.12

Hardness Data on Rotor Blades

Blade Ring/ Rotor Number		Hardness*
BR 2023 (as nitrided)		1178
R 1263 (hot press bonded)	Large Grains	1263
	Porous Area	739

*Vickers Hardness, diamond pyramid indentor, 5 Kg load.

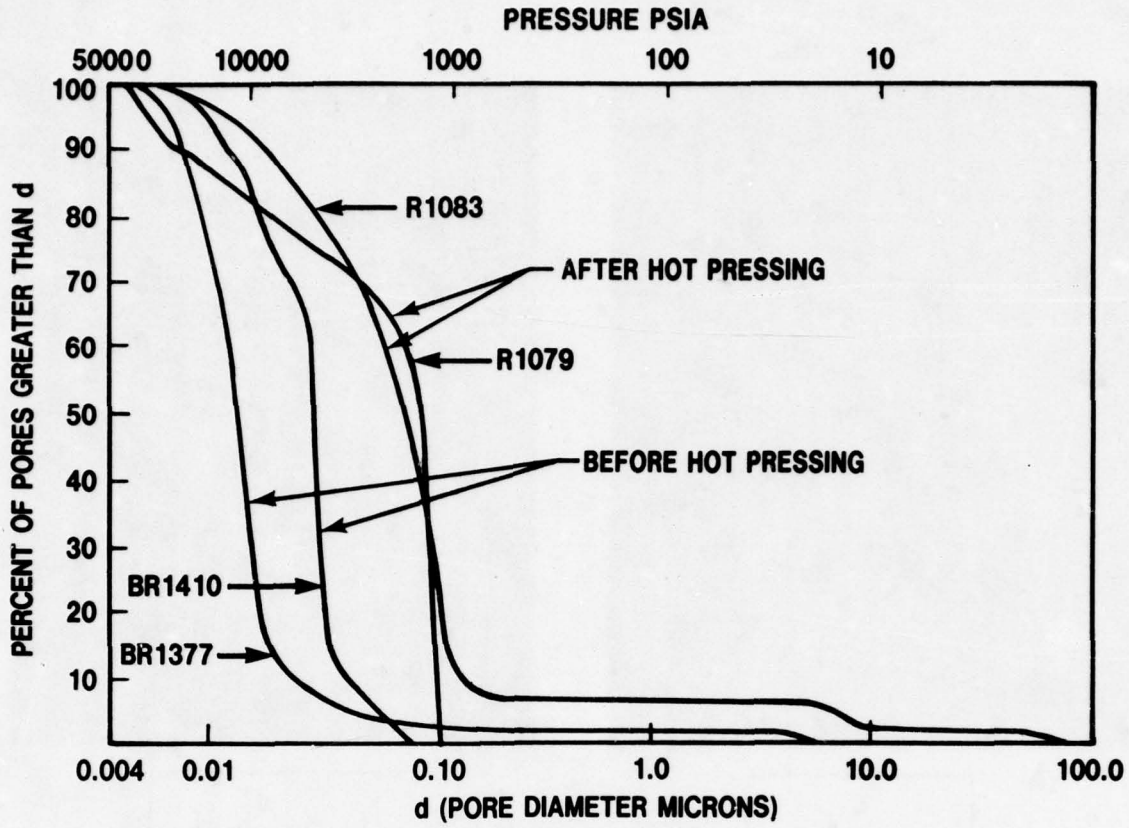

Figure 5.13 — Pore Size Distributions before and after Hot Press Bonding

6.0 ANALYTICAL CODES

Introduction

The development of analytical design codes and the application of these analytical techniques to the duo-density silicon nitride turbine rotor have been ongoing activities in the Ford/DARPA Brittle Materials Design Program and were continued in the Ford/ERDA program. This technology is an important part of the systems approach employed in this project for the development of high temperature gas turbine engines. The previous report[11] presented the analytical techniques used to statistically analyze data in addition to a life prediction method used to estimate the time dependent reliability of ceramic turbine rotors.

During this reporting period work continued on developing statistical tools, proof testing and life prediction analysis as applied to the duo-density silicon nitride turbine rotor.

Summary

Because strength assessment of ceramics is treated statistically, a procedure was prepared for determining whether statistically significant differences exist between two sets of data, known as 'Hypothesis Testing'. The test was applied to the duo-density turbine rotor and showed that blade strength does deteriorate after the press-bonding operation.

Use of proof-testing as a potential means of enhancing accuracy of life predictions was theoretically investigated. Analytical relations were derived for predicting the survival probability of a proof-tested component, and a procedure was outlined for maximizing the effectiveness of a proof-test.

Life-prediction relations derived in the previous report[11] were applied to the first-stage turbine rotor. Several disk contour modifications were studied as means of improving the life of the rotor under the ARPA duty cycle. The study showed that for given design constraints (space, inertia, etc.) and using material utilization as the criterion, the optimum disk configuration derived on the basis of fast fracture (time independent) mode of failure differed from the configuration derived from life considerations when the material is subject to static fatigue.

6.1 HYPOTHESIS TESTING

The development of statistical tools for the analysis of data continued during this reporting period. Methods to estimate Weibull parameters continue to be investigated while the bulk of the effort was in the field of hypothesis testing.

A very common problem encountered in dealing with statistical information is the determination of significance in the data. For example: given a change in a material process parameter, is there a significant change in the characteristic strength or the Weibull slope. This question recognizes that two independent statistical samples from the same distribution will never be exactly the same but that there are identifiable limits as to how much of a difference can be expected. Hypothesis testing is a procedure for drawing simple conclusions from observed data. It is a widely used and standardized convention and has been well documented[16-19].

Hypothesis tests may be either parametric or nonparametric in nature. Nonparametric or "distribution-free" tests[19] do not require the assumption that the form of the population distribution is known. When the underlying population distribution is known, a parametric test, more powerful than the nonparametric may be used. Parametric procedures which assume distributions such as the normal, the exponential, the log-normal and the Weibull exist in the literature.

Certain problems exist in the application of hypothesis testing. A hypothesis test is a point estimate and does not, by itself, provide a measure of the test uncertainty. Two types of errors may be committed in an hypothesis test. The first, the Type I error, is to reject the test hypothesis when in fact it is true. The second, the Type II error, is to accept the test hypothesis when in fact it is false. The probability of committing Type I or Type II errors are represented by α and β, respectively. The test sample size, N, used in the test and the probabilities α and β are not independent; any two may be specified, thus fixing the third. Usually, the test sample size is fixed by the practicalities of testing and α, often called the significance level, is set at some small probability such as 0.05 or 0.10. Information as to the level of β must accompany the results of the hypothesis test in order to provide a complete test. It is possible, particularly with small sample sizes, to conduct a test in which it is virtually impossible to detect a difference between two samples when in fact the difference exists. In this case the value of β is large. An Operating Characteristic (OC) Curve for a test does show the discriminating ability of the test but not in a straight forward manner. A more readily understood method for describing the uncertainty in a test is the use of the confidence interval type hypothesis test[20]. The width of the confidence interval calculated for the test is a measure of the quality of the test. Tests based on small sample sizes will exhibit very wide confidence intervals because of their high uncertainty.

Because the Weibull distribution has been chosen to characterize the strength of ceramic materials and the reliability of ceramic components, Weibull based hypothesis tests were studied and an interactive computer program was written to analyze data. Thoman and Bain[21] and McCool[22 and 23] have developed two simple hypothesis tests for the Weibull slope and the characteristic value. The critical values for the test statistics were found by Monte Carlo sampling and procedures were established for determining the test confidence intervals. A limitation of these tests is the assumption that both samples have the same size. When the samples are unequal, the actual values of α and β are changed and the degree of change is not known. The effects of unequal sample size should be investigated. The computer program, S.DIFF, which performs the hypothesis test is listed in Appendix I.

As an example, the rotor blade bend test data for the B-48 nitriding, reported in Section 5.4, was analyzed to determine if there was a statistically significant difference in blade strength as a result of hot press bonding. The blades from as-nitrided blade rings showed a characteristic breaking load of 89.8 pounds and a Weibull slope of 9.1, based on a sample of 52. A sample of 60 blades which had been press bonded had a characteristic load of 77.0 pounds and a Weibull slope of 6.9. The hypothesis test, at the 10 percent significance level, showed a statistically significant difference in both the Weibull slope and the characteristic value, indicating that the blade quality was degraded during the press-bonding operation. Details of the test are shown in Appendix II.

6.2 PROOF TESTING

Introduction

In the last report[11] equations were developed for predicting the time-dependent reliability of a ceramic component under a service load when the material is subject to so-called static fatigue resulting from subcritical crack growth.

In the above approach, the size of the strength controlling flaw and its distribution are inferred by way of fracture mechanics relations from statistical strength data. For reasons of economics these data are generated from relatively small (~ 30) sample sizes. Consequently, uncertainty exists as to the accuracy of predictions based on such limited information. Often, even less is known of the material strength in fabricated, geometrically complex structures, such as a turbine rotor, where the fabrication process itself may amplify the variability in strength properties. These difficulties may be overcome and the accuracy of predictions greatly enhanced by proof-testing of individual structures prior to service.

The purpose of proof-testing is to eliminate, by destructive testing, the occasional weak components and thus enhance the survival probability or strength of the truncated population of the components. In effect, proof testing establishes an upper limit on the allowable sizes of strength controlling flaws within the structure and should therefore improve the structure's probability of attaining specified life under a given loading condition.

Analysis

Let us consider a turbine rotor and assume that it is to withstand a service load for time τ with a probability of survival R_a. The load magnitude can either be constant or it may vary with time. Using an appropriate equation derived in the last report[11] an estimate can be obtained of the time to failure $(t_f)_{R_a}$ corresponding to the specified reliability R_a, or conversely one can compute the probability of attaining the desired life τ. Both R_a and τ are not likely to be satisfied simultaneously.

Let R be the probability of attaining life $\tau > (t_f)_{R_a}$ under a specified loading condition. Then using Weibull's notation

$$R = \exp\left\{-\sum_{i=1}^{N}\left(\frac{\tau}{t_{\theta_i}}\right)^{\frac{m}{n-2}}\right\} \tag{1}$$

or solving for τ

$$\left[\frac{\ell n\,\frac{1}{R_a}}{\sum_{i=1}^{N}\left(\frac{1}{t_{\theta_i}}\right)^{\frac{m}{n-2}}}\right]^{\frac{n-2}{m}} = (t_f)_{R_a} < \tau = \left[\frac{\ell n\,\frac{1}{R}}{\sum_{i=1}^{N}\left(\frac{1}{t_{\theta_i}}\right)^{\frac{m}{n-2}}}\right]^{\frac{n-2}{m}} \tag{2}$$

m is the Weibull slope and n is the crack propagation exponent. N is the number of uniformly stressed finite elements into which the rotor is subdivided for the purpose of analysis the $t_{\theta i}$ the characteristic time to failure of an individual rotor element at specified service loading and is given by[11]

$$t_{\theta_i} = \frac{2\alpha_{oi}}{(n-2)\,Vc_i}\left(\frac{S_\theta}{\sigma_1}\right)_i^{n-2} = \left(\frac{B}{\sigma_1^2}\right)_i\left(\frac{S_\theta}{\sigma_1}\right)_i^{n-2} \tag{3}$$

where

$$B_i = \frac{2}{(n-2)\, Y_i^2 A_i K_{IC_i}^{n-2}}$$

or expressed in terms of static fatigue strength parameters[24]

$$t_{\theta_i} = \frac{(\bar{S}_{\theta_i})^{n+1}_{t=o}}{\sigma_{1i}^{n}\,(n+1)\,\sigma}$$

$\left(\bar{S}_{\theta_i}\right)_{t=o}$ is the characteristic strength of rotor element evaluated at time t=0 at a constant stress rate $\dot{\sigma}$.

The unequality in equation (2) is satisfied only if $R<R_a$ and therefore in order to increase the probability of attaining the desired life τ to R_a, the strength of the rotor must be correspondingly increased. This can be achieved either through redesign or as we mentioned earlier by way of proof-testing according to the relation

$$R_\alpha = \frac{R}{R_p} \tag{4}$$

when R_p is the survival probability at proof test loading condition and is equal

$$R_p = \exp\left\{-\sum_{i=1}^{N}\left(\frac{\sigma_{1p}}{S_{\theta_p}}\right)_i^m\right\} \tag{5}$$

σ_{1pi} is the max principal tensile stress in a rotor element at proof test and $S_{\theta pi}$ is the characteristic strength of the element again at proof test conditions. Combining (1), (4) and (5)

$$R_\alpha = \prod_{i=1}^{N} \exp\left\{-\left[\left(\frac{\tau}{t_{\theta_i}}\right)^{\frac{m}{n-2}} - \left(\frac{\sigma_{1p}}{S_{\theta_p}}\right)_i^m\right]\right\} \tag{6}$$

or

$$\ell n\,\frac{1}{R_\alpha} = \sum_{i=1}^{N} \ell n\,\frac{1}{R_{\alpha i}} = \sum_{i=1}^{N}\left[\left(\frac{\tau}{t_{\theta_i}}\right)^{\frac{m}{n-2}} - \left(\frac{\sigma_{1p}}{S_{\theta_p}}\right)_i^m\right] \tag{7}$$

From the last equation one concludes that maximum benefit is realized from the proof test in terms of increased reliability when the distribution of reliabilities of individual rotor elements at proof test conditions approaches the distribution of the time dependent reliabilities at the specified time τ, i.e.

$$R_\alpha = \sum_{i=1}^{N} R_{\alpha i} \longrightarrow 1.0 \quad \text{when} \quad \left(\frac{\sigma_{1p}}{S_{\theta_p}}\right)_i \longrightarrow \left(\frac{\tau}{t_{\theta_i}}\right)^{\frac{1}{n-2}}$$

It is doubtful that this condition can be satisfied identically throughout the structure. Generally, an iterative process will be required to zero in on the appropriate proof-test load distribution that will result in the desired reliability level and that will be both practical and economical.

6.3 TURBINE DISK REDESIGN

Introduction

In the last report[11] a technique was outlined for predicting the life of a ceramic component under stress in the presence of subcritical crack growth (S.C.G.). In the current reporting period, this technique was applied to a duo-density rotor using estimated material characteristics to see whether modifications to the rotor disk design based on fast fracture considerations could improve rotor reliability for 25 hours of operation at maximum conditions. In order to perform the analysis, it was necessary to estimate strength and crack propagation parameters from preliminary and rather limited hot pressed ceramic nitride test data.

The analysis revealed that the disk configuration as originally designed for fast fracture failure was unsatisfactory when time-dependent failure modes were considered. Based on earlier work[24] a parametric study was conducted to find out what improvements, if any, in time-dependent reliability were attainable by way of disk contour redesigns where given design constraints. The results of this analysis indicated that a disk with a thicker throat was beneficial in terms of lifetime reliability.

Discussion

Disk redesigns studied were limited in scope so that any new disk configuration could be made from the existing hot pressing blank with minimal changes to the existing machining tools and so that existing blade tooling and rotor mounting hardware could be retained. Two disk contour modifications were investigated within these constraints. The first which is shown in Figure 6.1 has a throat thickness

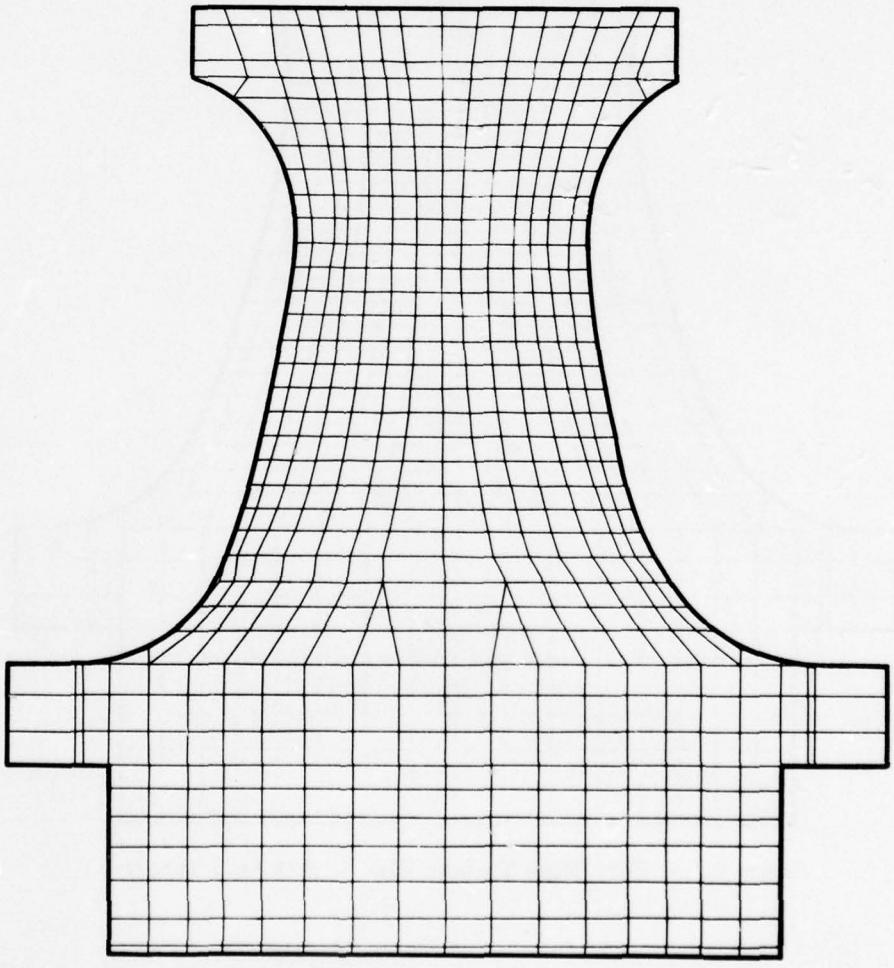

Figure 6.1 — First Stage Turbine Disk — 0.40 inch Throat

increased from .300 inch to .400 inch. The second with a throat thickness of .480 inch is shown in Figure 6.2. As will be shown later, both disk changes give a stress reduction in the throat without a significant increase in the stress levels in the disk bore.

Figures 6.3, 6.4 and 6.5 respectively show the calculated temperature contours in the .300, .400 and .480 inch throat disks at 2500°F TIT and 100% mechanical speed. Since the disk design modifications do not significantly alter the original disk contour geometry, (i.e. surface area) no major change in thermal loading is expected in the new rotor disk configurations for the same operating conditions. Consequently, the thermal boundary conditions calculated for the .300 inch disk were used in each instance.

The calculated maximum principle tensile stress contours for the original design and for the two modified designs at the full power loading (2500°F TIT and 100% speed) are shown in Figures 6.6, 6.7 and 6.8. A summary of maximum stress levels in the disk throat and bore areas for all three configurations is shown in Table 6.1.

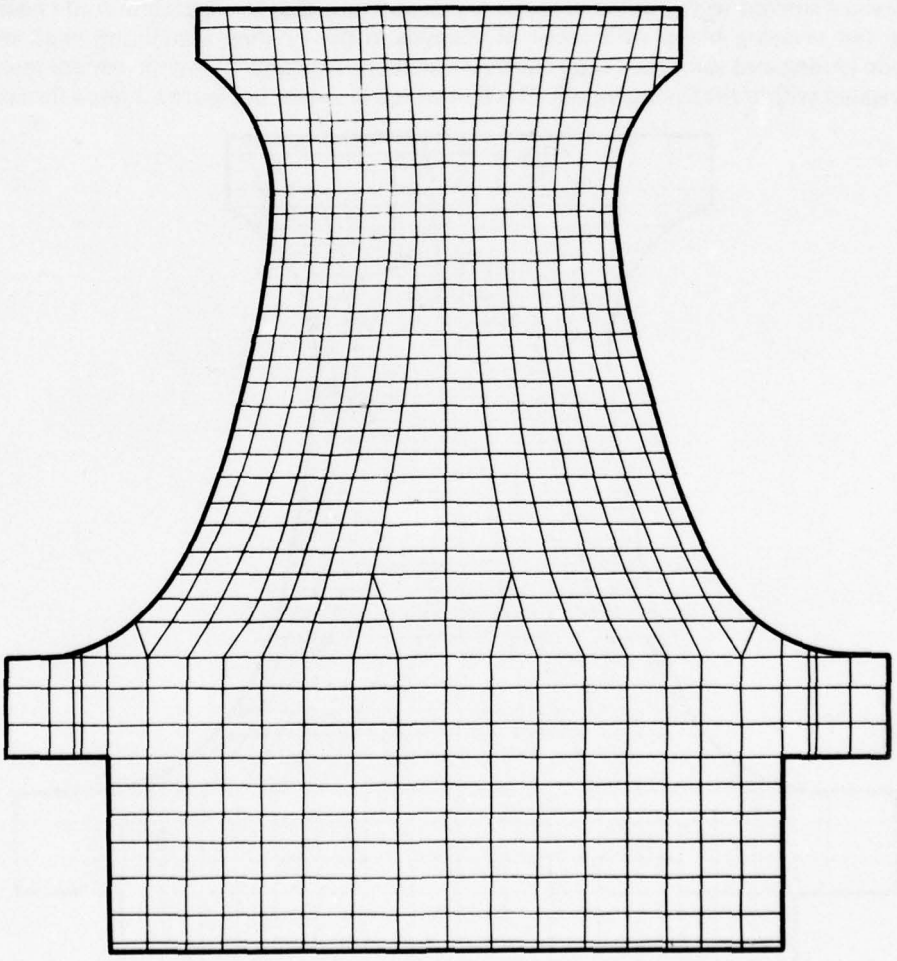

Figure 6.2 — First Stage Turbine Disk — 0.48 inch Throat

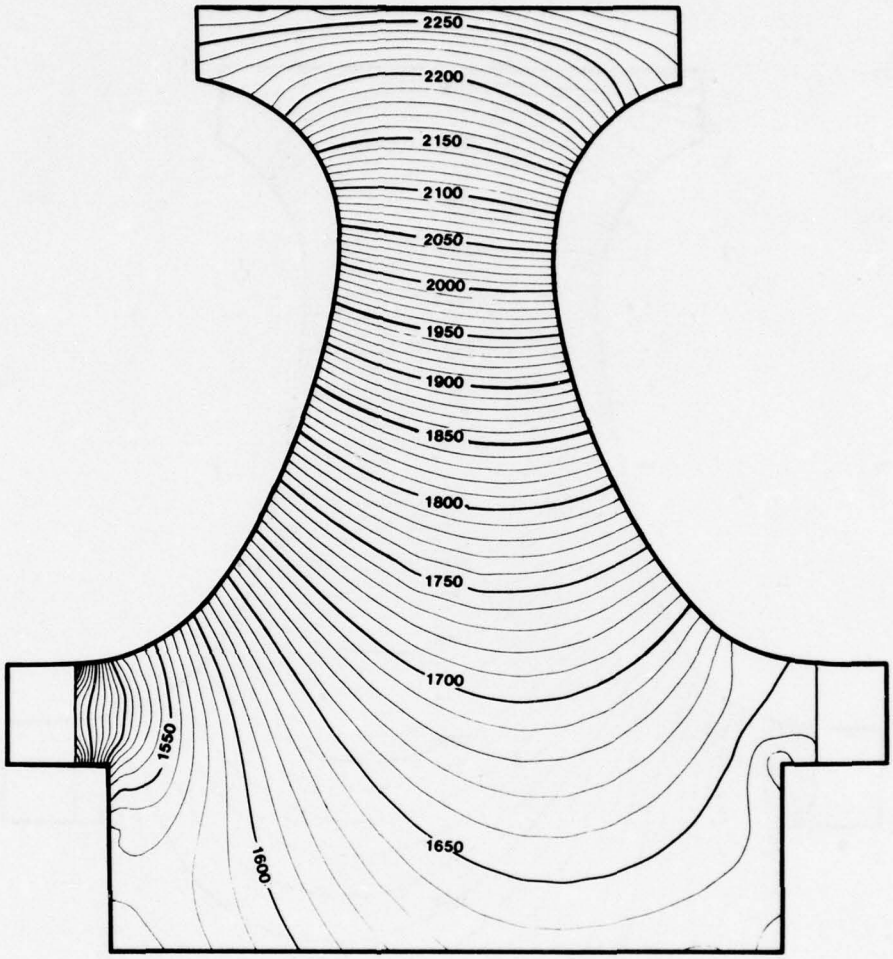

Figure 6.3 — First Stage Turbine Disk (0.30 inch Throat) Temperature (°F) Contours for 2500°F T.I.T. and 100% Speed

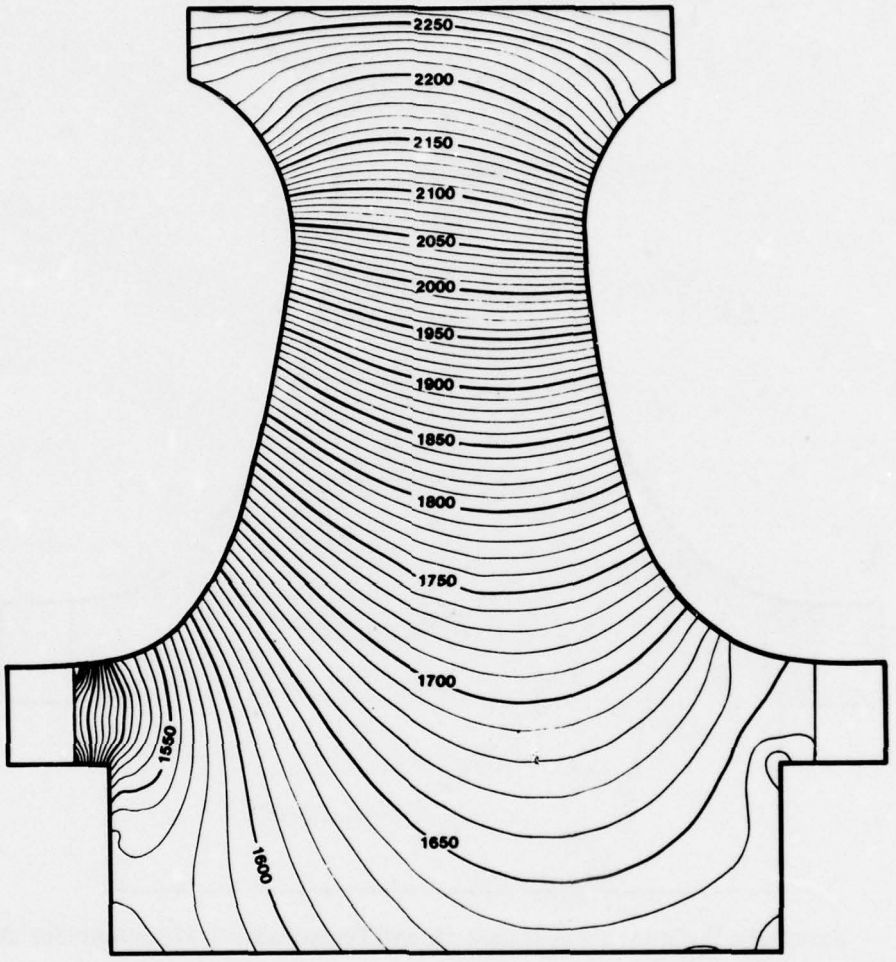

Figure 6.4 — First Stage Turbine Disk (0.40 inch Throat) Temperature (°F) Contours for 2500°F T.I.T. and 100% Speed

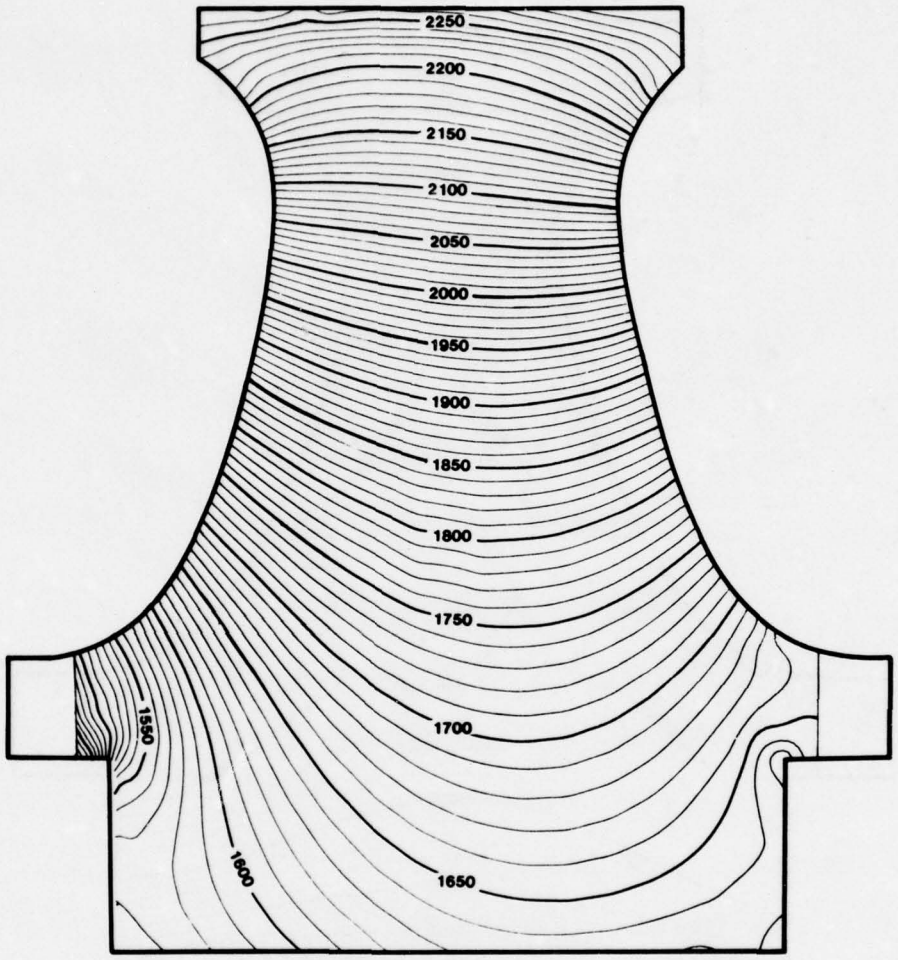

Figure 6.5 — First Stage Turbine Disk (0.48 inch Throat) Temperature (°F) Contours for 2500°F T.I.T. and 100% Speed

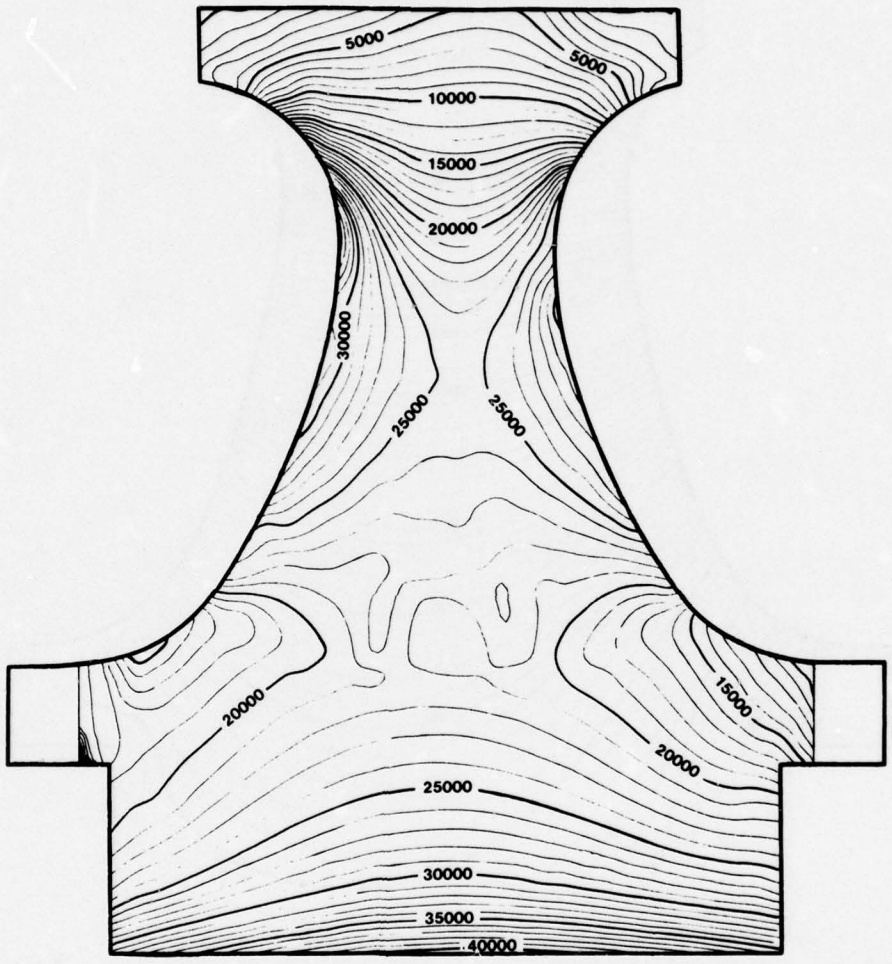

Figure 6.6 — Maximum Principle Tensile Stresses (Psi) for the First Stage Turbine Disk (0.30 inch Throat) at 2500°F T.I.T. and 100% Speed

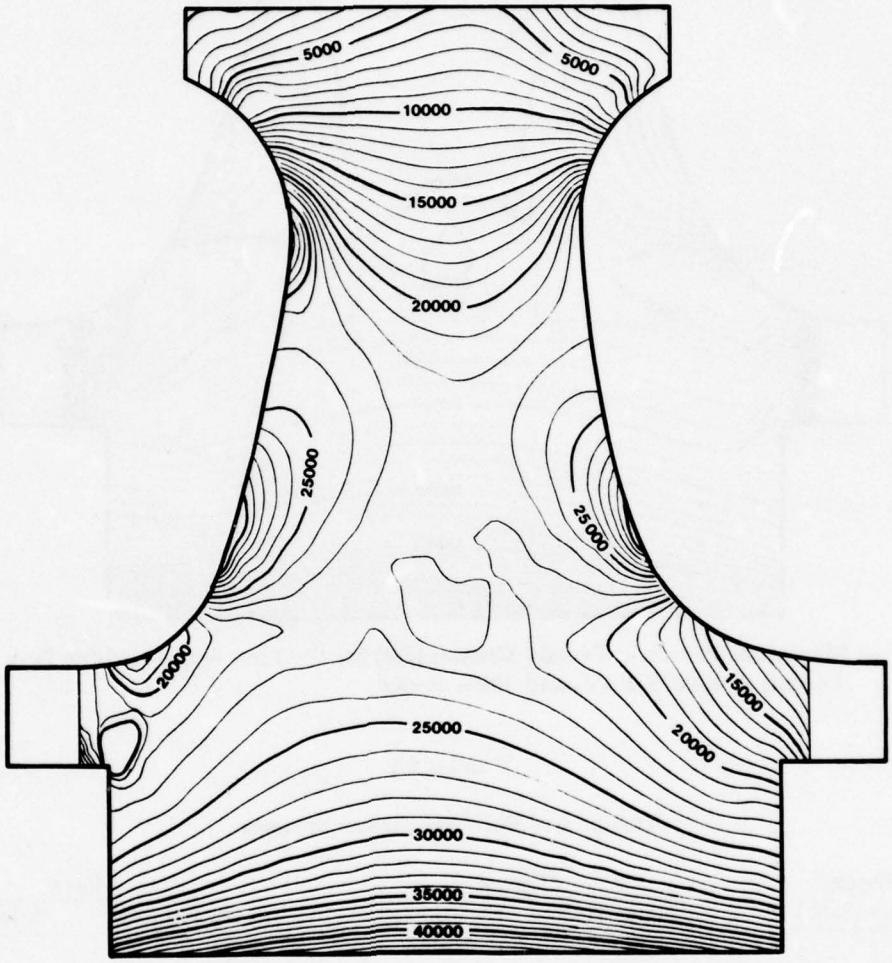

Figure 6.7 — Maximum Principle Tensile Stresses (Psi) for the First Stage Turbine Disk (0.40 inch Throat) at 2500°F T.I.T. and 100% Speed

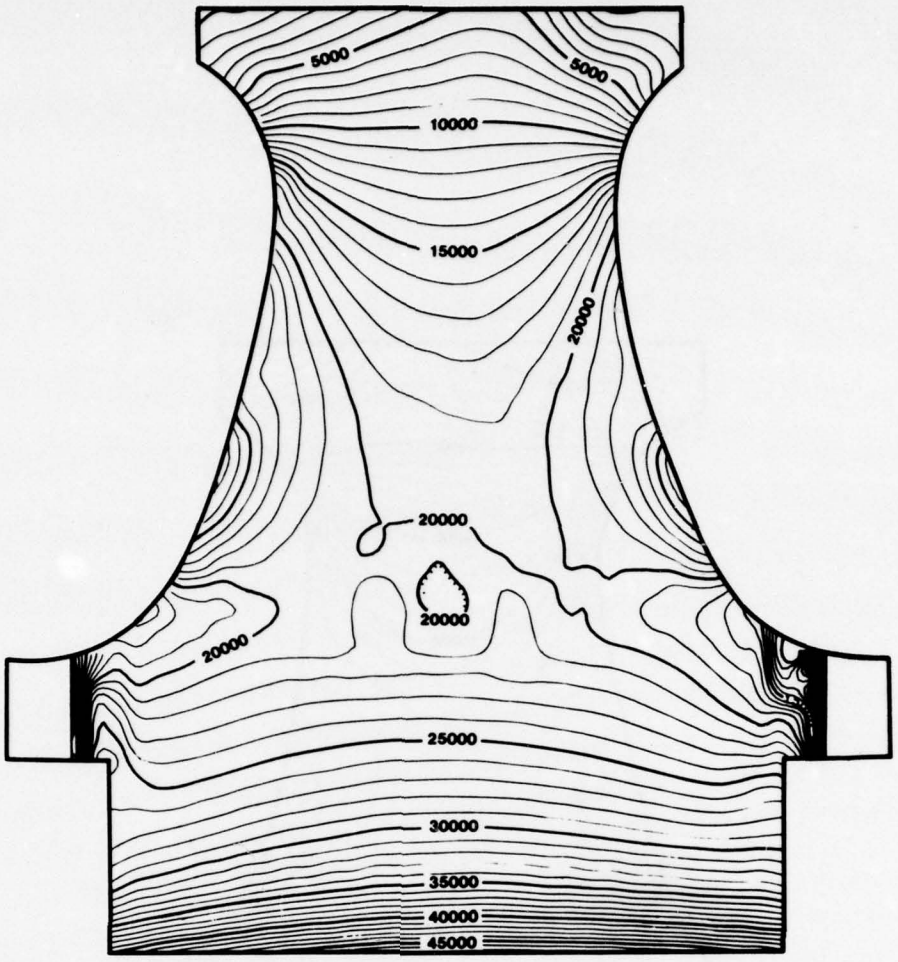

Figure 6.8 — Maximum Principle Tensile Stresses (Psi) for the First Stage Turbine Disk (0.48 inch Throat) at 2500°F T.I.T. and 100% Speed

TABLE 6.1

Throat and Bore Maximum Stresses

Disk Throat Thickness (inch)	Throat		Bore	
	Stress (psi)	% Reduction	Stress (psi)	% Increase
.300 (original)	34,000	—	40,000	—
.400	28,000	18%	44,000	10%
.480	20,000	41%	47,000	18%

Table 6.2 lists the thermal and physical properties of the HPSN and injection molded RBSN disk/blade materials that were used in the analysis. Hot pressed silicon nitride strength data for the study was estimated from preliminary material modulus of rupture test data.

The estimated strength data for the hub material is shown in Figure 6.9. It is based on limited MOR tests at various stress rates of "A" size bars of hot pressed silicon nitride hub material with 3½% MgO hot pressing additive. The solid line represents an estimate of material fast fracture strength while the broken lines represent a lower, static fatigue strength due to subcritical crack growth. The Weibull modulus which defines material strength scatter, m, was assumed independent of temperature for fast

fracture failure modes. The subcritical crack growth exponent, n, was estimated from preliminary material test data as also shown in Figure 6.9.

Discussion

In designing the original, .300 inch throat rotor, its geometry was optimized to produce almost the same failure probabilities at full power loading for the bore and throat regions with the higher bore stresses being offset by the larger volume of the throat region.

By increasing the throat thickness, the stresses and thus the fast fracture failure probabilities in that region have been reduced. Since the hub configuration remains unaltered the stresses in that region have increased and the reliability reduced enough to lower the fast fracture reliability of the overall

TABLE 6.2

Material Properties

	Temp. °F	Young's Modulus x10⁶ psi	Poisson's Ratio	Shear Modulus x10⁶ psi	Coefficient of Thermal Expansion in/in/°F x10⁻⁶
3.5% MgO Hot-Pressed Si_3N_4 (Hub)	78	43.5	.272	17.1	0.95
	500	44.1	.260	17.5	1.23
	1000	44.3	.251	17.7	1.54
Density = 3.18 gm/cm³	1500	43.5	.250	17.4	1.74
	2000	42.6	.246	17.1	1.89
	2500	41.3	.237	16.7	2.01
Injection Molded Si_3N_4	78	25.0	.187	10.5	.82
	500	24.7	.178	10.5	1.07
Density = 2.70 gm/cm³	1000	24.1	.164	10.3	1.46
	1500	23.3	.152	10.1	1.62
	2000	22.2	.140	9.8	1.70
	2500	21.5	.128	9.5	1.73

	Temp. °F	Thermal Conductivity Btu/hr-ft-°F	Specific Heat Btu/lb-°F
3.5% MgO Hot-Pressed Si_3N_4 (Hub)	78	17.0	.178
	500	15.0	.227
Density = 3.18 gm/cm³	1000	13.0	.263
	1500	11.0	.289
	2000	9.2	.328
	2500	8.0	.325
Injection Molded Si_3N_4	78	11.4	.150
	500	10.4	.230
Density = 2.70 gm/cm³	1000	8.1	.270
	1500	6.6	.280
	2000	5.5	.290
	2500	4.6	.300

rotor. Thus by trading off the reliabilities in these two regions, one can arrive at a rotor configuration that will be optimum from the standpoint of life considerations. This configuration will be different than that arrived at from the fast fracture point of view. Similarly as in the fast fracture approach an optimum configuration is defined as one for which the failure probabilities for the two regions are equalized at the time of failure. In this case this is represented by the .40 throat thickness which as seen from Table 6.3, gives the maximum probability of attaining the 25-hour life at full load.

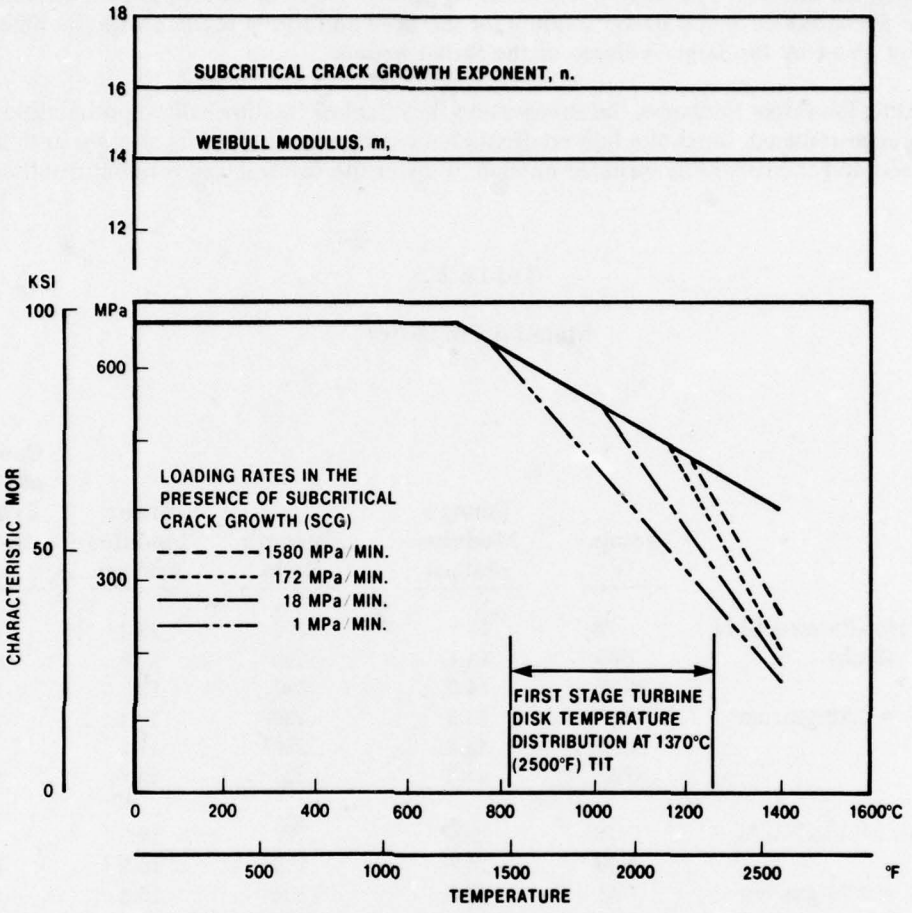

Figure 6.9 — Estimated Strength Characteristics of Rotor Hub Hot Pressed Silicon Nitride Used to Check Out Analytical Codes

TABLE 6.3

Fast Fracture and Time Dependent Reliability Estimates for the First Stage Turbine Disk (exluding Blades) 2500°F TIT and 100% Speed

Throat Thickness (Inches)	SCG Threshold Temperature (+) °C, °F	Reliability (Fast Fracture)	Reliability (Time Dependent, SCG) (25 Hours)	Critical SCG Disk Region
.300	770°, 1420°	.99787	.29156	Throat
.400	770°, 1420°	.99647	.82042	Throat
.480	770°, 1420°	.98986	.60986	Bore

(+): Threshold temperature for a loading rate of 1 MPa/min. (8.7 ksi/hr.) on the "A" size MOR test bar.

7.0 REFERENCES

1. McLean, A. F., Fisher, E. A., Harrison, D. E., "Brittle Materials Design, High Temperature Gas Turbine", AMMRC-CTR-72-3, Interim Report, March, 1972.

2. McLean, A. F., Fisher, E. A., Bratton, R. J., "Brittle Materials Design, High Temperature Gas Turbine", AMMRC-CTR-72-19, Interim Report, September, 1972.

3. McLean, A. F., Fisher, E. A., Bratton, R. J., "Brittle Materials Design, High Temperature Gas Turbine", AMMRC-CTR-73-9, Interim Report, March, 1973.

4. McLean, A. F., Fisher, E. A., Bratton, R. J., "Brittle Materials Design, High Temperature Gas Turbine", AMMRC-CTR-73-32, Interim Report, September, 1973.

5. McLean, A. F., Fisher, E. A., Bratton, R. J., "Brittle Materials Design, High Temperature Gas Turbine", AMMRC-CTR-74-26, Interim Report, April, 1974.

6. McLean, A. F. Fisher, E. A., Bratton, R. J., "Brittle Materials Design, High Temperature Gas Turbine", AMMRC-CTR-74-59, Interim Report, September, 1974.

7. McLean, A. F., Fisher, E. A., Bratton, R. J., Miller, D. G., "Brittle Materials Design, High Temperature Gas Turbine", AMMRC-CTR-75-8, Interim Report, April, 1975.

8. McLean, A. F., Fisher, E. A., Bratton, R. J., Miller, D. G., "Brittle Materials Design, High Temperature Gas Turbine", AMMRC-CTR-75-28, Interim Report, September, 1975.

9. McLean, A. F., Baker, R. R., Bratton, R. J., Miller, D. G., "Brittle Materials Design, High Temperature Gas Turbine", AMMRC-CTR-76-12, Interim Report, April, 1976.

10. McLean, A. F., Baker, R. R., "Brittle Materials Design, High Temperature Gas Turbine", AMMRC-CTR-76-31, Interim Report, October, 1976.

11. McLean, A. F., Fisher, E. A., "Brittle Materials Design, High Temperature Gas Turbine", AMMRC-CTR-77-20, Interim Report, June, 1977.

12. Katz, R. N., Gazza, G. E., "Grain Boundary Engineering and Control in Nitrogen Ceramics", Proceedings of Nato Advanced Study Institute on Nitrogen Ceramics, University of Kent, Canterbury, U.K., August 1976, p. 417.

13. Lange, F. F., Terwilliger, G. R., "Fabrication and Properties of Silicon Compounds" Naval Air Systems Command, Contract N0019-72-C-0278, Final Report, 1973.

14. Greskovich, C., Prochazka, S., Rosolowski, J. H., "Basic Research on Technology Development for Sintered Ceramics", Air Force Materials Laboratory, Contract AFML-TR-76-179, Final Report, November 1976.

15. Priest, H. F., Priest, G. L., Gazza, G. E., "Sintering of Si_3N_4 Under High Nitrogen Pressure", Journal of American Ceramic Society, 1977 page 81.

16. Mann, N. R., Schafer, R. E. and Singpurwalla, N. D.; Methods for Statistical Analysis of Reliability and Life Data; John Wiley and Sons, New York, 1974.

17. Benjamin, J. R. and Cornell, C. A.; Probability, Statistics and Decision for Civil Engineers; McGraw-Hill Book Co., 1970.

18. Davies, O. L. and Goldsmith, P. L.; Statistical Methods in Research and Production; Oliver and Boyd, Tweeddale Court, Edinburgh, 1976.

19. Siegel, S.; Nonparametric Statistics; McGraw-Hill Book Co., New York, 1956.

20. Natrella, M. G.; "The Relation Between Confidence Intervals and Tests of Significance," The American Statistician, v. 14, No. 1, February, 1960, p. 20.

21. Thoman, D. R. and Bain, L. J.; "Two Sample Test in the Weibull Distribution," Technometrics, v. 11, No. 4, p. 805.

22. McCool, J. I.; "Evaluating Weibull Endurance data by the Method of Maximum Likelihood," ASLE Transactions, 13, p. 189.

23. McCool, J. I.; "Multiple Comparison for Weibull Parameters," IEEE Transactions on Reliability, v. R-24, No. 3, p. 186.

24. Paluszny A., Nicholls P. F, Predicting time-dependent reliability of ceramic rotors" presented at the 5th Army Materials Technology Conference, "Ceramics for High Temperature Applications — II," Newport, Rhode Island, March 21-25, 1977.

APPENDIX I

FORTRAN LISTING OF HYPOTHESIS TESTING PROGRAM S. DIFF

```
 S.DIFF :

10**FTN S.DIFF=H.DIFF(OPTZ,NOGO,CORE=24K)
20C     PROGRAM WRITTEN BY RICHARD A. JERYAN, FORD MOTOR COMPANY
30C     GAS TURBINE RESEARCH DEPARTMENT, DEARBORN MI 48121
40C     (REF.: THOMAN AND BAIN; TECHNOMETRICS, V.11, P.805.)
50C     LAST REVISION 8/10/77
60 DIMENSION PPA(100), PPB(100)
70 REAL M1,M2,N1,N2,LBA,LBB,LBTHETAR
80 600 FORMAT(//'DO YOU WANT TO RUN ANOTHER TEST? (YES=1,NO=0)')
90 WRITE (6,10)
100 10 FORMAT(/'THIS PROGRAM WILL DETERMINE IF A STATISTICALLY
110& SIGNIFICANT'/'DIFFERENCE EXISTS BETWEEN TWO WEIBULL
120& DISTRIBUTIONS'/'BASED ON A TWO-SIDED TEST AT A 0.10
130& SIGNIFICANCE LEVEL'//'ENTER WEIBULL SLOPE, CHARACTERISTIC
140& VALUE AND SAMPLE SIZE')
150 11 WRITE (6,12)
160 12 FORMAT(//'SAMPLE 1:')
170 READ (5,500) M1,THETA1,N1
180 WRITE (6,20)
190 20 FORMAT (/'SAMPLE 2:')
200 READ (5,500) M2,THETA2,N2
210 N = MIN0(N1,N2)
220 IF(N.LT.5) GO TO 5000
230 IF(N.GT.100) GO TO 5003
240 IF(AMAX0(N1,N2)/AMIN0(N1,N2).LT.1.50) GO TO 30
250 WRITE (6,25)
260 25 FORMAT (/'***WARNING*** THERE IS CONSIDERABLE DIFFERENCE
270& BETWEEN THE'/'SAMPLE SIZES WHICH MAY CAUSE SOME ERROR IN
280& THIS TEST')
290C
300C     A: TEST STATISTIC FOR SHAPE PARAMETER RATIO
310C     B: TEST STATISTIC FOR SCALE PARAMETER RATIO
320C
330 30 A = M1/M2
340     C = THETA1/THETA2
350     B = ((M1+M2)/2.)*ALOG(C)
360C
370C     READ IN THE 95% PERCENTAGE POINTS TO DETERMINE THE
380C     95% CONFIDENCE INTERVALS FOR A AND B
390C
400 DATA PPA/1.0,1.0,1.0,1.0,2.765,2.465,2.246,2.093,1.983,1.897,
410& 1.829,1.774,1.727,1.688,1.654,1.624,1.598,1.574,1.553,1.534,
420& 1.519,1.501,1.487,1.473,1.461,1.449,1.439,1.428,1.419,1.409,
430& 1.401,1.393,1.380,1.378,1.372,1.365,1.359,1.353,1.348,1.342,
440& 1.337,1.332,1.328,1.323,1.319,1.314,1.310,1.306,1.303,1.299,
450& 1.296,1.292,1.289,1.285,1.282,1.279,1.277,1.274,1.271,1.268,
460& 1.266,1.263,1.261,1.258,1.256,1.253,1.251,1.249,1.247,1.245,
470& 1.243,1.241,1.239,1.237,1.235,1.233,1.232,1.230,1.229,1.227,
480& 1.226,1.224,1.223,1.221,1.220,1.218,1.217,1.215,1.214,1.212,
490& 1.211,1.209,1.208,1.207,1.206,1.204,1.203,1.202,1.200,1.199/
500 DATA PPB/1.,1.,1.,1.,1.670,1.404,1.215,1.086,0.992,0.918,
510& .860,.811,.770,.734,.704,.676,.654,.631,.611,.593,
520& .577,.561,.548,.534,.522,.510,.500,.490,.481,.472,
530& .464,.455,.448,.441,.434,.427,.421,.415,.410,.404,
540& .399,.394,.389,.384,.380,.376,.372,.367,.364,.360,
550& .356,.353,.350,.346,.343,.340,.337,.334,.331,.328,
560& .326,.323,.320,.317,.315,.313,.311,.308,.306,.304,
570& .302,.299,.297,.295,.293,.291,.290,.288,.286,.284,
580& .282,.281,.279,.278,.276,.274,.273,.271,.270,.268,
590& .267,.265,.264,.263,.262,.260,.259,.258,.256,.255/
600 500 FORMAT (V)
610C
620C     90% INTERVAL FOR A: (LBA*A, UBA*A)
630C     90% INTERVAL FOR C: (LBTHETAR, UBTHETAR)
```

```
*
640C
650C     TO BE CONSERVATIVE, CONDUCT TEST BASED ON THE
660C     SMALLER SAMPLE SIZE
670C
680 LBA = 1./PPA(N)
690 UBA = PPA(N)
700 LBB = -PPB(N)
710 UBB = PPB(N)
720 IF(A.LT.LBA) GO TO 50
730 IF(A.GT.UBA) GO TO 70
740 WRITE (6,40)
750 40 FORMAT (/' 1. THERE IS NO STATISTICALLY SIGNIFICANT
760& DIFFERENCE BETWEEN'/'     THE WEIBULL SLOPES')
770 GO TO 90
780 50 WRITE (6,60)
790 60 FORMAT(/' 1. THE WEIBULL SLOPE OF SAMPLE 1 IS SIGNIFICANTLY
800& SMALLER'/'     THAN THE WEIBULL SLOPE OF SAMPLE 2')
810 GO TO 90
820 70 WRITE (6,80)
830 80 FORMAT(/' 1. THE WEIBULL SLOPE OF SAMPLE 1 IS SIGNIFICANTLY
840& GREATER'/'     THAN THE WEIBULL SLOPE OF SAMPLE 2')
850 90 IF(B.LT.LBB) GO TO 110
860 IF(B.GT.UBB) GO TO 130
870 WRITE (6,100)
880 100 FORMAT(/'2. THERE IS NO STATISTICALLY SIGNIFICANT
890& DIFFERENCE BETWEEN'/'     THE CHARACTERISTIC VALUES')
900 GO TO 150
910 110 WRITE (6,120)
920 120 FORMAT(/'2. THE CHARACTERISTIC VALUE OF SAMPLE 1 IS
930& SIGNIFICANTLY SMALLER '/'     THAN THE CHARACTERISTIC VALUE
940& OF SAMPLE 2')
950 GO TO 150
960 130 WRITE (6,140)
970 140 FORMAT(/'2. THE CHARACTERISTIC VALUE OF SAMPLE 1 IS
980& SIGNIFICANTLY GREATER'/'     THAN THE CHARACTERISTIC VALUE
990& OF SAMPLE 2')
1000 150 WRITE (6,160) LBA*A, UBA*A
1010 160 FORMAT(/'THE 90 PERCENT CONFIDENCE INTERVAL FOR THE RATIO
1020& (M1/M2) OF THE'/'WEIBULL SLOPES IS:',/19X,'(',F6.4,',',F6.4,')')
1030 LBTHETAR = EXP(LBB*(2./(M1+M2)))*C
1040 UBTHETAR = EXP(UBB*(2./(M1+M2)))*C
1050 WRITE (6,170) LBTHETAR, UBTHETAR
1060 170 FORMAT(/'THE 90 PERCENT CONFIDENCE INTERVAL FOR THE RATIO
1070& (CV1/CV2) OF THE'/'CHARACTERISTIC VALUES IS:',/19X,'(',
1080& F6.4,',',F6.4,')')
1090 WRITE (6,600)
1100 READ (5,500) KK
1110 IF(KK.GT.0) GO TO 11
1120 STOP
1130 5000 PRINT,
1140 PRINT,'BE SERIOUS, YOU HAVE LESS THAN 5 DATA
1150& POINTS IN ONE OF YOUR SAMPLES;'
1160 PRINT,'DO MORE TESTS!!'
1170 WRITE (6,600)
1180 READ (5,500) KK
1190 IF(KK.GT.0) GO TO 11
1200 STOP
1210 5003 PRINT,
1220 PRINT,'THIS PROGRAM WILL NOT HANDLE SAMPLE SIZES OVER 100'
1230 WRITE (6,600)
1240 READ (5,500) KK
1250 IF(KK.GT.0) GO TO 11
1260 STOP
1270 END
```

APPENDIX II

NUMERICAL EXAMPLE OF HYPOTHESIS TESTING

A sample of 52 as-nitrided blades were tested and the maximum likelihood estimates of the Weibull parameters were calculated to be

$$\hat{m}_1 = 9.1$$

$$\hat{\theta}_1 = 89.9$$

A sample of 60 blades, after hot press bonding, were tested and the Weibull parameter estimates were

$$\hat{m}_2 = 6.9$$

$$\hat{\theta}_2 = 77.0$$

The caret mark is used above the symbols to indicate that they are maximum likelihood estimators of the true parameters.

Testing for equality of the Weibull slopes, the significance level is

$$\alpha = 0.10$$

The null hypothesis is

$$H_0 : m_1 = m_2$$

The alternative hypothesis is

$$H_1 : m_1 \neq m_2$$

To test H_0 against H_1, H_0 is accepted if

$$\ell_{\alpha/2} < \hat{m}_1/\hat{m}_2 < \ell_{1-\alpha/2}$$

where ℓ_γ is taken from Table 1 of Reference 21.

Assuming that both samples are composed of 52 items, the null hypothesis is accepted if

$$0.774 < \hat{m}_1/\hat{m}_2 < 1.292$$

Because $\hat{m}_1/\hat{m}_2 = 1.319$ and does not fall within the above acceptance region, the hypothesis that both samples come from Weibull distributions with the same slope may not be accepted. The 90% interval estimate for the ratio of the true Weibull slopes is

$$\ell_{\alpha/2}\,(\hat{m}_1/\hat{m}_2) < \hat{m}_1/\hat{m}_2 < \ell_{1-\alpha/2}\,(\hat{m}_1/\hat{m}_2)$$

or

$$1.021 < m_1/m_2 < 1.704$$

The ratio of Weibull slopes of the true populations is between 1.021 and 1.704 with 90% confidence. It should also be noted that there is 95% confidence that the ratio is greater than 1.021.

Testing for equality of the characteristic value, the significance level is

$$\alpha = 0.10$$

The null hypothesis is

$$H_0: \theta_1 = \theta_2$$

The alternative hypothesis is

$$H_1: \theta_1 \neq \theta_2$$

To test H_o against H_1, H_o is accepted if

$$\ell_{\alpha/2} < \left(\frac{\hat{m}_1 + \hat{m}_2}{2}\right) \ell n \left(\theta_1 / \theta_2\right) < \ell_{1-\alpha/2}$$

where ℓ_γ is taken from Table 2 of Reference 21.

Again assuming that both samples are composed of 52 samples, the null hypothesis is accepted if

$$-0.353 < \left(\frac{\hat{m}_1 + \hat{m}_2}{2}\right) \ell n \left(\hat{\theta}_1 / \hat{\theta}_2\right) < 0.353$$

Since

$$\left(\frac{\hat{m}_1 + \hat{m}_2}{2}\right) \ell n \left(\hat{\theta}_1 / \hat{\theta}_2\right) = 1.239$$

and does not fall within the above acceptance region, the hypothesis that both samples come from Weibull distributions with the same characteristic value may not be accepted. The 90% interval estimate for the ratio of the true characteristic values is

$$\left(\hat{\theta}_1 / \hat{\theta}_2\right) \exp\left[\frac{2\ell_{\alpha/2}}{\hat{m}_1 + \hat{m}_2}\right] < \left(\theta_1 / \theta_2\right) < \left(\hat{\theta}_1 / \hat{\theta}_2\right) \exp\left[\frac{2\ell_{1-\alpha/2}}{\hat{m}_1 + \hat{m}_2}\right]$$

or

$$1.117 < \theta_1 / \theta_2 < 1.220$$

The ratio of characteristic strengths of the true populations is between 1.117 and 1.220 with 90% confidence. There is a 95% confidence that the ratio is greater than 1.117

APPENDIX III

FORTRAN LISTING OF MAXIMUM-LIKELIHOOD ESTIMATION PROGRAM AND DATA FILES

The listing of the Fortran computer program which calculates the maximum-likelihood estimates of Weibull parameters was incomplete in the 11th report [11]. The complete listing follows.

```
S.MLE :
1*#FTN S.MLE=H.MLE(OPTZ,NOGO,CORE=24K,ULIB)LIB/FORD
2CC     PROGRAM WRITTEN BY RICHARD A. JERYAN, FORD MOTOR COMPANY
30C     GAS TURBINE ENGINEERING DEPARTMENT, DEARBORN, MI 48121
35C     (REF: THOMAN, BAIN AND ANTLE: TECHNOMETRICS, V.11, P.455)
40C     LAST REVISION 4/11/77
5C DIMENSION X(200),BN(196),ELM(2,116),ELO(2,116)
60 DIMENSION AMRANK(20,20),AMR(200),D2CR(25)
7C DIMENSION U05(30),U95(30)
75C     POLYNOMIAL APPROXIMATION FOR GAMMA FUNCTION. REF: EQN. 6.1.36,
76C     "HANDBOOK OF MATHEMATICAL FUNCTIONS," NBS AMS 55
80 F(AX)=1.-0.577191652*AX+C.988205891*AX^2-0.897056937*AX^3
9C&+0.918206857*AX^4-0.7567C4078*AX^5+0.482199394*AX^6
1CC8-0.193527818*AX^7+0.035868343*AX^8
120 CALL YOPEN(02,"QK051509/ENFORMLE$BRUCE,R;")
130 CALL YOPEN(03,"QK051509/INTFORM$BRUCE,R;")
140 CALL YOPEN(04,"QK051509/INTFORO$BRUCE,R;")
15C REAL MO,M,LBM,LBO,LBXB1C
160 PRINT,
17C PRINT,
180 PRINT,'THIS PROGRAM WILL CALCULATE THE UNBIASED MAXIMUM LIKELIHOOD ESTIMATOR'
190 PRINT,'FOR THE WEIBULL SHAPE PARAMETER AND CHARACTERISTIC VALUE'
200 READ(02,500) BN
210 READ(03,500) (ELM(1,I), ELM(2,I),I=1,116)
220 READ(04,500) (ELO(1,I),ELO(2,I), I=1,116)
230 8 CONTINUE
240 READ(01,500,END=5000) N,(X(I), I=1,N)
25C 500 FORMAT (V)
26C IF (N.LT.5) GO TO 4000
270 IT=50
280CFIRST ESTIMATE OF THE SLOPE IS CALCULATED AS THE SLOPE OF THE
290C LINE BETWEEN THE FIRST AND THE LAST DATA POINTS.
3CC CALL SORTS(X,N,"A",ERR)
310 MO=(ALOG(ALOG((N+.4)/.7))-ALOG(ALOG((N+.4)/(N-.3))))/
320&(ALOG(X(N))-ALOG(X(1)))
33C A=0.
340 ERROR=0.001
350 A=X(N)
360 DO 10 I=1,N
370 X(I)=X(I)/A
380 10 CONTINUE
39C S1=0.
4CC S2=0.
410 S3=0.
420 S4=0.
430 DO 100 I=1,N
440 S1=S1+ALOG(X(I))
450 S2=S2+X(I)^MO
460 S3=S3+ALOG(X(I))*(X(I)^MO)
470 S4=S4+((ALOG(X(I)))^2)*(X(I)^MO)
480 100 CONTINUE
490 DO 200 I=1,IT
5CC M=((1./MO)+(S1/N)-(S3/S2))/((1./MO^2)+((S4/S2)-((S3/S2)^2)))
510 M=M+MO
520 S2=0.
530 S3=0.
540 S4=0.
55C DO 300 J=1,N
560 S3=S3+ALOG(X(J))*(X(J)^M)
570 S4=S4+((ALOG(X(J)))^2)*(X(J)^M)
580 S2=S2+X(J)^M
590 300 CONTINUE
600 DLOM=(N/M)-N*(S3/S2)+S1
610 MO=M
620 IF(ABS(DLOM)-ERROR) 250,250,200
```

```
630 200 CONTINUE
640 WRITE (6,2000)
650 2000 FORMAT('NO SOLUTION FOUND')
660 GO TO 5000
670 250 THETA=0.
680 DO 400 I=1,N
690 THETA=THETA + X(I)^MO
700 400 CONTINUE
710 WRITE (6,2001)
720 2001 FORMAT (//"SAMPLE VALUES:"//)
730 WRITE (6,2002) (A*X(I), I=1,N)
740 2002 FORMAT (1X,6F10.1)
750 THETA = A*(THETA/N)^(1./MO)
760C MULTIPLY BY UNBIASING FACTOR
770 MO = MO*BN(N-4)
775C   IF (N.LE.120) CALCULATE PARAMETER INTERVAL ESTIMATES
780 IF (N.GT.120) GO TO 2005
790 WRITE (6,2003)
800 2003 FORMAT(/37X,"POINT",15X,"90 PERCENT",/35X,"ESTIMATES",
810& 9X,"INTERVAL ESTIMATES")
820 UBM = MO/ELM(1,N-4)
830 LBM = MO/ELM(2,N-4)
840 UBO = THETA/EXP(-ELO(1,N-4)/MO)
850 LBO = THETA/EXP(ELO(2,N-4)/MO)
860 WRITE (6,2004) MO,LBM,UBM
870 2004 FORMAT(/"WEIBULL SHAPE PARAMETER=",9X,F10.5,6X,
880& "(",F10.5,",",F10.5,")")
890 WRITE (6,2006) THETA,LBO,UBO
900 2006 FORMAT("WEIBULL CHARACTERISTIC VALUE= ",F10.2,
910& 9X,"(",F10.2,",",F10.2,")")
920 GO TO 2025
930 2005 WRITE (6,2010) MO
940 2010 FORMAT (//'WEIBULL SHAPE PARAMETER=          ',F10.5)
950 WRITE (6,2020) THETA
960 2020 FORMAT ('WEIBULL CHARACTERISTIC VALUE= ',F10.2)
970C   DISTRIBUTION MEAN=
980 2025 AAX= 1./MO
990 AAF=1.0
995C   RECURSION FORMULA FOR GAMMA FUNCTION
1000 2026 IF (AAX.LE.1.00) GO TO 2027
1010 AAF = AAF*AAX
1020 AAX = AAX - 1.00
1030 GO TO 2026
1040 2027 AMEAN = THETA*AAF*F(AAX)
1050C   DISTRIBUTION VARIANCE AND STANDARD DEVIATION
1060 AAAX=2./MO
1070 AAAF=1.0
1080 2028 IF (AAAX.LE.1.00) GO TO 2029
1090 AAAF = AAAF*AAAX
1100 AAAX = AAAX - 1.00
1110 GO TO 2028
1120 2029 VARI= (THETA^2)*(AAAF*F(AAAX)-((AAF*F(AAX))^2))
1130 STDDEV= SQRT(VARI)
1140C VALUE OF X AT W(X;M,0)=0.10; ( B10 )
1150 XB10 = THETA*(0.10536052^(1./MO)).
1160 WRITE (6,2030) AMEAN
1170 2030 FORMAT (/'DISTRIBUTION MEAN=                ',F10.2)
1180 WRITE (6,2040) STDDEV
1190 2040 FORMAT ('DISTRIBUTION STANDARD DEVIATION= ',F10.2)
1195C  IF (N.LE.30) CALCULATE B10 INTERVAL ESTIMATES
1200 IF (N.GT.30) GO TO 2045
1210 DATA U05/1.,1.,1.,1.,-1.422,-1.125,-1.015,-.955,-.915,-.8794,-.852,
1220& -.826,-.802,-.78,-.7648,-.741,-.722,-.706,-.69,-.674,-.662,
1230& -.648,-.637,-.626,-.616,-.605,-.596,-.587,-.578,-.5672/
1240 DATA U95/1.,1.,1.,1.,4.4453,3.76,3.10,2.64,2.24,2.1304,1.95,1.82,1.7,
1250& 1.6,1.5091,1.44,1.38,1.32,1.27,1.2262,1.18,1.14,1.1,1.07,1.04,1.01,
1260& .99,.96,.94,.9147/
1270 LBXB10 = XB10/(EXP(U95(N)/MO))
1280 UBXB10 = XB10*(EXP(-U05(N)/MO))
1290 WRITE(6,2051) XB10,LBXB10,UBXB10
1300 2051 FORMAT('B10 VALUE=',23X,F10.2,6X,'(',F10.2,',',F10.2,')')
1310 GO TO 2052
```

```
1320 2045 WRITE(6,2050) XB1C
1330 2050 FORMAT ('B10 VALUE=                              ',F10.2)
1340 2052 CONTINUE
1350C     K-S GOODNESS OF FIT TEST
1360C     .20 SIGNIFICANCE LEVEL (NONPARAMETRIC)
1370 IF(N.GT.25) GO TO 2055
1380 DATA D2CR/.900,.684,.585,.494,.446,.410,.381,.358,.339,.322,
1390& .307,.295,.284,.274,.266,.258,.250,.244,.237,.231,
1400& .227,.223,.218,.214,.21/
1410 D2CRIT = D2CR(N)
1420 GO TO 2060
1430 2055 D2CRIT = 1.07/SQRT(N)
1440 2060 IF(N.GT.20) GO TO 3500
1445C  READ MEDIAN RANK TABLE
1450 CALL YOPEN(05,"QK051509/MRDATA$BRUCE,R;")
1460 DO 3000 I=1,20
1470 DO 3000 J=1,20
1480 3000 AMRANK(I,J) = 0.0CC
1490 DO 3010 I=1,20
1500 READ (05,500) (AMRANK(I,K),K=I,20)
1510 3010 CONTINUE
1520 DO 3020 I=1,N
1530 AMR(I)=AMRANK(I,N)
1540 3020 CONTINUE
1550 GO TO 3600
1560 3500 DO 3030 I=1,N
1570 AMR(I)=(I-.3)/(N+.4)
1580 3030 CONTINUE
1590 3600 CONTINUE
1600 D2=0.0
1610 DO 3620 I=1,N
1620 3610 FF = 1.-EXP(-(((A*X(I))/THETA)^MO))
1630 D1 = ABS(FF-AMR(I))
1640 IF(D1.LE.D2CRIT) GO TO 3616
1650 WRITE (6,3615)
1660 3615 FORMAT("****",/,"****THE DATA EXCEEDS THE GOODNESS-
1661& OF-FIT LIMITS OF THE",/,"KOLMOGOROV-SMIRNOV TEST AT THE
1662& 20% SIGNIFICANCE LEVEL",/,"****")
1663 D2=D1
1665 GO TO 3625
1670 3616 IF(D1.LE.D2) GO TC 3620
1680 D2 = D1
1690 3620 CONTINUE
1700 3625 WRITE (6,3630) D2
1710 3630 FORMAT ("D2=                                      ",F10.6)
1720 GO TO 8
1730 4000 PRINT,"BE SERIOUS, YOU HAVE LESS THAN FIVE SAMPLES;"
1740 PRINT,"DO SOME MORE TESTS"
1750 GO TO 8
1760 5000 PRINT,"END OF DATA"
1770 STOP
1780 END
```

BNFORMLE ·

```
.70,.752,.792,.820,.842,.859,.872,.883,.893,.901,.908,.914,.9185
.923,.927,.931,.9345,.938,.9405,.943,.945,.947,.949,.951,.953,.955
.9565,.958,.959,.960,.961,.962,.963,.964,.965,.966,.967,.968
.969,.670,.9705,.971,.9715,.972,.9725,.973,.9735,.974,.9745,.975
.9755,.976,.9765,.977,.9775,.978,.9785,.979,.9795,.980,.980,.980
.9805,.981,.981,.981,.9815,.982,.982,.982,.9825,.983,.983,.983,.9835
.984,.9842,.9844,.9846,.9848,.985,.9852,.9854,.9856,.9858,.986
.9861,.9862,.9863,.9864,.9865,.9866,.9867,.9868,.9869,.987
.9872,.9873,.9875,.9876,.9878,.9879,.9881,.9882,.9884,.9885
.9887,.9888,.9890,.9891,.9893,.9894,.9896,.9897,.9899,.9900
.9901,.9901,.9902,.9903,.9903,.9904,.9904,.9905,.9906,.9906
.9907,.9908,.9908,.9909,.9909,.9910,.9911,.9911,.9912,.9913
.9913,.9914,.9914,.9915,.9916,.9916,.9917,.9918,.9918,.9919
.9919,.9920,.9921,.9921,.9922,.9923,.9923,.9924,.9924,.9925
.9926,.9926,.9927,.9928,.9928,.9929,.9929,.9930,.9931
.9931,.9932,.9933,.9933,.9934,.9934,.9935,.9936,.9936,.9937
.9938,.9938,.9939,.9939,.994C,.9941,.9941,.9942,.9943,.9943
.9944,.9944,.9945,.9945,.9946,.9947,.9948,.9948,.9949,.9949
.9950
```

INTFORM :

```
.683,2.779,.697,2.436,.709,2.183,.720,2.015,.729,1.896,.738,1.807,.745,1.738
.752,1.682,.759,1.636,.764,1.597,.770,1.564,.775,1.535,.779,1.510,.784,1.487
.788,1.467,.791,1.449,.795,1.434,.798,1.418,.802,1.405,.805,1.392,.808,1.381
.810,1.370,.813,1.361,.815,1.351,.818,1.343,.820,1.334,.822,1.327,.824,1.319
.826,1.313,.828,1.306,.830,1.300,.832,1.294,.834,1.288,.835,1.283,.837,1.278
.839,1.273,.841,1.269,.842,1.265,.844,1.261,.845,1.256,.846,1.253,.847,1.249
.849,1.246,.850,1.242,.851,1.239,.852,1.235,.853,1.232,.854,1.229,.856,1.227
.857,1.224,.858,1.221,.859,1.218,.860,1.216,.861,1.213,.862,1.211,.863,1.208
.864,1.206,.864,1.204,.865,1.202,.866,1.200,.867,1.198,.868,1.196,.869,1.194
.869,1.192,.870,1.190,.871,1.188,.872,1.187,.872,1.185,.873,1.184,.874,1.182
.875,1.181,.875,1.179,.876,1.178,.876,1.176,.877,1.175,.878,1.173,.879,1.172
.879,1.170,.880,1.169,.880,1.167,.881,1.166,.881,1.165,.882,1.164,.882,1.162
.883,1.161,.883,1.160,.884,1.159,.884,1.158,.885,1.157,.885,1.156,.886,1.155
.886,1.154,.887,1.153,.887,1.152,.888,1.151,.888,1.150,.889,1.149,.889,1.148
.890,1.147,.890,1.146,.891,1.146,.891,1.145,.892,1.144,.892,1.143,.893,1.142
.893,1.141,.893,1.140,.894,1.139,.894,1.139,.895,1.138,.895,1.137,.895,1.136
.896,1.135,.896,1.135,.897,1.134,.897,1.133
```

INTFORØ :

```
1.247,1.107,1.007,.939,.874,.829,.784,.751,.717,.691,.665,.644,.622,.605
.587,.572,.557,.544,.532,.520,.509,.499,.489,.480,.471,.463,.455,.447
.441,.433,.428,.421,.416,.410,.404,.398,.394,.389,.384,.379,.376,.371
.367,.362,.360,.355,.352,.347,.345,.341,.338,.334,.332,.329,.326,.323
.321,.318,.315,.312,.310,.307,.305,.302,.301,.298,.296,.293,.292,.289
.288,.285,.284,.282,.280,.278,.277,.275,.273,.271,.270,.268,.266,.264
.263,.261,.260,.258,.257,.256,.254,.253,.252,.250,.249,.247,.247,.245
.244,.243,.242,.241,.239,.238,.237,.236,.234,.233,.232,.231,.230,.229
.228,.227,.226,.225,.224,.223,.222,.221,.220,.220,.218,.218,.217,.216
.215,.214,.213,.213,.211,.211,.210,.210,.208,.208,.207,.207,.205,.205
.204,.204,.202,.202,.201,.201,.199,.199,.198,.198,.197,.197,.196,.196
.194,.194,.193,.193,.191,.191,.190,.190,.189,.189,.188,.188,.186,.187
.185,.186,.184,.185,.183,.184,.182,.183,.181,.181,.180,.180,.179,.179
.178,.178,.177,.177,.176,.177,.175,.176,.174,.175,.173,.174,.172,.173
.171,.172,.170,.171,.170,.171,.169,.170,.168,.169,.167,.168,.166,.167
.165,.166,.164,.165,.164,.165,.163,.164,.162,.163,.162,.163,.161,.162
.160,.161,.159,.160,.159,.160,.158,.159
```

MRDATA :

```
.5,.2929,.2063,.1591,.1294,.1091,.0943,.083,.0741,.067,.0611,.0561
.0519,.0483,.0452,.0424,.04,.0378,.0358,.0341
.7071,.5,.3864,.3147,.2655,.2295,.2021,.1806,.1632,.1489,.1368,.1266,.1178
.1101,.1034,.0975,.0922,.0874,.0831
.7937,.6136,.5,.4218,.3648,.3213,.2871,.2594,.2366,.2175,.2013
.1873,.1751,.1644,.155,.1465,.139,.1322
.8409,.6853,.5782,.5,.4404,.3935,.3557,.3244,.2982,.276,.2568,.2401
.2254,.2125,.2009,.1905,.1812
.8706,.7345,.6352,.5596,.5,.4519,.4122,.3789,.3506,.3263,.3051
.2865,.27,.2553,.2421,.2302
.8909,.7705,.6787,.6065,.5481,.5,.4596,.4253,.3958,.37,.3475,.3275,.3097
.2937,.2793
.9057,.7979,.7129,.6443,.5878,.5404,.5,.4653,.435,.4085,.385,.3641
.3453,.3283
.917,.8194,.7406,.6756,.6211,.5747,.5347,.5,.4695,.4425,.4184,.3968
.3774
.9259,.8368,.7634,.7018,.6494,.6042,.565,.5305,.5,.4728,.4484,.4264
.933,.8511,.7825,.724,.6737,.63,.5915,.5575,.5272,.5,.4755
.9389,.8632,.7987,.7432,.6949,.6525,.615,.5816,.5516,.5245
.9439,.8734,.8127,.7599,.7135,.6725,.6359,.6032,.5736
.9481,.8822,.8249,.7746,.73,.6903,.6547,.6226
.9517,.8899,.8356,.7875,.7447,.7063,.6717
.9548,.8966,.845,.7991,.7579,.7207
.9576,.9025,.8535,.8095,.7698
.96,.9078,.861,.8188
.9622,.9126,.8678
.9642,.9169
.9659
```

Army Materials and Mechanics Research Center
Watertown, Massachusetts 02172

AD ____________

BRITTLE MATERIALS DESIGN
HIGH TEMPERATURE GAS TURBINE
VOLUME 2 CERAMIC TURBINE ROTOR TECHNOLOGY

Arthur F. McLean, Robert R. Baker,
Ford Motor Company, Dearborn, Michigan 48121

Technical Report AMMRC TR-78-14, March, 1978
93 pages, 44 illus., 21 tables, 24 references
Contract DAAG 46-71-C-0162, ARPA Order Number
1849, Twelfth Report, January 1, 1977 to September 30, 1977

Key Words

Gas Turbine Engine
Brittle Design
Ceramics
High Temperature Materials
Silicon Nitride
Silicon Carbide
Non-Destructive Tests
Mechanical Properties

ABSTRACT

The progress in the last nine months on ERDA supported programs within the joint DARPA/ERDA supported "Brittle Materials Design, High Temperature Gas Turbine" Program is reported on in this volume. Volume 1 covers the progress on the DARPA supported Ceramic Turbine Testing Program.

Investigations of the materials used to fabricate duo-density ceramic turbine rotors were conducted on injection molded reaction bonded and hot pressed silicon nitride. The starting silicon powder, used to injection mold rotor blade rings, was found to contain contaminates in the form of iron and chromium. Microstructural examination of both silicon nitride test bars and rotor blades indicated a definite correlation between strength and the size of microscopic flaws due to contamination. Magnetic separator equipment was ordered and received so that all starting silicon powder can be cleaned in-house. Approximately 30 hot pressings were made with various purity level starting powders and a variety of hot pressing aids. The high temperature strength will be determined to identify the best candidates for further study.

The injection molding process, utilized to fabricate rotor blade rings, was improved by optimizing the molding parameters with the automated control system and improving the molding mixture. The installation of nozzles, to apply mold release, and air blast jets, to clean the die and evenly distribute the mold release, resulted in a noticeable improvement in the surface finish of the blade rings. Significant improvements were made in the hot press bonding process used to fabricate duo-density turbine rotors. Control of the hot pressing load was refined and temperature measurement improved. The graphite tooling was redesigned and blade filling process was modified. These two changes resulted in the most significant improvement in the yield of hot pressings to date; 70% of the rotors fabricated were free of flaws induced by hot pressing. Alternate approaches were investigated to produce duo-density turbine rotors.

Duo-density turbine rotors were tested in the cold spin pit to evaluate the hot press to reaction sintered bond joints and the effect of I.D. voids, in the blade ring rim, on blade failure speeds. Degradation of the room temperature strength of the reaction bonded silicon nitride rotor blades was identified as resulting from the press-bonding operation. Blade strength decreases of 14 to 38% were measured by the blade bend test. Analysis of the blades indicated they change from a shiny black to a gray color after hot pressing with a corresponding increase in non-uniform porosity; phase analysis indicated that the reaction bonded silicon nitride had changed from an average of 70% α, 29% β before press bonding to an average of 22% α, 75% β and 3% silicon oxynitride after press-bonding.

Army Materials and Mechanics Research Center
Watertown, Massachusetts 02172

AD ____________

BRITTLE MATERIALS DESIGN
HIGH TEMPERATURE GAS TURBINE
VOLUME 2 CERAMIC TURBINE ROTOR TECHNOLOGY

Arthur F. McLean, Robert R. Baker,
Ford Motor Company, Dearborn, Michigan 48121

Technical Report AMMRC TR-78-14, March, 1978
93 pages, 44 illus., 21 tables, 24 references
Contract DAAG 46-71-C-0162, ARPA Order Number
1849, Twelfth Report, January 1, 1977 to September 30, 1977

Key Words

Gas Turbine Engine
Brittle Design
Ceramics
High Temperature Materials
Silicon Nitride
Silicon Carbide
Non-Destructive Tests
Mechanical Properties

ABSTRACT

The progress in the last nine months on ERDA supported programs within the joint DARPA/ERDA supported "Brittle Materials Design, High Temperature Gas Turbine" Program is reported on in this volume. Volume 1 covers the progress on the DARPA supported Ceramic Turbine Testing Program.

Investigations of the materials used to fabricate duo-density ceramic turbine rotors were conducted on injection molded reaction bonded and hot pressed silicon nitride. The starting silicon powder, used to injection mold rotor blade rings, was found to contain contaminates in the form of iron and chromium. Microstructural examination of both silicon nitride test bars and rotor blades indicated a definite correlation between strength and the size of microscopic flaws due to contamination. Magnetic separator equipment was ordered and received so that all starting silicon powder can be cleaned in-house. Approximately 30 hot pressings were made with various purity level starting powders and a variety of hot pressing aids. The high temperature strength will be determined to identify the best candidates for further study.

The injection molding process, utilized to fabricate rotor blade rings, was improved by optimizing the molding parameters with the automated control system and improving the molding mixture. The installation of nozzles, to apply mold release, and air blast jets, to clean the die and evenly distribute the mold release, resulted in a noticeable improvement in the surface finish of the blade rings. Significant improvements were made in the hot press bonding process used to fabricate duo-density turbine rotors. Control of the hot pressing load was refined and temperature measurement improved. The graphite tooling was redesigned and blade filling process was modified. These two changes resulted in the most significant improvement in the yield of hot pressings to date; 70% of the rotors fabricated were free of flaws induced by hot pressing. Alternate approaches were investigated to produce duo-density turbine rotors.

Duo-density turbine rotors were tested in the cold spin pit to evaluate the hot press to reaction sintered bond joints and the effect of I.D. voids, in the blade ring rim, on blade failure speeds. Degradation of the room temperature strength of the reaction bonded silicon nitride rotor blades was identified as resulting from the press-bonding operation. Blade strength decreases of 14 to 38% were measured by the blade bend test. Analysis of the blades indicated they change from a shiny black to a gray color after hot pressing with a corresponding increase in non-uniform porosity; phase analysis indicated that the reaction bonded silicon nitride had changed from an average of 70% α, 29% β before press bonding to an average of 22% α, 75% β and 3% silicon oxynitride after press-bonding.

Army Materials and Mechanics Research Center
Watertown, Massachusetts 02172

AD ____________

BRITTLE MATERIALS DESIGN
HIGH TEMPERATURE GAS TURBINE
VOLUME 2 CERAMIC TURBINE ROTOR TECHNOLOGY

Arthur F. McLean, Robert R. Baker,
Ford Motor Company, Dearborn, Michigan 48121

Technical Report AMMRC TR-78-14, March, 1978
93 pages, 44 illus., 21 tables, 24 references
Contract DAAG 46-71-C-0162, ARPA Order Number
1849, Twelfth Report, January 1, 1977 to September 30, 1977

Key Words

Gas Turbine Engine
Brittle Design
Ceramics
High Temperature Materials
Silicon Nitride
Silicon Carbide
Non-Destructive Tests
Mechanical Properties

ABSTRACT

The progress in the last nine months on ERDA supported programs within the joint DARPA/ERDA supported "Brittle Materials Design, High Temperature Gas Turbine" Program is reported on in this volume. Volume 1 covers the progress on the DARPA supported Ceramic Turbine Testing Program.

Investigations of the materials used to fabricate duo-density ceramic turbine rotors were conducted on injection molded reaction bonded and hot pressed silicon nitride. The starting silicon powder, used to injection mold rotor blade rings, was found to contain contaminates in the form of iron and chromium. Microstructural examination of both silicon nitride test bars and rotor blades indicated a definite correlation between strength and the size of microscopic flaws due to contamination. Magnetic separator equipment was ordered and received *so that all starting silicon powder can be cleaned* in-house. Approximately 30 hot pressings were made with various purity level starting powders and a variety of hot pressing aids. The high temperature strength will be determined to identify the best candidates for further study.

The injection molding process, utilized to fabricate rotor blade rings, was improved by optimizing the molding parameters with the automated control system and improving the molding mixture. The installation of nozzles, to apply mold release, and air blast jets, to clean the die and evenly distribute the mold release, resulted in a noticeable improvement in the surface finish of the blade rings. Significant improvements were made in the hot press bonding process used to fabricate duo-density turbine rotors. Control of the hot pressing load was refined and temperature measurement improved. The graphite tooling was redesigned and blade filling process was modified. These two changes resulted in the most significant improvement in the yield of hot pressings to date; 70% of the rotors fabricated were free of flaws induced by hot pressing. Alternate approaches were investigated to produce duo-density turbine rotors.

Duo-density turbine rotors were tested in the cold spin pit to evaluate the hot press to reaction sintered bond joints and the effect of I.D. voids, in the blade ring rim, on blade failure speeds. Degradation of the room temperature strength of the reaction bonded silicon nitride rotor blades was identified as resulting from the press-bonding operation. Blade strength decreases of 14 to 38% were measured by the blade bend test. Analysis of the blades indicated they change from a shiny black to a gray color after hot pressing with a corresponding increase in non-uniform porosity; phase analysis indicated that the reaction bonded silicon nitride had changed from an average of 70% α, 29% β before press bonding to an average of 22% α, 75% β and 3% silicon oxynitride after press-bonding.

Army Materials and Mechanics Research Center
Watertown, Massachusetts 02172

AD ____________

BRITTLE MATERIALS DESIGN
HIGH TEMPERATURE GAS TURBINE
VOLUME 2 CERAMIC TURBINE ROTOR TECHNOLOGY

Arthur F. McLean, Robert R. Baker,
Ford Motor Company, Dearborn, Michigan 48121

Technical Report AMMRC TR-78-14, March, 1978
93 pages, 44 illus., 21 tables, 24 references
Contract DAAG 46-71-C-0162, ARPA Order Number
1849, Twelfth Report, January 1, 1977 to September 30, 1977

Key Words

Gas Turbine Engine
Brittle Design
Ceramics
High Temperature Materials
Silicon Nitride
Silicon Carbide
Non-Destructive Tests
Mechanical Properties

ABSTRACT

The progress in the last nine months on ERDA supported programs within the joint DARPA/ERDA supported "Brittle Materials Design, High Temperature Gas Turbine" Program is reported on in this volume. Volume 1 covers the progress on the DARPA supported Ceramic Turbine Testing Program.

Investigations of the materials used to fabricate duo-density ceramic turbine rotors were conducted on injection molded reaction bonded and hot pressed silicon nitride. The starting silicon powder, used to injection mold rotor blade rings, was found to contain contaminates in the form of iron and chromium. Microstructural examination of both silicon nitride test bars and rotor blades indicated a definite correlation between strength and the size of microscopic flaws due to contamination. Magnetic separator equipment was ordered and received so that all starting silicon powder can be cleaned in-house. Approximately 30 hot pressings were made with various purity level starting powders and a variety of hot pressing aids. The high temperature strength will be determined to identify the best candidates for further study.

The injection molding process, utilized to fabricate rotor blade rings, was improved by optimizing the molding parameters with the automated control system and improving the molding mixture. The installation of nozzles, to apply mold release, and air blast jets, to clean the die and evenly distribute the mold release, resulted in a noticeable improvement in the surface finish of the blade rings. Significant improvements were made in the hot press bonding process used to fabricate duo-density turbine rotors. Control of the hot pressing load was refined and temperature measurement improved. The graphite tooling was redesigned and blade filling process was modified. These two changes resulted in the most significant improvement in the yield of hot pressings to date; 70% of the rotors fabricated were free of flaws induced by hot pressing. Alternate approaches were investigated to produce duo-density turbine rotors.

Duo-density turbine rotors were tested in the cold spin pit to evaluate the hot press to reaction sintered bond joints and the effect of I.D. voids, in the blade ring rim, on blade failure speeds. Degradation of the room temperature strength of the reaction bonded silicon nitride rotor blades was identified as resulting from the press-bonding operation. Blade strength decreases of 14 to 38% were measured by the blade bend test. Analysis of the blades indicated they change from a shiny black to a gray color after hot pressing with a corresponding increase in non-uniform porosity; phase analysis indicated that the reaction bonded silicon nitride had changed from an average of 70% α, 29% β before press bonding to an average of 22% α, 75% β and 3% silicon oxynitride after press-bonding.

UNCLASSIFIED

SECURITY CLASSIFICATION OF THIS PAGE *(When Data Entered)*

REPORT DOCUMENTATION PAGE

READ INSTRUCTIONS BEFORE COMPLETING FORM

1. REPORT NUMBER: AMMRC TR 78-14 Volume 2	2. GOVT ACCESSION NO.
3. RECIPIENT'S CATALOG NUMBER	
4. TITLE *(and Subtitle)*: Brittle Materials Design, High Temperature Gas Turbine Volume 2 Ceramic Turbine Rotor Technology	5. TYPE OF REPORT & PERIOD COVERED: Interim Report Number 12, 1-1-77 to 9-30-77
	6. PERFORMING ORG. REPORT NUMBER: DAAG 46-71-C-0162 ✓
7. AUTHOR(s): A. F. McLean, Ford Motor Company; R. R. Baker, Ford Motor Company	8. CONTRACT OR GRANT NUMBER(s)
9. PERFORMING ORGANIZATION NAME AND ADDRESS: Ford Motor Company, Dearborn, MI 48121	10. PROGRAM ELEMENT, PROJECT, TASK AREA & WORK UNIT NUMBERS: D/A Project: ARPA Order 1849; AMCMS Code: ; Agency Accession: DA OD 4733
11. CONTROLLING OFFICE NAME AND ADDRESS: Army Materials and Mechanics Research Center, Watertown, Massachusetts 02172	12. REPORT DATE: March, 1978
	13. NUMBER OF PAGES: 93
14. MONITORING AGENCY NAME & ADDRESS *(if different from Controlling Office)*	15. SECURITY CLASS. *(of this report)*: Unclassified
	15a. DECLASSIFICATION/DOWNGRADING SCHEDULE

16. DISTRIBUTION STATEMENT *(of this Report)*

Approved for public release: distribution unlimited.

17. DISTRIBUTION STATEMENT *(of the abstract entered in Block 20, if different from Report)*

18. SUPPLEMENTARY NOTES

19. KEY WORDS *(Continue on reverse side if necessary and identify by block number)*

Gas Turbine Engine	Silicon Nitride
Brittle Design	Silicon Carbide
Ceramics	Non-Destructive Test
High Temperature Materials	Mechanical Properties

20. ABSTRACT *(Continue on reverse side if necessary and identify by block number)*

(See reverse side)

DD FORM 1 JAN 73 1473 EDITION OF 1 NOV 65 IS OBSOLETE

UNCLASSIFIED

SECURITY CLASSIFICATION OF THIS PAGE *(When Data Entered)*

ABSTRACT

The progress in the last nine months on ERDA supported programs within the joint DARPA/ERDA supported "Brittle Materials Design, High Temperature Gas Turbine" Program is reported on in this volume. Volume 1 covers the progress on the DARPA supported Ceramic Turbine Testing Program.

Investigations of the materials used to fabricate duo-density ceramic turbine rotors were conducted on injection molded reaction bonded and hot pressed silicon nitride. The starting silicon powder, used to injection mold rotor blade rings, was found to contain contaminates in the form of iron and chromium. Microstructural examination of both silicon nitride test bars and rotor blades indicated a definite correlation between strength and the size of microscopic flaws due to contamination. Magnetic separator equipment was ordered and received so that all starting silicon powder can be cleaned in-house. Approximately 30 hot pressings were made with various purity level starting powders and a variety of hot pressing aids. The high temperature strength will be determined to identify the best candidates for further study.

The injection molding process, utilized to fabricate rotor blade rings, was improved by optimizing the molding parameters with the automated control system and improving the molding mixture. The installation of nozzles, to apply mold release, and air blast jets, to clean the die and evenly distribute the mold release, resulted in a noticeable improvement in the surface finish of the blade rings. Significant improvements were made in the hot press bonding process used to fabricate duo-density turbine rotors. Control of the hot pressing load was refined and temperature measurement improved. The graphite tooling was redesigned and blade filling process was modified. These two changes resulted in the most significant improvement in the yield of hot pressings to date; 70% of the rotors fabricated were free of flaws induced by hot pressing. Alternate approaches were investigated to produce duo-density turbine rotors.

Duo-density turbine rotors were tested in the cold spin pit to evaluate the hot press to reaction sintered bond joints and the effect of I.D. voids, in the blade ring rim, on blade failure speeds. Degradation of the room temperature strength of the reaction bonded silicon nitride rotor blades was identified as resulting from the press-bonding operation. Blade strength decreases of 14 to 38% were measured by the blade bend test. Analysis of the blades indicated they change from a shiny black to a gray color after hot pressing with a corresponding increase in non-uniform porosity; phase analysis indicated that the reaction bonded silicon nitride had changed from an average of 70% α, 29% β before press bonding to an average of 22% α, 75% β and 3% silicon oxynitride after press-bonding.

A procedure for determining whether statistically significant differences exist between two sets of data, known as the 'Hypothesis Testing' was outlined. The test was applied to data from duo-density turbine rotors and showed that blade strength did deteriorate after the press-bonding operation. Use of proof-testing as a means of enhancing the accuracy of life predictions was discussed. Analytical relations were derived for predicting the survival probability of a proof-tested component, and a procedure was outlined for maximizing the effectiveness of a proof-test. Life prediction relations derived in the previous report were applied to the first-stage turbine rotor. Several disk contour modifications were studied as means of improving the life of the rotor under the DARPA duty cycle. The study showed that for given design constraints (space, inertia, etc.) and using material utilization as the criterion, the optimum disk configuration derived on the basis of fast fracture (time independent) mode of failure differed from the configuration derived from life considerations when the material is subject to static fatigue.